IMPROVEMENTS TO OPTICAL COMMUNICATION CAPABILITIES ACHIEVED THROUGH THE OPTICAL INJECTION OF SEMICONDUCTOR LASERS

Timothy P. Locke, Captain, USAF
AFIT/GE/ENG/12-27

DEPARTMENT OF THE AIR FORCE
AIR UNIVERSITY

AIR FORCE INSTITUTE OF TECHNOLOGY

Wright-Patterson Air Force Base, Ohio

AFIT/GE/ENG/12-27

IMPROVEMENTS TO OPTICAL COMMUNICATION CAPABILITIES ACHIEVED THROUGH THE OPTICAL INJECTION OF SEMICONDUCTOR LASERS

THESIS

Presented to the Faculty

Department of Electrical and Computer Engineering

Graduate School of Engineering and Management

Air Force Institute of Technology

Air University

Air Education and Training Command

In Partial Fulfillment of the Requirements for the

Degree of Master of Science in Electrical Engineering

Timothy P. Locke, B.S.E.E.

Captain, USAF

March 2012

AFIT/GE/ENG/12-27

IMPROVEMENTS TO OPTICAL COMMUNICATION CAPABILITIES ACHIEVED THROUGH THE OPTICAL INJECTION OF SEMICONDUCTOR LASERS

Timothy P. Locke, B.S.E.E.
Captain, USAF

Approved:

Michael C. Pochet, Maj, Ph.D. (Chairman)	5 Mar 2012 Date
Mark D. Silvius, Maj. Ph.D. (Member)	5 Mar 2012 Date
Nicholas G. Usechak, Ph.D. (Member)	5 Mar 2012 Date

Abstract

This research investigates the degree to which optical injection improves the communication capability of directly modulated semiconductor lasers and evaluates the suitability of optical injection for telecommunications applications. An end-to-end digital communication system which directly modulates the bias-current of a Fabry–Pérot laser diode is used to investigate the bit-rate-distance improvements achieved using optically injected Fabry–Pérot laser diodes. The injection strength and detuning frequency of the injection signal was varied to determine their impact on the optical communication link's characteristics. This research measured a 25 fold increase in the bit-rate-distance product using optical injection locking as compared to the injected laser's free-running capability. A 57 fold increase was measured in the bit-rate-distance product when signal power is considered in a power-penalty measurement. This increased performance is attributed to the injected signals tolerance to dispersion given its reduced linewidth and chirp.

This work also investigates the suitability of optical injection for radio over fiber applications using the period-one dynamic of optical injection. The all-optically generated, widely tunable microwave subcarrier frequency, well above the 3-dB cutoff frequency of the laser's packaging electronics, is modulated with the same baseband electronics. This optically carried, ultra-wide spread spectrum signal is transported 50km through standard single-mode fiber. After detection with a high-speed photodetector followed by removal of the baseband modulation component, the resultant signal was found to be suitable for broadcasting with an antenna or added to a frequency division multiplexed channel.

Acknowledgments

I would like to express my sincere appreciation to my faculty advisor, Maj. Michael C. Pochet for his patient guidance and support throughout the course of this thesis effort. The insight and experience was certainly appreciated. Thank you for your leadership.

I would like to thank my thesis committee member and sponsor Dr. Nicholas G. Usechak, who entertained my many interruptions in his optical research laboratory and whose knowledge and experience helped me greatly with physical laboratory setup and proper use of equipment. Thanks for providing me with significant theoretical grounding. I would also like to thank my thesis committee member Maj. Mark D. Silvius who provided significant guidance for my research into the analog and linear systems theory and practice for this research. Thank you.

This research relied heavily on the discoveries and knowledge of Dr. Vassilios Kovanis who is responsible for many analytical models of optical injection, Dr. Julie A Jackson for her help modeling eye diagrams with random frequency components, LtCol Geoffrey A Akers who allowed use of his microwave electronics, Maj. Milo W. Hyde for use of his eye analyzer, and Dr. William Zortman for knowledge of external modulation and power penalty metric.

Most of all, I'd like to thank my wife, who believed in me through it all. Your encouragement and support gave me the strength I needed to push through to the end. Thank you for standing with me… I love you more than the optical injection of semiconductor lasers! Timothy P. Locke

Table of Contents

List of Figures

Page

List of Tables

IMPROVEMENTS TO OPTICAL COMMUNICATION CAPABILITIES ACHIEVED THROUGH THE OPTICAL INJECTION OF SEMICONDUCTOR LASERS

1. Introduction

1.1. General Issue

This chapter provides motivation for researching improvements in optical communications in the context of warfighter needs and provides a general overview of the nature of work investigated in this thesis.

This work centers on the application of previously theoretically derived parameters of optical injection for improved baseband telecommunication and informatic modulation on injected laser dynamics. This study uses optical injection locking to improve the bit-rate-distance product of directly modulated semiconductor lasers by decreasing the linewidth and chirp of a semiconductor laser under stable optical injection. Moreover, the ability to use the optical injection concept to all-optically generate and modulate a highly tunable microwave carrier frequency (8 – 26+ GHz) is also explored.

1.2. Problem Statement

The nonlinear dependence of the index of refraction on photon wavelength causes chromatic dispersion which limits the data rate and/or distance capabilities of a given optical communication signal. In addition, the inherent relationship of a semiconductor

laser's relaxation oscillation frequency and damping rate limit its maximum achievable direct modulation rate. The improvement of the bit-rate-distance product, while maintaining an acceptable bit error ratio (BER) for a guided optical communications link, has the potential to improve overall distance and data rate capabilities. This potential improvement has attracted considerable research interest over the past two decades in a number of fields. Within this breadth of research, the concept of optical injection locking has garnered interest for its promise to improve optical communication capabilities, specifically in enhancing a laser's relaxation oscillation frequency, and through the suppression of the deleterious effects of chromatic dispersion. Given the ubiquity of optical communications in civil and military communication networks, the reduction of system cost, complexity and/or improvement of system performance will yield great benefits.

In this work, a directly modulated Fabry–Pérot semiconductor laser operating near 1550 nm under stable optical injection by a distributed feedback laser is used to communicate over 60 km of standard optical fiber. The improvements offered by injection-locking are then discussed. Improvements to directly modulated semiconductor lasers under injection-locking are shown to include the reduction of the optical linewidth, increased modulation bandwidth, suppression of nonlinear distortion, and reduction of relative intensity noise, mode hopping and chirp [1-5]. Various experimental and theoretical analyses of the physical mechanisms resulting in bandwidth and resonant frequency enhancement in injection-locked systems have been published [6-10]; however, what is missing in the literature is the engineering applicability of injection-

locked lasers on optical communication links. One objective of this thesis is to demonstrate and evaluate this engineering applicability and associated limitations.

Next, this thesis uses optical injection to excite the injected laser into what is referred to as the period-one state, where its resonance frequency is enhanced and un-damped. This excited state is on-off keyed for the transmission of digital data. The potential of this capability will be discussed in detail, along with potential limitations and instabilities.

1.3. Overview of Optical Communications

Guided-wave optical communication has been adopted as the primary technology used in long distance and high demand terrestrial communication applications because of its advantageous properties including significantly lower attenuation, lower interference, and higher bandwidth compared to electrical transmission over copper wires, wireless radio in mobile applications, and free-space optical communications.

There are several significant advantages to guided optical communications, especially for communication distances over 30 km. One advantage is the very large theoretical bandwidth of a standard single-mode fiber (SMF). The difference between the longest and shortest wavelengths supported by SMF translates to a frequency difference of over 40 THz. That theoretical bandwidth is more than two orders of magnitude greater compared to the total free-space radio frequency communications bandwidth defined by the International Telecommunication Union's Radio Regulations board (3 Hz to 300 GHz). A second advantage of optical communication is the low attenuation associated

with SMF (≈0.2 dB/km). This value is over an order of magnitude better than copper electric waveguides (in reference to low data rate communications over copper cables; attenuation increases significantly with data rate in copper cables). The low attenuation per kilometer allows comparatively longer SMF cable runs without the need for repeaters or amplifiers.

Another advantage of using standard SMF is near complete immunity to electromagnetic interference, including electromagnetic pulses associated with nuclear weapon detonation. Optical signals do not distort in high magnetic environments and because standard SMF is an electrical insulator, ground currents have no effect [11]. Optical fibers are also significantly lighter than similarly performing copper and emit very little electromagnetic radiation.

Never the less, guided optical communication does not dominate the entire communications industry since copper wires still provide significant benefits for certain applications, especially for metropolitan-area networks and last-mile communication links. Provided the communication link operates at a slow bit-rate over a short distance (by today's standards), a single communication link can be established for a lower cost using copper cables. If the system relies entirely on electronics, the cost savings is due to the elimination of the laser diodes and photonic detectors. Furthermore, installation of copper network infrastructure is simpler and requires less complicated tools for physical layer connectivity. Indeed, this is the reason most last mile communication links in the United States rely on copper cables. This dependency is partly due to legacy infrastructure, partly due to the low material cost in small quantities, and partly due to the

comparative ease of installation. Moreover, at low bit rates, electric transmitters and receivers are significantly less expensive and can easily be made to operate in a linear mode.

Wireless radio frequency communication systems possess similar data rates to guided electrical systems, with the key advantage that they allow communication without a physical connection. Wireless communication is primarily used for spacecraft, mobile platforms, or remote locations where it is either impossible or prohibitively expensive to install a communication medium like cables or fibers. The relatively low infrastructure expense makes last-mile wireless communication quite attractive, but ultimately limits each user's data rates because of multiple access interference issues.

In guided communications applications devices connect through separate physical channels and can communicate without using any of the available bandwidth over adjacent physical channels. In contrast, wireless communication, which occurs in the presence of multiple devices, is subject to multiple access interference that impedes the performance of other devices' communications. Multiple access interference has led wireless communications engineers to develop ways of separating communication signals from each other using one or more of six different signal separation domains: Amplitude, Frequency, Code, Polarity, Spatial, or Time [12].

Because of frequency allocation limitations, wireless communication devices are forced to use their frequency bandwidth more efficiently by communicating more than 1 bit per communication symbol. Multiple bits per communication symbol is commonly referred to as M-Ary communication [13] and has received very little attention in guided

optical communications until recent attempts to modulate the intensity of a laser signal with radio frequency signals, generically referred to as radio over fiber [46]. One possible path towards the implementation of radio-over-fiber schemes in optical communication is to convert amplitude modulated (AM) signals into frequency modulated (FM) signals using various approaches. The approach to achieve the AM-to-FM conversion investigated in this work is the use of the period one dynamic of optically injected lasers.

1.4. Overview of Optical Injection

One objective of this research is to use optical injection to reduce the wavelength chirp associated with a directly modulated semiconductor laser used as the transmitter in optical communications. Additionally, optical injection-locking will be used to mitigate dispersion effects resulting through long distances of standard SMF [14-16]. A reduction in temporal dispersion can be achieved by either reducing the dispersion parameter of the communication medium, or by reducing the optical spectrum the communication signal occupies. Previous research shows that it should be possible for a laser communication system to communicate through a significant length of standard SMF under stable optical injection, while, without injection, the communication system is unable to communicate [17-18]. A direct result of this demonstration is an increase in the bit-rate-distance product, a key metric in long distance telecommunications.

A basic description of optical injection is given in Figure 1.1 whereby a narrow linewidth laser (referred to as the master laser) is injected into a second laser (referred to

as the slave laser) that is electrically pumped above threshold. The key parameters and constraints to stable injection-locking, namely the detuning frequency between the injected and injecting laser and the injection strength, will be discussed in Chapter 2. In basic terms, a stably locked Fabry—Pérot laser diode can communicate further and faster than the same, free running laser diode [19-20].

The spectral and modulation bandwidth improvements achieved through injection locking are shown in Figure 1.2. The optical power spectra show that under injection, the multi-mode Fabry–Pérot laser operates in a single transverse mode. Here, the power in the one supported mode is increased at the expense of a reduction in the optical power of all other Fabry–Pérot modes, thereby reducing detrimental impact of dispersion effects when significant lengths of SMF are involved. The modulation bandwidth (S21 response) in Figure 1.2 also shows that the maximum possible modulation rate is greatly improved over the non-injected case [21, 22].

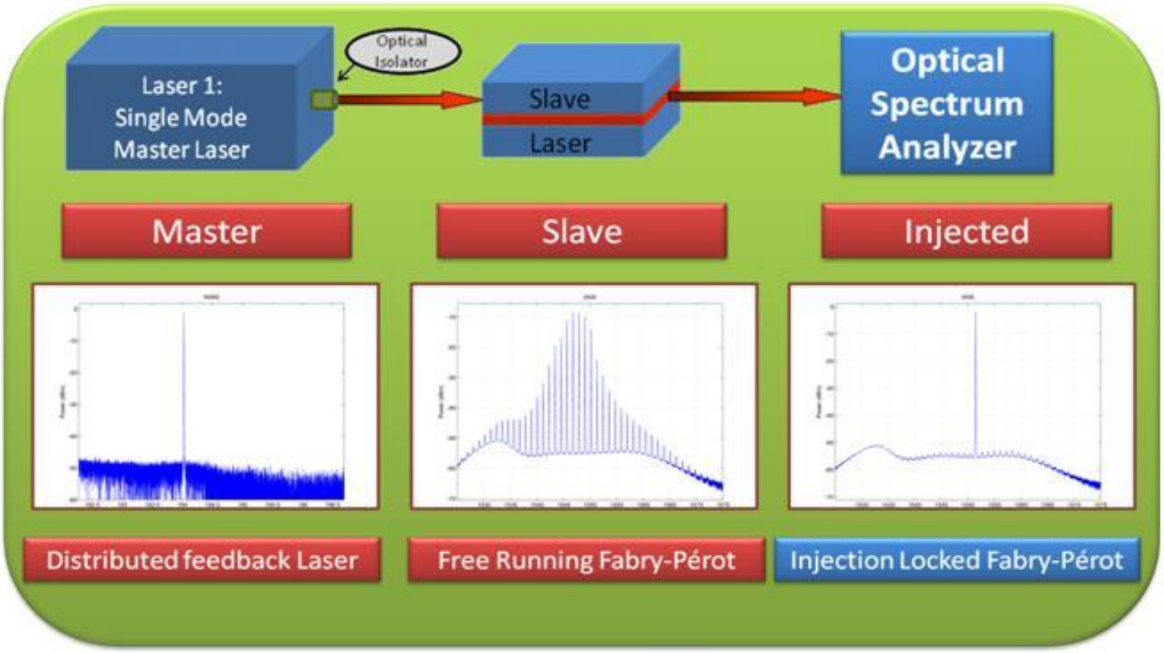

Figure 1.1. Basic description of optical injection with example stably locked optical spectra.

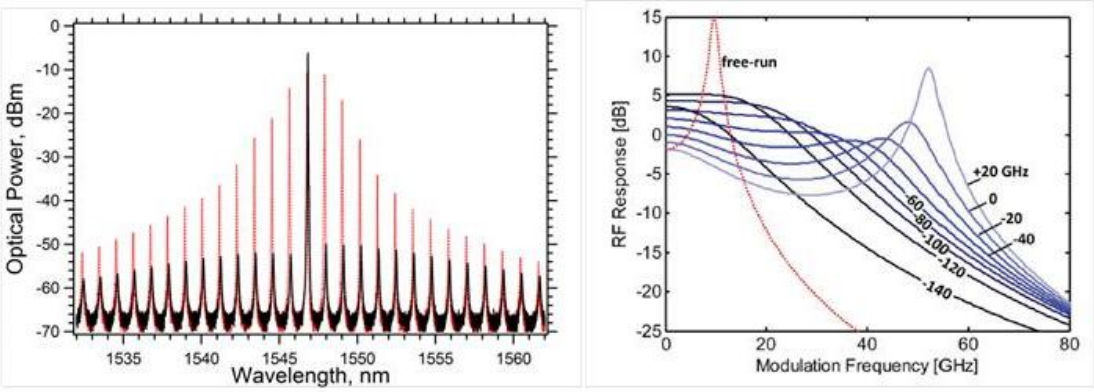

Figure 1.2: Left: shown on left in black, a Fabry-Pérot laser free running, in red, optically injected. Right: the modulation response of the laser under optical injection for varied frequency detuning conditions and the free-running case.

A second objective of this research is to demonstrate for the first time, the direct generation of consecutively-sequenced spread-spectrum (CSSS) communication symbols (compliant with IEEE 802.11a or WiFi) on a widely tunable microwave frequency exclusively using baseband electronics requiring no electrical local oscillator. This novel modulation architecture reduces the complexity of modulating a microwave frequency, effectively introducing a completely new orthogonal domain of communication into the field of guided optical communications accessible using baseband electronics. The technique on-off-shift keys (OOSK) a microwave frequency which is generated optically, utilizing the period-one dynamic of an optically injected semiconductor laser.

A semiconductor laser's period-one dynamic or un-damped relaxation oscillation frequency due to optical injection can be created using DC electronics and the dynamical state conditions can be changed using baseband electronics for frequency or amplitude

modulation of the microwave subcarrier. By selecting the detuning frequency and injection strength such that a period-one frequency is generated under constant wave (CW) injection conditions and then modulating the bias current of the slave laser, an optically generated amplitude shift keyed microwave subcarrier frequency is generated.

This important demonstration shows that the dynamical states of optical injection, particularly the period-one dynamical state, as a viable contender for radio over fiber technology. These dynamical states are orthogonal to baseband communication symbols on the same optical carrier wavelength and accessible using baseband electronics. This introduces the possibility of M-Ary communication techniques in guided optical communications without high-frequency microwave support electronics as well as a new wavelength division multiplexing technique. Baseband wavelength division multiplexed signals' spectral separation is limited by random four-wave-mixing noise which is a function of dispersion. Coherent generation of these signals reduces or even eliminates random four-wave mixing noise, allowing carrier wavelengths closer than the current standard 20 GHz separation.

1.5. Research Focus

The research investigates the suitability of optical injection for application in telecommunication. Previous research has produced parameters that describe and suggest an ability to control the complex interaction between injection-locked lasers. This research uses those parameters to modulate information onto optical carriers using baseband electronics at data-rates consistent with long-haul telecommunications. These

experiments focus on the two states of optical injection called optical injection-locked (OIL) and period-one (P1) dynamical states of optical injection to show improvements in guided optical communications through a significant length standard SMF. It shows a reduction in optical linewidth of the optical communication signal while improving modulation rate of the laser. This allows an increase in the bit-rate-distance product of a given optical communication system. It shows an ineffective communication link, using a Fabry–Pérot laser as the transmitter, can be made viable by injection locking this laser.

This research demonstrates for the first time the ability to create on-off-shift keyed microwave frequencies at data-rates appropriate for long-haul telecommunication applications using baseband electronics. This novel experiment is executed by taking advantage of the P1 dynamic of optically injected semiconductor lasers. After finding a suitable detuning frequency by injecting a slave Fabry–Pérot laser with a master laser and tuning the wavelength of each to find the P1 dynamic, the bias current of the slave laser is then modulated using relatively simple baseband electronics which changes the dynamical states of the optically injected system. This shows, for the first time, the ability to use baseband electronics to create communication symbols at data-rates competitive with telecommunications applications on a microwave subcarrier.

1.6. Investigative Questions

This research investigates the degree to which optical injection improves the telecommunication capability of directly-modulated semiconductor lasers by implementing an end-to-end telecommunication system which directly modulates the bias

current of slave laser diodes. This research demonstrates a communication link with a Fabry–Pérot laser and characterizes its modulation rate and its bit-rate-distance product. This is the first demonstration of an end-to-end communication system operating at telecommunication data-rates through representative telecommunication distances using a directly-modulated Fabry–Pérot laser diode with baseband support electronics and no optical filter. These experiments quantify the degree to which stably-locked optical injection (OIL) improves the bit-rate-distance product of a Fabry–Pérot semiconductor laser diode under these conditions. This research further investigates the suitability of the P1 dynamical state for telecommunications applications. This novel communication architecture provides direct access for a baseband communication signal to a microwave subcarrier frequency using only baseband electronics at long-haul telecommunication bit-rates.

The first step in the OIL investigation experimentally measures the direct modulation rate and distance under free-running conditions while the base-band electric signal modulates the bias-current using support electronics with cut-off frequency well below that of the free-running laser diode itself. The next step characterizes the communication link after the Fabry–Pérot laser has been optically injected. These two metrics are finally capered at a given bit error rate and signal power. The result is that the injected laser has a higher bit-rate-distance product for a given bit error ratio. This portion of the work will also investigate the relationship between wavelength detuning of the master laser, and the master laser power under stable injection-locking to the link bit error rate.

After characterizing communication capability under stably-locked optical injection, the P1 dynamic is experimentally explored. The microwave subcarrier frequency produced using the P1 dynamical state of optical injection has proven to be quite unstable, moving in the frequency domain by as much as 300MHz. The novel experimental setup used in this research proves to not only stabilize the P1 frequency, but also improves the signal-to-noise ratio (SNR) of the resulting orthogonal-to-baseband signal by over 10 dB. This signal is an optically generated on-off-shift-keyed microwave subcarrier frequency using baseband electronics. The P1 detuning frequency is found by varying the difference between the free running master and slave lasers until a suitable microwave frequency is intensity modulating the output of the slave laser. Then the bias current on the slave laser is modulated directly which changes the injection strength in the slave laser cavity enough that it operates between the P1 dynamical state and the OIL state. The frequency of the P1 dynamic is present when the bias current is high and absent when the bias current is low. The stability and tunability of the generated microwave sub-carrier frequency is analyzed, along with the degree to which the signal is orthogonal with baseband communication signals on the same optical carrier.

1.7. Methodology

A block-diagram of this experimental laboratory setup allowing optical injection is schematically depicted in Figure 1.3. Here, a distributed feedback (DFB) master laser is injected into a Fabry–Pérot slave laser in a polarization maintaining manner through an optical circulator. The master laser has a built-in optical isolator which prevents optical

feedback and mutual injection-locking between the lasers' optical cavities. The injection strength can be controlled by changing the bias current on the master laser or by using a polarization-maintaining fiber amplifier at the output of the master laser whose output is connected to port 1 of the optical circulator. The optical output of the *Fabry–Pérot* slave laser is then connected to port 2 of the optical circulator. Finally, the DC bias current from the slave laser is connected to the DC port of the bias tee while the output voltage of a signal generator is connected to the RF port of the bias tee through a short coaxial cable with SMA connectors.

The optical output from port 3 of the optical circulator is split into two paths: one path is input to an optical spectral analyzer used to observe the coupled systems' optical spectra while the second path is passed through a length of standard SMF. At the output of the length of optical fiber, the optical signal is converted into an electric signal using a high-speed photo detector, amplified, and characterized by a power spectrum analyzer, oscilloscope, or bit-error-rate detector.

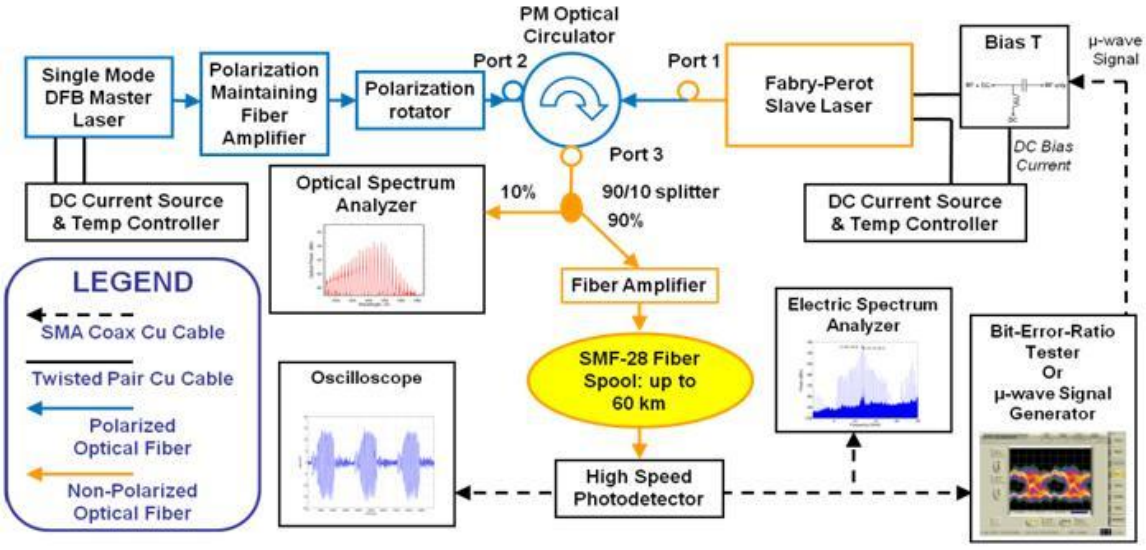

Figure 1.3: Notional setup of optical injection experiment.

1.8. Organization of Thesis

This thesis is organized as follows: Chapter 2 describes previous work published on optical injection of semiconductor lasers. It introduces the field of optical communication, then describes common telecommunication metrics, then focuses on optical injection-locking and the P1 dynamic of optical injection.

Chapter 3 discusses the novel methods of measuring the degree to which optical injection is suitable for guided optical telecommunication applications. It starts with a description of the laboratory setup allowing direct modulation of high-frequency communication symbols onto an optical carrier and microwave subcarrier using only low-pass baseband electronics. Then it describes the process through which the bit-rate-distance product is measured for an optimum bit-error ratio through different lengths of fiber at different modulation rates comparable to telecommunication applications.

Finally, chapter 3 discusses the testing and measuring methods to determine the suitability of the P1 dynamical state in telecommunication and radio-over-fiber applications. This test method effectively provides a direct method of accessing this orthogonal domain in guided optical communications using only baseband electronics.

In chapter 4, the laboratory results are presented and analyzed. It quantifies the degree to which stably-locked optical injection improves the bit-rate-distance product of a directly-modulated Fabry–Pérot laser diode at data-rates appropriate for optical communications (57 fold). Then it describes the method and effectiveness of directly accessing the orthogonal microwave frequencies offered by the un-damped relaxation oscillation frequency of the slave laser. It explores the degree to which the P1 frequency can be stabilized resulting in signal-to-noise ratio improvement (over 10dB) by selecting appropriate baseband modulation rates. Furthermore, it demonstrates, for the first time, data-rates appropriate for telecommunication applications using the large-signal modulation of the P1 dynamical state.

Chapter 5 then briefly summarizes the findings and proposes future research which should be undertaken to further explore the practicality of this approach to improve system performance. This research includes characterizing the dynamics of simultaneously locking multiple slave laser diodes, demonstrating the ability to use the P1 dynamical state for frequency division multiple access within the same ITU band. Another research area includes all-optical microwave mixing using the P1 dynamical state of multiple lasers allowing the optical generation of microwave frequencies below the relaxation oscillation fluency using dually-locked Fabry–Pérot laser diodes. Potential

all-optical P1 frequency detection is proposed using either the optical-mixing properties of optical injection or the nonlinear amplification of optical signals by placing a Fabry–Pérot laser nearly into stably-locked optical injection conditions.

Appendix A provides information on baseband modulation and demodulation techniques. It shows the results of several simulations showing both the frequency and time-domain responses of different modulation techniques, focusing mainly on the Unipolar Rectangular PAM used in the laboratory experiments. Finally, Appendix A introduces the analytical tool called the eye diagram and eye analyzer. This qualitative tool is useful, but limited since digital sampling rates of communication symbols are as much as two-orders of magnitude slower than the communication data-rate.

2. Literature Review

This chapter introduces the metrics and tools used to evaluate the optical communication system created for this research. This chapter also summarizes the pertinent research accomplished in the field of optical communications and optically injected semiconductor lasers. It starts by introducing an optical communication link's general framework and methods used to evaluate a communications link. Next, detrimental optical dispersion effects on long-haul optical communications are discussed, followed by an overview of various types of semiconductor lasers implemented as transmitters.

It also provides an overview of optical injection and discusses the effects optical injection has on directly modulated semiconductor lasers. It discusses the stably-locked optical injection state and the benefits of injection locking. Finally it presents the P1 dynamical state of optical injection, and emphasizes the two key parameters used to control the frequency and modulation depth of the P1 dynamical state.

2.1. Optical Communication and Semiconductor Laser Introduction

A graphical illustration of an optical communication scheme based on a directly modulated semiconductor laser is given in Figure 2.1. In Figure 2.1, a Bit Error Ratio Tester (BERT) producing a baseband binary rectangular passive amplitude modulated (PAM) electrical signal is used to modulate a laser diode's bias current through a bias tee. The resultant intensity modulated optical signal emitted by the laser diode can be coupled into a significant length of SMF. A distant photo detector can receive and convert the

intensity modulated photon stream into a usable microwave electric signal. The signal from the photo-detector can be placed into an electric microwave baseband receiver or input port of the BERT. This section discusses the features and limitations of this optical signal.

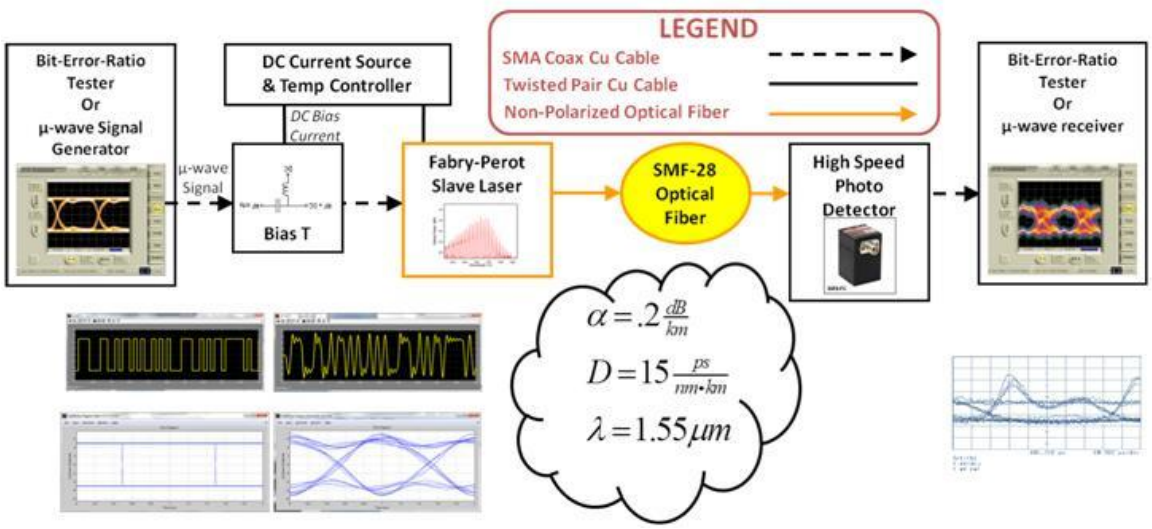

Figure 2.1: Cartoon of a directly modulated optical communications system. A description of the pulse modulation scheme can be found in Appendix A.

Directly modulating a laser diode, as described in Figure 2.1, is one of the most efficient techniques for gigabit and higher communication rates, because of the compact nature and comparatively low fabrication cost compared to external modulation schemes. The relatively simple task of modifying the bias level of the laser diode's bias current above the laser-action threshold allows for both simpler and higher bandwidth modulation electronics which, in turn, requires significantly lower modulation energy per bit. One drawback, however, is that the output wavelength of the laser depends on the applied current since the semiconductor's refractive index depends on carrier density

[29]. This relationship between modulated current and wavelength shift is referred to as *wavelength chirp*, and causes spectral distortion of the optical gain of the laser. This additional spectral breadth results in detrimental effects when the optical signal is passed through dispersive media such as long SMF.

External modulation schemes are more common in commercial optical communications systems. External modulation does not experience wavelength chirp and currently holds the highest bit-rate-distance product at the cost of system complexity and cost. A comparison between direct and external modulation schemes is given in Figure 2.2. The advantage of external modulation is that separate devices are used to generate the light and to modulate it. This allows a more spectrally pure laser source and avoids the detrimental impact associated with wavelength chirp. External modulation also allows the emitter and modulator to be individually optimized for overall optimization of system performance.

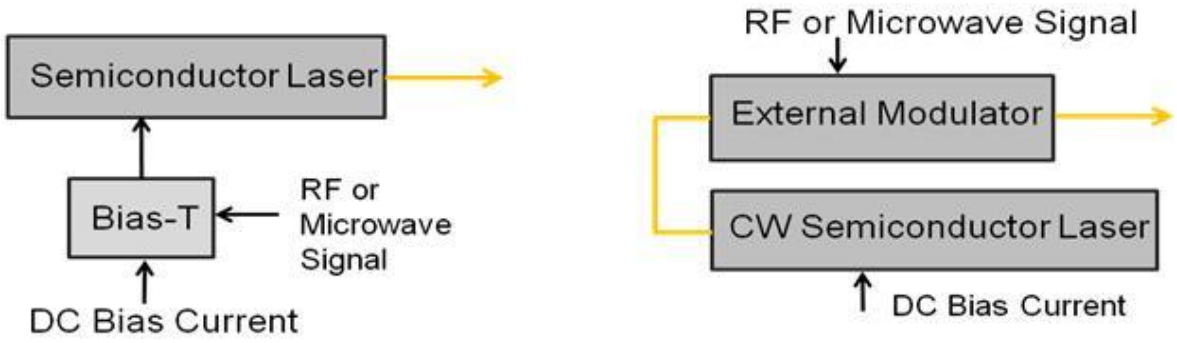

Figure 2.2: Block diagram comparing direct modulation to external modulation.

Since external modulation does not require a laser diode with high-speed modulation response to changes in the laser diode's bias current, the typical trade-off

between modulation response and spectral purity is avoided. As a result, semiconductor lasers for externally modulated architectures are designed to have optimized linewidth, or high-Q, properties, and ignore the direct-modulation response.

Semiconductor lasers used in externally modulated architectures typically have extremely narrow optical linewidths, in the range of 80-200 kHz. Indeed, a literature review shows that a remarkable full-width half max linewidth of 780Hz in a semiconductor laser diode has recently been achieved by using microsphere resonators [45]. In laser cavities delivering extremely narrow linewidths, the photon lifetime is too long for **direct** modulation to be practical, as there will not be enough time between communication symbols for the light intensity to change. Ironically, the disadvantage of externally modulated communications systems is the same as its advantage examined from a contradicting viewpoint: there is added system cost and complexity associated with having separate components for light generation and modulation.

Semiconductor lasers, regardless of the method by which they are modulated, have an inherent optical linewidth. This linewidth is indicative of the notion that laser devices do not generate a delta-function-like irradiance at a single wavelength. Indeed a more realistic output profile for a laser is a Lorentzian-like peak encompassing a range of wavelengths. This spectral shape is best described by the band structure of the semiconductor laser's active region and the laser's cavity design. This concept is described in Figure 2.3 for a bulk semiconductor material [24]; increased degrees of carrier confinement achieved using quantum-well and quantum-dot type active region lasers show improved levels of optical linewidths [30,31].

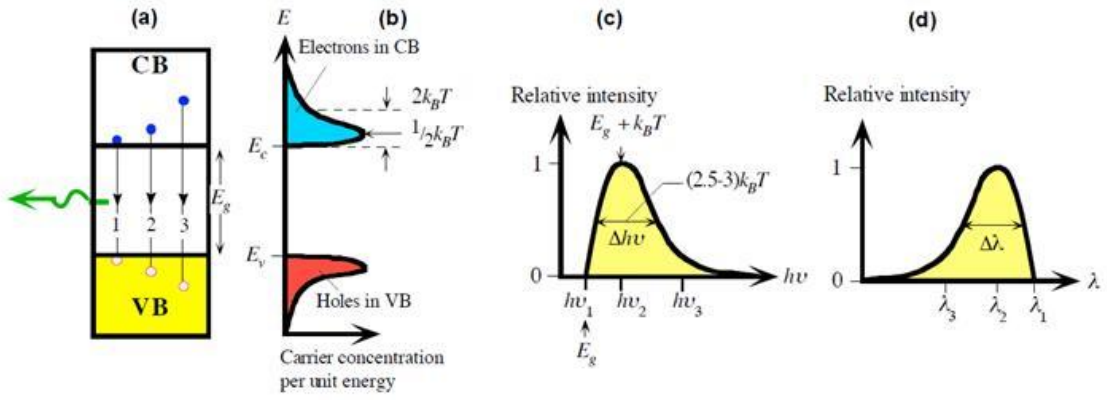

Figure 2.3: (a) Energy band diagram with possible recombination paths. (b) Energy distribution of electrons in the conduction band (CB) and holes in the valence band (VB). The highest electron concentration is (1/2)k_BT above the conduction band edge, E_c. (c) The relative light intensity as a function of photon energy based on (b). (d) Relative intensity as a function of wavelength in the output spectrum based on (b) and (c) [24].

The non-zero linewidth of the carrier laser combined with its chirp results in communication limiting effects over lengths of optical fiber due to the relationship between the index of refraction of the optical fiber and the wavelength of light coupled into the fiber. The group propagation velocity, V_g, of guided light through the fiber core depends on the index of refraction of the core, which in turn is a function of wavelength, making the group velocity a function of wavelength. As a consequence, the group velocity is, in reality, a function of wavelength as shown pictorially in the top sketch of Figure 2.4, $V_g(\lambda_1) \neq V_g(\lambda_2)$. This type of dispersion is called material dispersion and is illustrated in Figure 2.4 and Figure 2.5. Figure 2.4 shows how a very short light pulse with optical spectrum ranging from λ_1 to λ_2 at time zero, decreases in intensity, and increases in time duration as it travels through a dispersive medium for a given

transmission time τ, because of the wavelength dependence of the fiber-optic material's index of refraction.

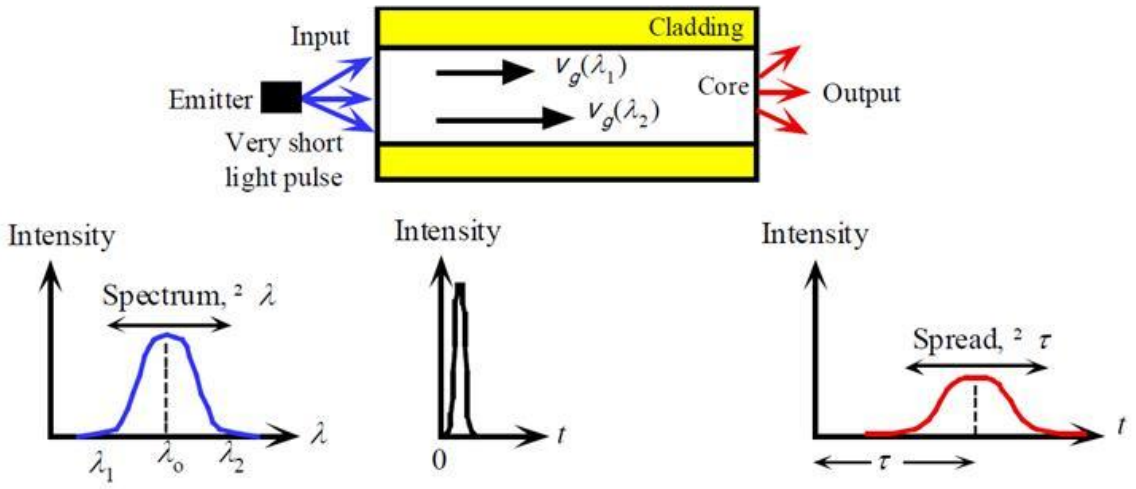

Figure 2.4. Illustration of the spreading of the optical pulse as a result of material dispersion [24].

Figure 2.5 illustrates that the pulse rate or bit rate modulated onto the semiconductor laser, represented by 1/T, will be dispersion limited for a given distance of optical fiber depending on the dispersion coefficient of the fiber at the carrier's wavelength, (λ_0) and the spectral width of the signal $\Delta\lambda$. To quantify the pulse spreading, $\Delta\tau$, the dependency of group velocity V_g on wavelength through the index of refraction's (n_g) dependence on wavelength λ_0 needs to be evaluated as well as the spectrum of the light source emitted. $\Delta\tau$ increases with fiber length because slower moving photons fall further behind the faster ones over longer distances. As a result, dispersion is normally expressed as a spread per unit length and is given by Equation(1).

$$\frac{\Delta\tau}{L} = |D_m|\Delta\lambda \tag{1}$$

In Equation (1) D_m is called the material dispersion coefficient and is approximated as the second derivative of the index of refraction with respect to free-space wavelength λ.

$$D_m \approx -\frac{\lambda}{c}\left(\frac{d^2 n}{d\lambda^2}\right) \tag{2}$$

Though D_m can be positive or negative, the width of the received pulse due to dispersion, ($\Delta\tau$), is always positive, given the absolute value of D_m is in Equation(1). Popular SMF has dispersion coefficients ranging from -20 to 25 (ps km^{-1} nm^{-1}) for center wavelengths between 1.1μm and 1.6μm, crossing the zero-dispersion value at approximately 1.3μm.

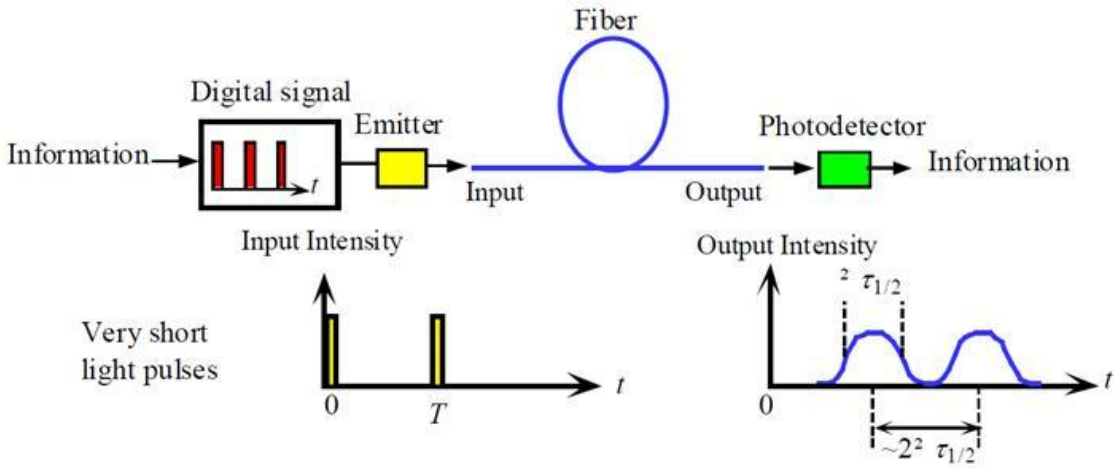

Figure 2.5. Demonstration of the effect of dispersion on a train of optical pulses [24].

For a fixed length of dispersive fiber, L, which causes a light pulse to have a full-width-half-max (FWHM) power spread, $\Delta\tau_{1/2}$, there exists a maximum pulse-rate or

minimum T shown in Figure 2.5, at which the light pulses blur into each other so much that the pulses are indecipherable thus placing a limit on the pulse-rate capacity for a given length of fiber channel. For binary (M=2), return-to-zero type PAM encoded signals, the maximum bit rate, B, is intuitively the rate at which the time between pulses, T, is equal to 2 FWHM spread times, after that point the inter-symbol interference will degrade the performance of the receiver [24]. This relationship is described in Equation(3).

$$B_{RZ} \approx \frac{\log_2(M)}{2\Delta\tau_{1/2}} \tag{3}$$

Generally, non-return-to-zero coding schemes, such as the rectangular PAM simulated for the generation of Figure 6.10 have twice the bit-rate capacity for any given length of optical fiber compared to similarly shaped return-to-zero coding schemes. Therefore, in order to correctly compare the communication capability of a given semiconductor laser, effects of modulation schemes and long distance channel effects must also be taken into account.

The pulse shape, both in terms of intensity versus time and intensity versus wavelength, also affects the total channel bit-rate capacity. As shown in Figure 2.3, real-world light emitters have a statistical distribution that is not perfectly flat, possibly allowing the intensity of slower moving photons to be lower in magnitude than the intensity of fast moving photons from the following pulse. Pulse shaping leads to an output temporal pulse shape (intensity versus time) that may allow more pulse-time

overlap than described in Equation (3). This in turn could allow a higher bit-rate capacity for a given channel at the acceptable bit error ratio.

With this understanding, it is less important to know the full-width-half-max power but instead the relationship between the bit-rate capacity, B, and the root-mean-square dispersion, represented by σ. For a reference, taking a Gaussian shape into account, the bit rate distance product of a fixed length of fiber is approximately 18% higher. With this in mind, Equation (3), with M=2 (binary) becomes:

$$B \approx \frac{.25}{\sigma} \tag{4}$$

For Gaussian pulses, $\sigma=0.425\ \Delta\tau_{1/2}$ for the 18% increase in bit-rate capacity expressed above. Since the dispersion limit increases with fiber length and the range of source wavelengths, $\Delta\lambda_{1/2}$, it is customary to specify the product of the bit-rate and the length at the operating wavelength for a given emitter. So, if D_{ch} is the chromatic dispersion coefficient, then the dispersion of the light pulse is $LD_{ch}\sigma_{\lambda}$. That makes the bit-rate-distance product, BL, equal to Equation (5).

$$BL \approx \frac{.25L}{\sigma} = \frac{.25}{|D_{ch}|\sigma_{\lambda}} \tag{5}$$

The BL of a fiber optic communication system is a function of both the dispersion coefficient of the channel, D_{ch}, and of the chromatic content of the optical emitter, or laser diode. For this research, the objective of which is to increase the communication capability of a Fabry–Pérot semiconductor laser, the channel characteristics are set by the use of Corning's SMF-28e+ standard single-mode optical fiber with a dispersion coefficient of approximately 17.4 ($ps \cdot nm^{-1}\ km^{-1}$) at 1550 nm.

The linewidth of a semiconductor laser may be understood by looking at the supported band-gap energy between electrons in the conduction band and holes in the valence band of the semiconductor material as shown in Figure 2.3. The band-gap energy distribution directly affects the output wavelength of the laser, as described in Equation (6). In Equation (6), the wavelength is equal to Plank's constant, h, times the speed of light, c, divided by the band-gap energy times the effective index of refraction of the laser gain medium. The wavelength distribution of the output is more appropriately described by the carrier distribution in both the conduction and valance bands, depicted in Figure 2.3(b). Here, the case for a bulk semiconductor active region is shown, where the carrier distribution in both the conduction and valence bands can be controlled through the use of carrier confinement, as achieved using quantum-well and quantum-dot type active regions (the quantum dynamics associated with both are beyond the scope of this work).

$$E_g = E_c - E_v = h\nu = \frac{hc}{n\lambda} \qquad E_g = \frac{1.24}{\lambda} \tag{6}$$

When a bias current above the laser's threshold, shown in Figure 2.6, is applied through the active region of the semiconductor laser, illustrated in Figure 2.7, many electron-hole pairs are created and spontaneously recombine. This electron-hole recombination induces packets of electromagnetic radiation (photons) with random direction, random phase, and energy equal to the band-gap as, described by Equation (6).

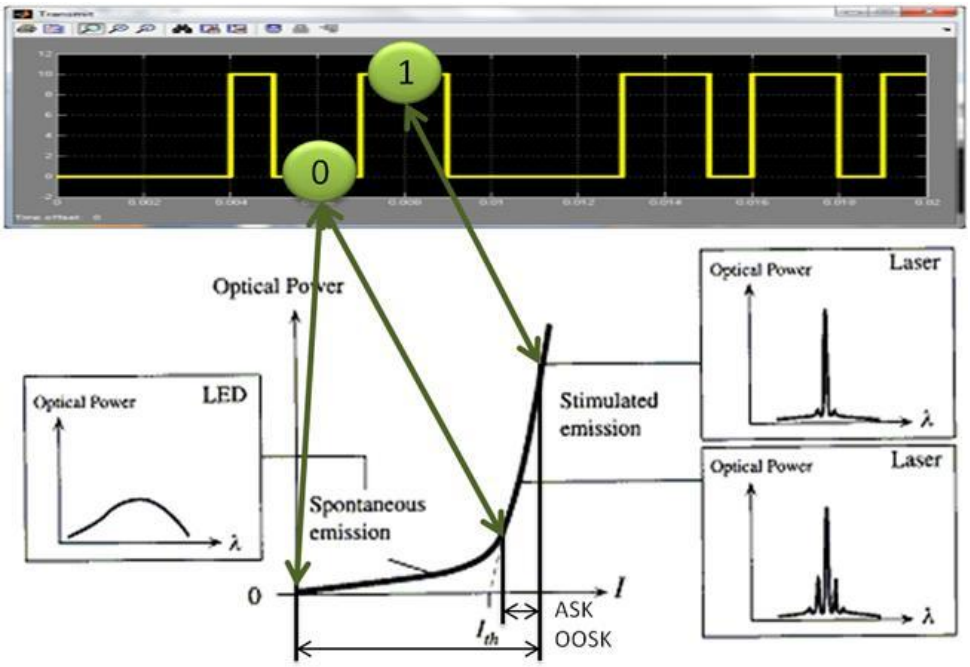

Figure 2.6: Driving the laser diode directly with the PAM communication signal to On-Off-Shift Key (OOSK) the laser diode requires significantly more modulating current then small-signal Amplitude Shift Keying (ASK) of the laser diode through a bias tee [24].

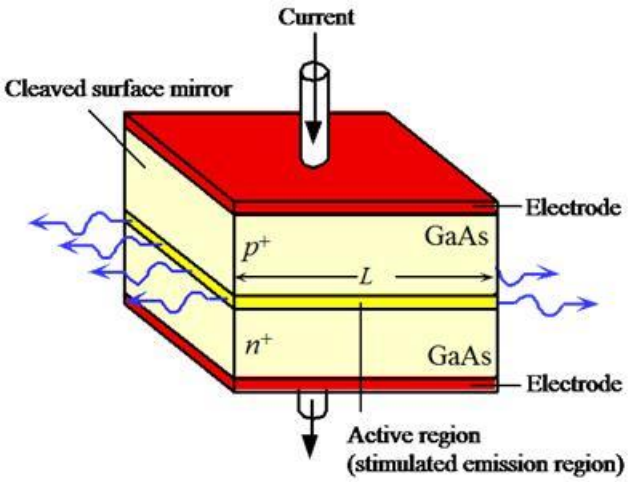

Figure 2.7: schematic of a Fabry–Pérot homojunction laser diode [24].

Initially, as the laser transitions from spontaneous emission to stimulated emission states, most of these randomly directed photons are simply absorbed by the bulk material surrounding the active region. The small remaining portion of photons have direction, phase, frequency and polarization supported by the Fabry-Pérot laser cavity, reflect back, and stimulate emission in the gain region. These stimulated photons have the same direction, perpendicular to the cleaved surfaces, and the same phase, adding to the magnitude of the standing electric and magnetic-fields building inside the Fabry–Pérot laser cavity.

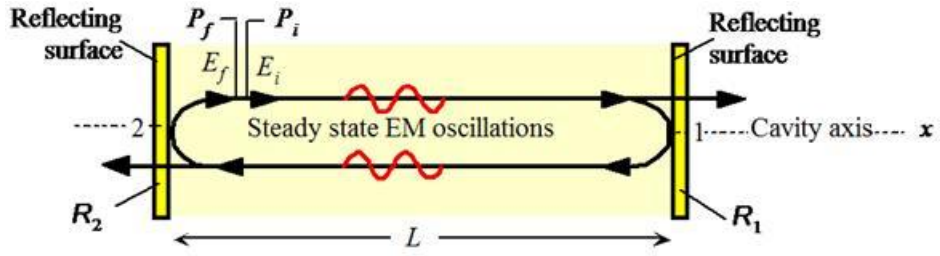

Figure 2.8: Illustration of an optical cavity resonator [24].

While traveling through the gain medium, optical power is reduced by the reflectance of each facet, absorption and scattering while propagating through the medium. In order for the optical cavity to begin to resonate, these losses, γ, have to be replaced with stimulated emission, or effective optical gain, g. Note that γ represents all losses in the cavity and on its walls except the light that is transmitted through the facets. Therefore, assuming an initial power P_i, after a single round trip path of 2L, shown in Figure 2.8, the final power P_f of the electromagnetic radiation is given by equation (7).

$$P_f = P_i R_1 R_2 e^{g(2L)} e^{-\gamma(2L)} \tag{7}$$

The simple observation that coherent optical power will not build up unless P_f is at least equal to P_i allows an expression for the threshold optical gain, which will in turn allow the calculation of threshold current, beneath which, the optical output of the laser is much the same as an LED, and above which, the light is coherent, as a laser diode. That threshold gain expression is given by equation (8).

$$g_{th} = \gamma + \frac{1}{2L}\ln\left(\frac{1}{R_1 R_2}\right) \tag{8}$$

If a laser bias current is changed quickly and crosses the threshold current, I_{th}, the optical output can overshoot the steady state value. This overshoot, called relaxation oscillation frequency is common in optical communication systems and can be seen in the eye-diagram in Figure 6.24 (right) found in Appendix A. Optical telecommunications systems often compensate for predictable overshoot by incorporating it into the communication symbol, thus making pulse position modulation more common in optical communications.

Having a high enough bias current to exceed the gain condition in equation (8) is a necessary condition for lasing. Equally important is that the electric-field, after one full round trip (2L) through the gain medium, be in phase with the electric-field it started with, $\Delta\phi_{2L} = m(2\pi)$. If the initial electric-field, E_i, is not in phase with the final electric-field, E_f, the fields will add destructively. This reduces the number of stimulated photons of that wavelength, eventually substituted with photons whose frequency completes an integer number of cycles, m, in one round-trip. So, if $k = 2\pi/\lambda$ is the free-space

wavelength and k_m is the special subset of k which satisfies equation (8), photons are amplified by the Fabry–Pérot resonator, leading to the usual mode condition:

$$m\left(\frac{\lambda_m}{2n}\right) = L \tag{9}$$

These longitudinal axial modes are controlled primarily by the length of the optical cavity, L, and the effective index of refraction of the gain medium, n. The resulting optical spectrum from a constant wave Fabry–Pérot laser diode looks roughly like the line-shape function, derived from the energy versus density of states function of a given semiconductor material, convolved with a comb function, who's peak locations correspond to the wavelengths which satisfy equation (9). This idea is graphically represented in the cartoon in Figure 2.9.

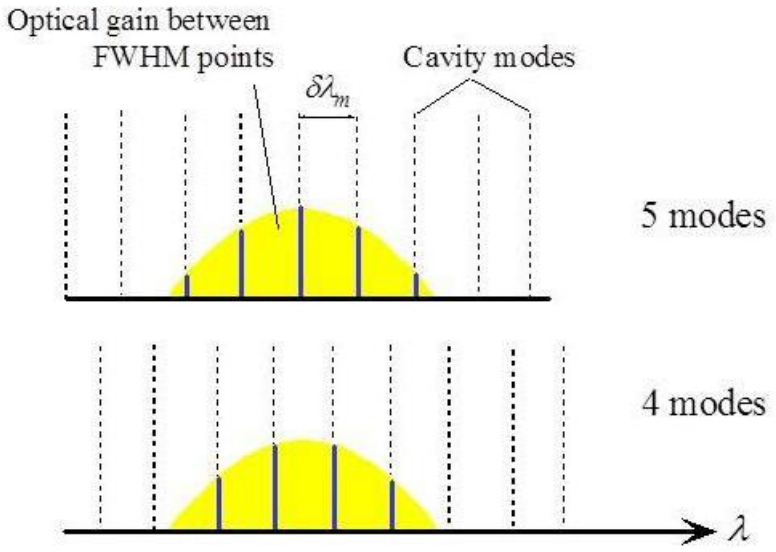

Figure 2.9: Cartoon showing optical gain convolved with cavity mode spectra. By adjusting the center frequency of a given optical gain, the number of supported modes can change [24]. Additionally, the relative intensity of each supported mode can change. Only

Since the index of refraction is partially a function of carrier density, the wavelength of each supported longitudinal axial mode shifts with respect to laser diode bias current. Furthermore, the index of refraction and therefore optical cavity length is a function of temperature, both the position of each cavity mode as well as the wavelength difference, $\delta\gamma_m$, also changes with respect to temperature. Another important factor is the non-flat nature of the optical gain envelope, which causes the relative intensity of each Fabry-Pérot mode to change with respect to temperature. These features of Fabry-Pérot laser diodes make temperature control a key issue in optical injection and optical communications.

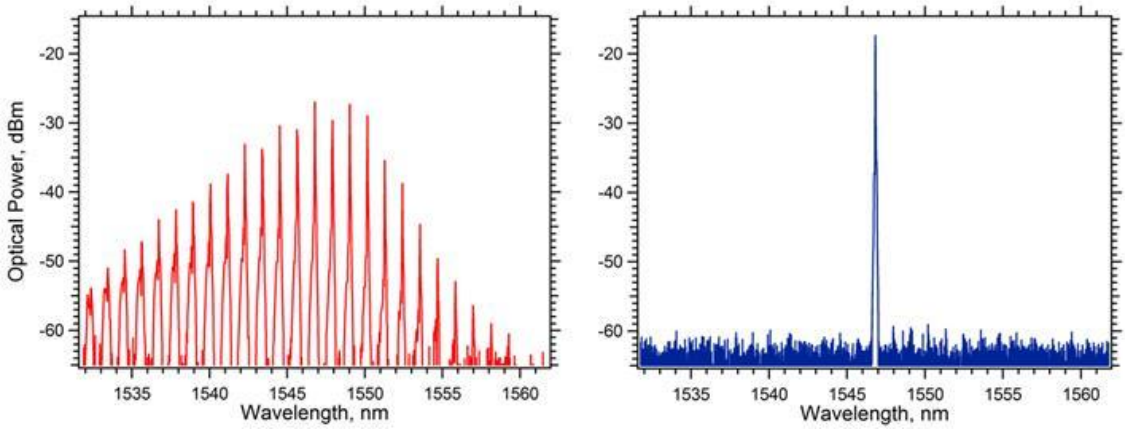

Figure 2.10: Left, an example optical spectrum of a laser diode supporting multiple axial longitudinal modes compared to the same laser diode, on right, operating with a single supported longitudinal axial mode.

Although Figure 2.8 and Figure 2.9 illustrate the concept of a multi-mode Fabry-Pérot semiconductor laser, more sophisticated laser designs are able to produce single-mode devices. The most commonly used single-mode device design is referred to as a

distributed feedback (DFB) laser. In a DFB laser design, rather than using the two-mirror scheme of Fabry–Pérot laser, a grating throughout the device is used as the wavelength selective element. Figure 2.10 shows the difference in multi-mode versus single-mode operation of Fabry–Pérot and DFB lasers, respectively.

Dispersion effects in modern optical communication schemes are minimized by choosing operation wavelengths that result in a minimal amount of optical dispersion. The ideal, near-zero dispersion wavelength for standard single-mode fiber occurs at 1310 nm. However, wavelength division multiplexed channels require that a number of carrier wavelengths be outside the minimally dispersive carrier wavelength region. Furthermore, phase noise due to four-wave-mixing in wavelength division multiplexed systems increases as the carrier wavelengths of each channel are placed closer to one-another.

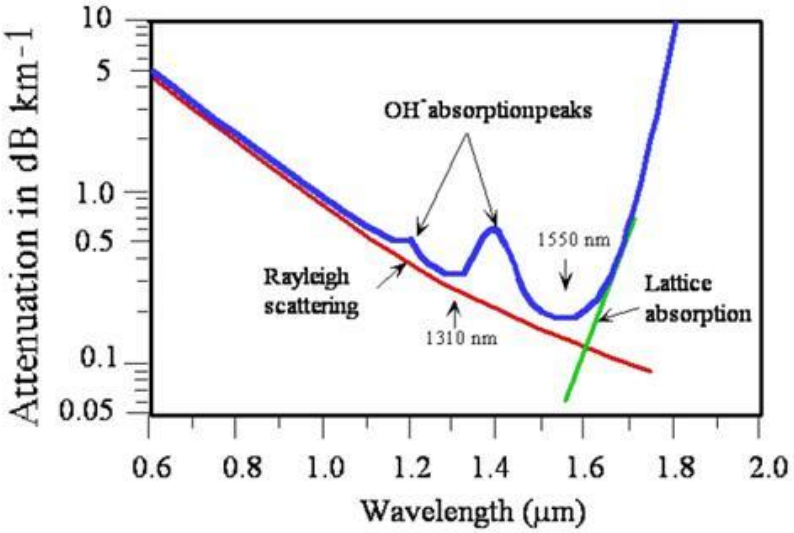

Figure 2.11. Illustration of a typical attenuation vs. wavelength characteristics of a silica based optical fiber like the standard single-mode fiber used in this research showing the two most commonly used carrier wavelengths of 1310nm and 1550nm [24].

Additional considerations, when choosing an operational wavelength, are the noise floor and attenuation as a function of wavelength [24]. With respect to loss, the ideal operation wavelength occurs at 1550 nm, which is the wavelength of focus in this work. Figure 2.11 illustrates the attenuation as a function of wavelength.

2.2. Channel Capacity

Single-mode Fiber has a very large low-loss bandwidth. Moreover, Corning Inc., a manufacturer of high-quality SMF, reports less than 0.2 dB per km attenuation between the optical wavelengths of 1525 and 1575 nm. As shown in Equation (10) and (11), the bandwidth available across this wavelength range equates to 6.5 THz, with the entire band experiencing less than 20 dB per 100 km.

$$f = \frac{c}{\lambda}$$
$$f_{1525nm} - f_{1575nm} \tag{10}$$

$$\frac{2.99E8}{1.525E-6} - \frac{2.99E8}{1.575E-6} \rightarrow 196.59THz - 190.34TH = 6.5THz \tag{11}$$

For comparison, LMR™, a manufacturer of copper and aluminum coaxial cables for used to drive microwave antennas, advertizes their lowest attenuation cable to be 6.65 mm diameter copper tube which has 4.9 dB attenuation per 100 ft. For comparable bandwidth distance per dB attenuation, one would need 3,650 copper tubes from LMR™ to equal the performance of a single optical fiber from Corning, and this comparison only included a narrow transmission window around the fiber's lowest attenuation. In fact, Corning publishes that its ultra low-loss single-mode fiber has less than 0.31 dB/km

across the entire band from 1260nm to 1625nm, a bandwidth of 53.44 THz, which explains why optical fiber is the transportation channel of choice in 'long-haul' telecommunications.

With such a high bandwidth, the optical fiber itself is seldom limits the bandwidth in any optical communications system. The maximum modulation bandwidth of directly modulated semiconductor lasers is more appropriately given by the laser diode's modulation response. This modulation response is a result of the complex internal dynamics of translating changes in bias current to changes in optical output. Similarly, the bandwidth limiting device in an external modulated optical communication system is typically the external modulation device itself, also not the SMF.

To measure the modulation response of a system, a frequency sweep of a small-signal applied to the input of the system is performed while measuring the output signal. That output response, divided by the input response, is then plotted with respect to frequency in a plot commonly referred to as an S21 curve. An ideal system will have infinite bandwidth and a perfectly flat and smooth modulation response. A real system, however, will look more like the example S21 plot shown in Figure 2.12. Notice how even the best case modulation response illustrated has more than a 3dB drop between its peak modulation response and the response at half its peak frequency.

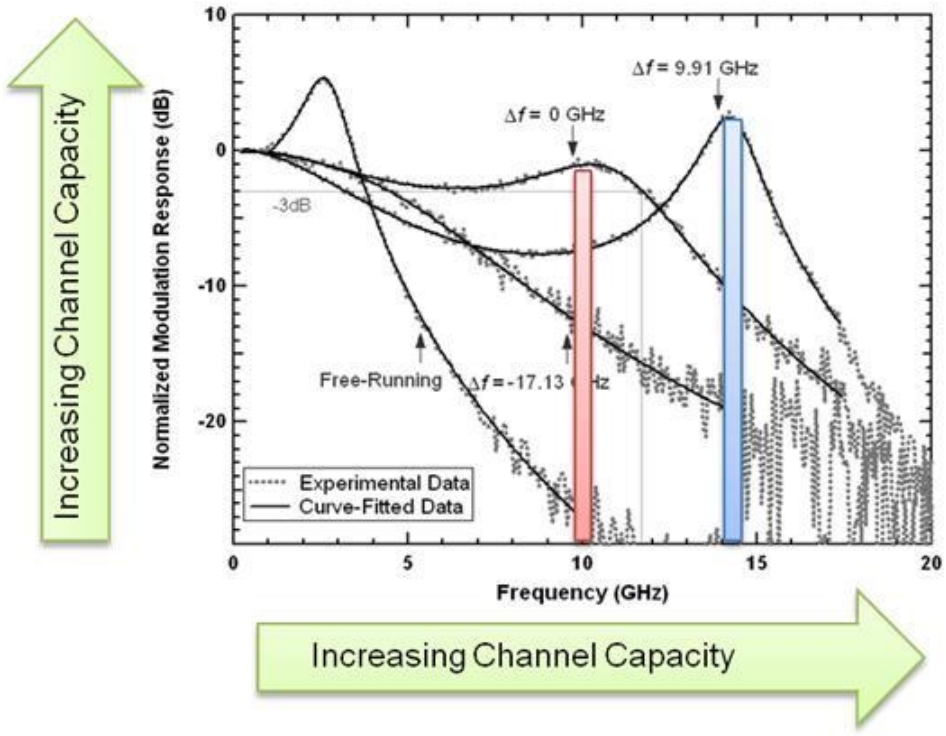

Figure 2.12: Significantly enhanced modulation bandwidth of Fabry–Pérot laser diodes has been observed under injection-locked conditions [33]. Generically, increasing the modulation bandwidth increases channel capacity for a given modulation response.

The work performed in this thesis is motivated by previous studies that have shown that stably-locked lasers (both single-mode DFB and multi-mode Fabry–Pérot) have significantly increased modulation responses over the same lasers under free-running conditions. An example of a normal modulation response of a semiconductor laser is given in Figure 2.12, labeled as free-running [33]. Figure 2.12 also illustrates the modulation response of a semiconductor laser under stable injection locking, whereby the maximum modulation frequency is roughly four times that of the free-running laser; this equates to being able to pass approximately 4X the data using the optically-injected

device versus the same device without optical injection. Stated in another fashion, the optically injection-locked device can replace up to 4 separate laser transmitters.

The following section discusses the impact of the finite slope, and shape modulation response curve's shape on the communication system's operation.

2.3. Non-Flat S21 response

As shown in Figure 2.12, the direct modulation response of a Fabry–Pérot laser is not flat over the pass band. Since rectangular PAM modulation produces very high-frequency spectral components (see Figure 6.14 in Appendix A), a number of frequencies are modulated with higher gain than others. This causes distortion of the baseband signal produced by common bit error ratio testers (BERTs) including the Synthesis BERTScope used in this research. The effect this will have on a random bit sequence is that high frequency bit sequences such as [0101010] communicated at bit rates equal to the peak modulation frequency could cause an eye diagram that looks clear, open, and tightly overlaid while mid frequency bit sequences such as [10011001] will not overlay well. For the [10011001] bit sequence case, the first to second bit transition will respond well, but when the BERT paints the third bit (second zero) the system will have settled up and a trace will appear above the first because of the channel's complex impedance shown as decreased magnitude in the S21 curve. Figure 2.13 qualitatively shows how an optical communication link can be improved by trading bandwidth for spectral predictability since spectral components can more easily be chosen with predictable communication symbols.

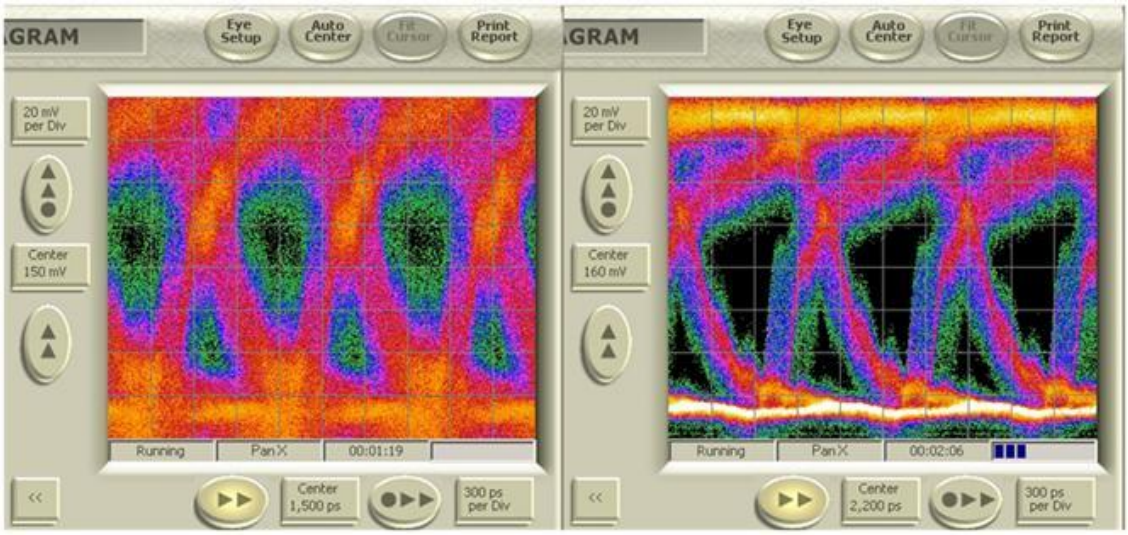

Figure 2.13: Two example eye diagrams, both at the same data rate. Left, a PRBS-7 sequence and on the right a user-defined sequence with the same spectral components as differential Manchester line coding.

2.4. Optical Injection

A great amount of research has been devoted to the modulation enhancement capabilities of semiconductor lasers and their associated support electronics. Optical injection provides many improvements and in specific cases, allows all-optical generation of microwave frequencies, removing the limitations inherent in modulation electronics. Enhancing these parameters with optical injection makes direct-modulation of semiconductor lasers a more attractive architectural choice (as opposed to external modulation) for optical transmitters. Table 1 summarizes various fundamental limits of directly modulated semiconductor lasers and how optical injection-locking (OIL) has been shown to improve these limitations.

Table 1: List of limitations of directly modulated lasers and improvements from optical injection-locking [22].

Fundamental Limits		Benefits from OIL
Laser	Optical Dispersion-Signal Linewidth	Linewidth enhancement
	Nonlinear electron-photon coupling	Reduced nonlinearities
	Amplified Spontaneous Emission Noise	Reduced Relative Intensity Noise (RIN)
	Relaxation Oscillation Frequency	Enhanced Relaxation Oscillation Frequency
	Wavelength chirp (non-zero α parameter)	Reduced chirp
	Mode Partition Noise (Fabry–Pérot laser)	Single-mode with Side-Mode Suppression
Link	Differential quantum efficiency <1	Increased link gain
	Double-Sideband Modulation	Near-single-sideband modulation

2.5. Optical Injection Configurations

There are two possible configurations to accomplish the basic OIL objective of injecting light from a master laser into a slave laser cavity, and both are shown in Figure 2.14. In transmission style optical injection (a) light from a master laser is coupled to a slave laser facet through an optical isolator which prevents mutual injection-locking. The injected output is then taken from the other facet of the slave laser. Transmission style injection requires two optical coupling systems with the slave laser [22]. The second possible configuration, the reflection style, is shown in Figure 2.14 (b) and uses the same type of setup adopted in this research. In reflection style optical injection, a three-port device called an optical circulator is used in place of an optical isolator to prevent mutual locking and only one optical coupling system is required for the slave laser.

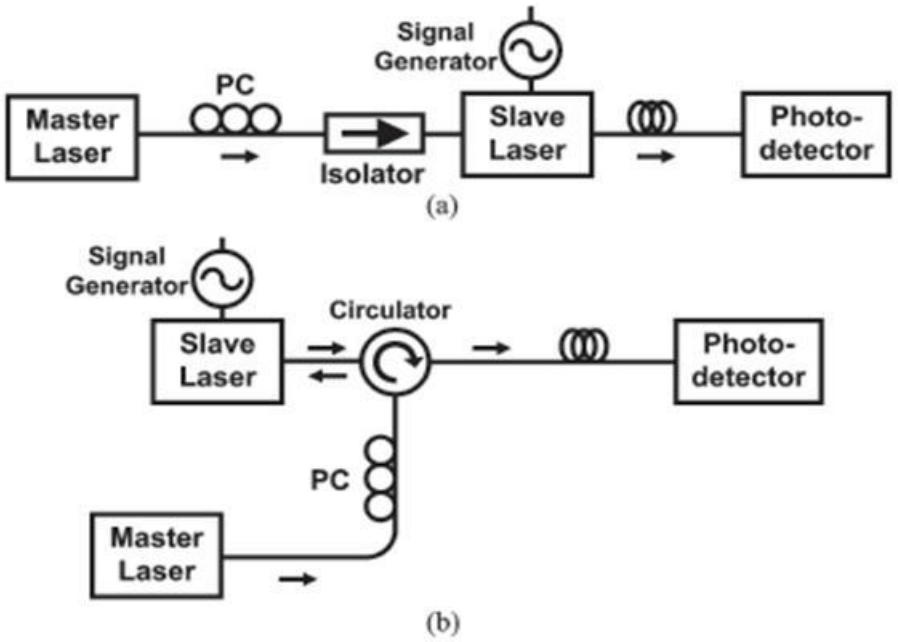

Figure 2.14: The basic optical injection schematic showing transmission style (a) and reflection style (b) optical injection setups [22].

2.6. Optical Injection Parameters

The master laser's center wavelength and optical power are the two major parameters to consider when directly modulating an injection-locked laser compared to a free-running laser. The master laser power conveys into the injection strength parameter, which is given by [33]

$$\eta_{ratio} = \frac{(1-R)}{\sqrt{R}} \sqrt{\frac{P_{master}}{P_{slave}}} = \mathrm{k_c} \frac{\mathrm{A_{inj}}}{\mathrm{A_o}} \tag{12}$$

While the wavelength detuning factor or detuning frequency given by [33]

$$2\pi\Delta\omega = \Delta f = f_{master} - f_{slave} \tag{13}$$

For constant wave applications, the reflectivity of the slave laser is not changed nor is the injection power. Therefore, the injection ratio can be reported as a constant, k_c, called the coupling coefficient, times the ratio of injected field amplitude divided by the slave's field amplitude. The optical power and field magnitude are directly related ($P \propto A^2$). Therefore, the injection ratio in this research is measured externally as the ratio of master optical power divided by slave optical power and is usually reported in units of dB, or $(10\log_{10}(P_{master} / P_{slave}))$ [33].

The wavelength detuning frequency is also a very important metric in optical injection and is usually reported in terms of frequency (GHz), or wavelength (pm). The wavelength detuning frequency is measured as the distance from the center frequency of the master laser minus the center frequency of the nearest supported longitudinal mode of the slave laser. The direct modulation dynamics of the slave laser are not symmetrical, and therefore are affected by the sign as well as the magnitude of the detuning frequency. Negative detuning frequencies lead to stably locked operation under strong optical injection while positive detuning frequencies tend to lead to more complex dynamical operation like the P1 dynamical state [33].

For a rough conversion estimate, -10 pm change in wavelength at 1550 nm is approximately +1.25 GHz in frequency. In general, when the magnitude of the wavelength detuning frequency is too high, the injected optical power enters the slave laser cavity which is geometrically incorrectly sized to support that photon wavelength, which likely only makes a single or small integer number of reflections or passes through the optical gain medium. During this small time inside the slave laser's optical cavity, it

induces very few stimulated emissions and experiences very little absorption, leading to very little attenuation or gain, and exits the slave laser cavity without interacting significantly with the slave laser's optical spectrum or modulation dynamics. This state is described as 'unlocked.' Generically, the larger the frequency detuning and the higher the facet reflectivity of the slave laser, the higher the measured external injection ratio has to be to stably lock a Fabry–Pérot laser cavity [22].

2.7. Modulation Response under Optical Injection

By introducing an injection ratio and detuning frequency, the small-signal modulation response, or transfer function, of a directly modulated laser transforms from a quadratic equation with a set relaxation oscillation frequency to a higher-order differential equation governed by the following three rate equations [34]. The A_{inj} terms in (1.13 and (1.14) represent the injected master laser; for cases where A_{inj} is equal to zero, the standard free-running rate equations remain.

$$\frac{dA(t)}{dt} = \frac{1}{2}\Gamma g A(t) - \frac{1}{2}\gamma_c A(t) + k_c A_{inj}\cos(\theta(t)) \tag{14}$$

$$\frac{d\theta(t)}{dt} = \frac{\alpha}{2}\Gamma g - \frac{\alpha}{2}\gamma_c - \Delta\omega - k_c \frac{A_{inj}}{A(t)}\sin(\theta(t)) \tag{15}$$

$$\frac{dN(t)}{dt} = J(t) - \gamma_s N(t) - gA^2(t) \tag{16}$$

Table 1: Variables used in the three rate equations governing optical injection [34].

$A(t)$	electric field magnitude	$\Delta\omega$	detuning frequency
$N(t)$	carrier density	k_c	coupling coefficient
$\theta(t)$	phase between master and slave	g	gain coefficient
A_{inj}	magnitude of the injected field	γ_c	photon decay rate
α	linewidth enhancement factor	$J(t)$	bias current density

Generically, these equations allow the modulation response of an optically injected semiconductor laser to be calculated. These three rate equations differ from the free-running direct-modulation response of a semiconductor laser with the added requirement that the phase offset, $\theta(t)$, between the master and slave fields be accounted for. In the free-running case, phase has little meaning beyond the static requirement that the field fit geometrically inside the laser cavity. From a small-signal point of view, many of the variables in these rate equations remain fairly constant, leaving the terms $k_c A_{inj} \cos(\theta(t))$ as the dominant term that describes the amplitude of the small-signal response and $k_c \frac{A_{inj}}{A(t)} \sin(\theta(t))$ to describe the frequency or change in phase ($f = \frac{d\theta}{dt}$) response to small-signal modulation [33].

Put more simply, during optical injection-locking, light from the master laser combines coherently with the light from the slave laser in the slave's optical cavity. This causes changes in the slave's internal field compared to free-running conditions. When the dynamics settle, the slave's wavelength and phase matches that of the master. If the

master laser's wavelength changes, the slave laser wavelength changes within a certain detuning frequency range, partly determined by the optical injection strength of the master laser. Outside of that range, the slave laser unlocks and lases much as it would under free-running conditions. Figure 2.15 shows operation maps of a selected Fabry–Pérot laser under different levels of optical injection [22]. Of particular interest to directly modulated semiconductor lasers is that the resonance frequency, a key metric in modulation frequency response, increases with increased optical injection strength. Also, the relaxation oscillation dampening coefficient increases as optical injection strength increases.

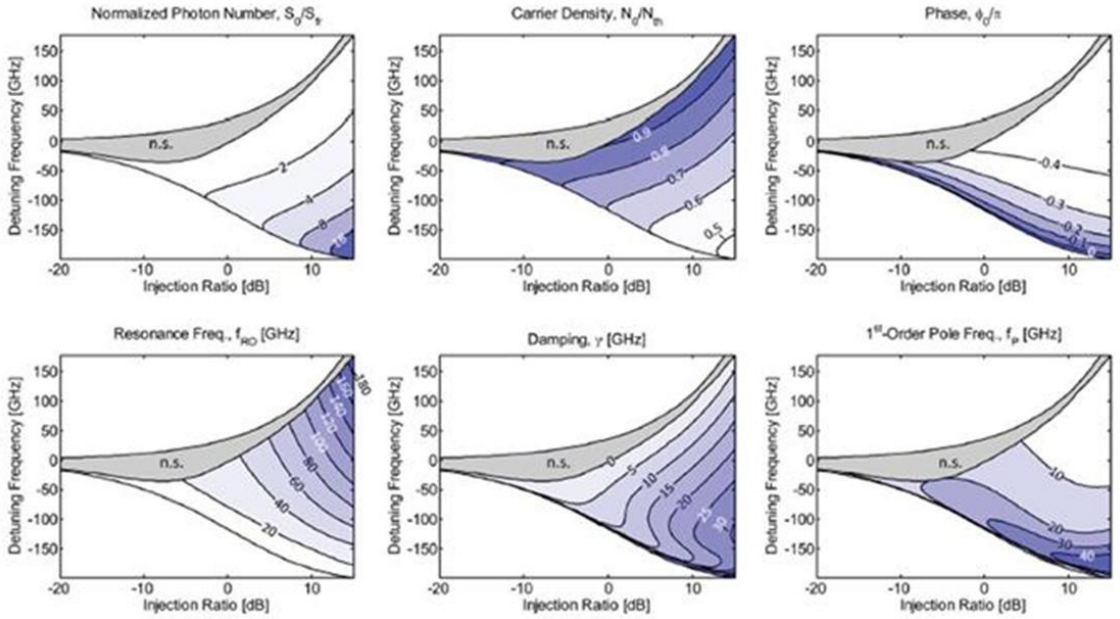

Figure 2.15 : Optical Injection-Locking map for various states. Top three maps are steady-state phton number, carrier density, and phase relationships with respect to injection strength and the bottom three are dynamical values of resonance frequency, damping ratio and the location (frequency) of the first order pole. n.s. indicates unstable locking region [22].

The small-signal modulation responses or S21 curves for different detuning frequencies at fixed injection strength are shown in Figure 2.16 [22, 38]. Notice the significant peak located at approximately 60 GHz for the positive detuning frequency of 20 GHz, as the positive detuning frequency continues to increase, the relaxation oscillation frequency will become un-damped and the dynamical P1 oscillation state will be entered. As the detuning frequency continues to increase, it will eventually unlock and the slave will behave as it would under free-running conditions.

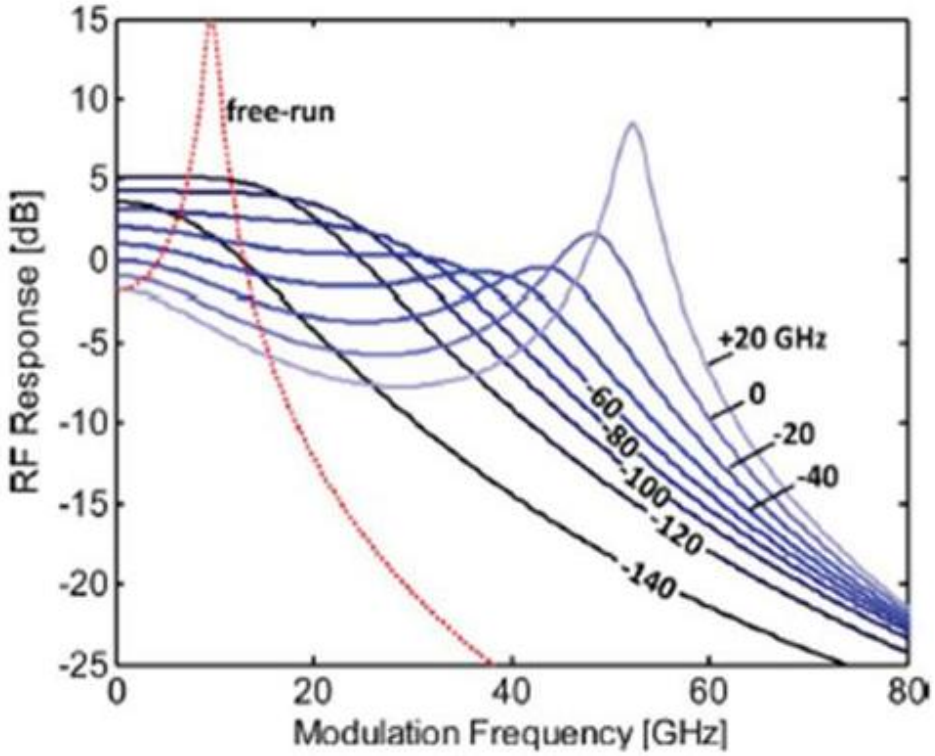

Figure 2.16: small-signal modulation response for various detuning frequencies given optical injection strength of 4dB [22].

As shown in Figure 2.16, significant low-frequency direct-modulation gain has been demonstrated well above that observed under free-running conditions [22, 35]. This

technique can improve optical communication link performance by combining the optical power of a laser with narrow linewidth and poor **direct**-modulation response with the optimized direct modulation properties of a slave laser with poor optical spectral qualities. To achieve this effect, a high injection strength at a low negative detuning frequency is typically necessary [22].

2.8. Optical Injection Affects on Noise

Relative Intensity Noise (RIN), a common metric in the calculation of noise floor in optical-communication links, is largely caused by random carrier recombination and generation events [36]. By improving RIN in an optical communication system, the signal-to-noise ratio will increase which will in turn increase the information carrying capacity of the laser. In optically injection-locked lasers, the intensity and phase fluctuations of the injected light also contribute to system noise [37, 39]. The RIN contributions from the master laser can be considered small-signal, broad-spectrum modulation of injected master light. This causes frequency-domain photon, phase, and carrier Langevin noise sources [22].

Langevin noise sources are frequency independent, stationary, and memoryless (ergodic) processes so the Wiener—Khinchin theorem may be used [36]. Generally, RIN decreases as injection strength increases and (negative) detuning frequency increases. See Figure 2.17 for a graphical representation of how RIN changes under different injection-locking conditions. Under positive detuning conditions however, a different interesting phenomenon occurs, where the peak of the Langevin noise power with respect to

frequency can be adjusted with injection strength and (positive) frequency detuning. This could allow a communication system the ability to choose a frequency location for the Langevin noise that does not interfere with modulation near the free-running resonance frequency [22].

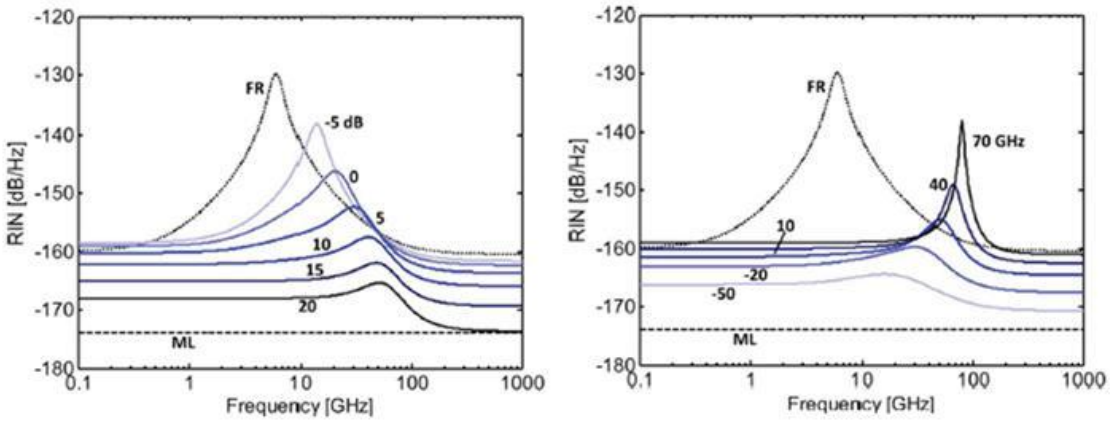

Figure 2.17: Relative Intensity Noise (RIN) under optical injection-locking: Left, fixed detuning frequency of -5GHz for various injection ratios, Right, 10 dB injection strength at different detuning frequencies.

2.9. Optical Injection Technique for Single Sideband Modulation

In dispersion limited guided wave communications applications, single-sideband modulation can significantly improve the bit-rate-distance product or reduce periodic signal fading [42]. Optical injection provides a technique for single-sideband modulation of optical communication systems [37]. When an optical signal $\cos(ft)$ is modulated by a base-band communication signal $x(t)$ the resulting signal $y(t)$ is simply the optical signal with a proportional amplitude described by the baseband signal, $y(t) = x(t)\cos(ft)$. Taking the Fourier transform of this process reveals how a baseband signal winds up

occupying twice the bandwidth while it is on a photon carrier compared to the baseband electric bandwidth shown in Figure 6.14 or Figure 6.18 [25].

$$\begin{aligned} Y(f) &= X(f) * \tfrac{1}{2}\left[\delta(f - f_0) + \delta(f + f_0)\right] \\ Y(f) &= \tfrac{1}{2}\left[X(f - f_0) + X(f + f_0)\right] \end{aligned} \tag{17}$$

A more spectral efficient modulation technique, called single sideband (SSB) modulation, can be achieved electrically by passing $Y(f)$ through a band-pass filter centered on the sideband of interest, such as $\cos\left(\frac{f + f_0}{2}\right)$ for the upper sideband, to attenuate the unwanted sideband. SSB modulation is less of an issue in wireless communication systems since the added complexity does not improve the channel's SNR for additive-white-Gaussian-noise channels. This is explained by assuming the best a wireless communications engineer can achieve is half the signal power divided by half the noise power resulting in the same SNR as DSB modulation. In practice, SSB wireless communications systems have lower SNR than DSB wireless systems because the slope at the filter's cutoff frequency not ideal. SSB modulation is employed in wireless applications for other reasons, especially in ultra-wideband applications where one sideband can be significantly distorted [25].

Through linearly dispersive transmission mediums, however, SSB can reduce the dispersion penalty [43], and effectively provide significantly higher SNR at the receiver. The spectral broadening due to modulation can be quite significant, as discussed with the 2-Gbps rectangular PAM signal in Figure 6.14b, appendix A, spectral components exist as far as 160 GHz corresponding to a ±Δλ of approximately ±500 pm at carrier

wavelength 1550 nm. Assuming a more spectrally efficient base-band shape such as raised cosine PAM shown in Figure 6.18, appendix A [22], the optical signal still must spread in frequency a minimum of ½ the bit-rate [12].

If this modulation is occurring through the direct modulation of the bias current of a Fabry–Pérot laser diode, as described in Figure 6.6, the laser has to support the broadened optical signal inside its laser cavity. Assuming the cavity gain is symmetric, each modulated signal sideband will be attenuated equally, creating a symmetric double-side-band modulated signal.

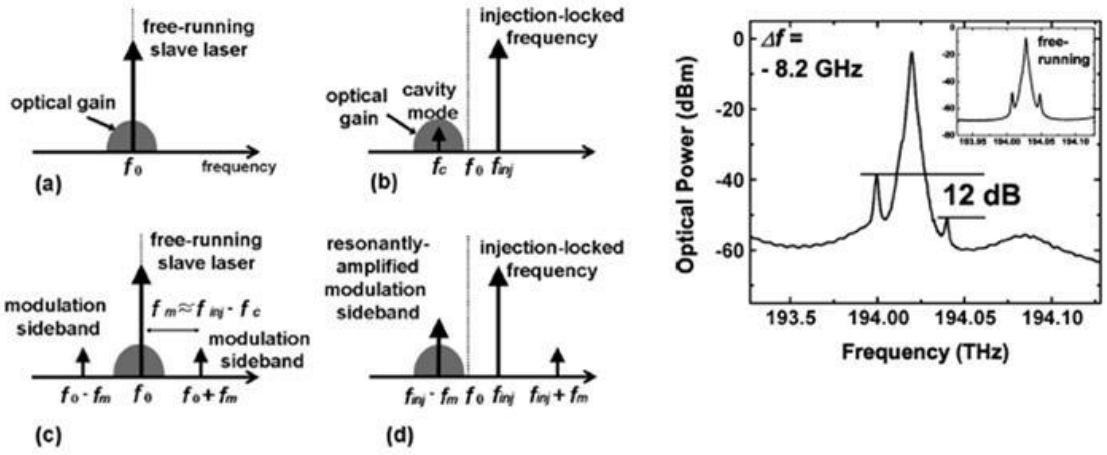

Figure 2.18: Cartoon illustrating SSB amplification while directly modulating an injection-locked laser, correctly detuning the master laser to place one of the modulation sidebands into a geometrically supported Fabry–Pérot mode while the other sideband remains unsupported leading to near-single-sideband modulation [43].

If the laser diode is optically injection-locked (OIL), the carrier wavelength will be located at the injection-locked wavelength, not the geometrically supported wavelength expected under free-running conditions. Figure 2.18 graphically illustrates

this concept [43]. When the OIL carrier linewidth spreads to accommodate the modulation bandwidth, a portion of the modulation signal power will be located within the optical gain of a supported Fabry–Pérot mode. That modulation power will be resonantly amplified by the cavity mode [43], while the other side of the modulation power will be further attenuated, as its wavelength is suppressed.

2.10. Side-Mode Suppression and Mode-Partition Noise Reduction

A common theme for improving communication capability of directly modulated semiconductor lasers is to reduce the linewidth through stably-locked injection. The discrete delta-function-like nature of Fabry–Pérot longitudinal modes in the frequency domain makes mode partition noise particularly unique. As a short-time pulse from a multi-mode Fabry–Pérot laser travels through a linearly dispersive medium, each spectral component travels at a different speed. Rather than showing up at the receiver as a smoothly slurred communication symbol the group shows as a series of discrete pulses with time delay between pulses appropriately spaced for the distance traveled through the dispersive fiber. Figure 2.19 shows pictorially how the time domain received pulse looks after one longitudinal mode completely overtook the other mode of the previous pulse. Research performed in 1982 showed how optical injection could suppress Fabry–Pérot modes and significantly reduce mode-partition noise [44].

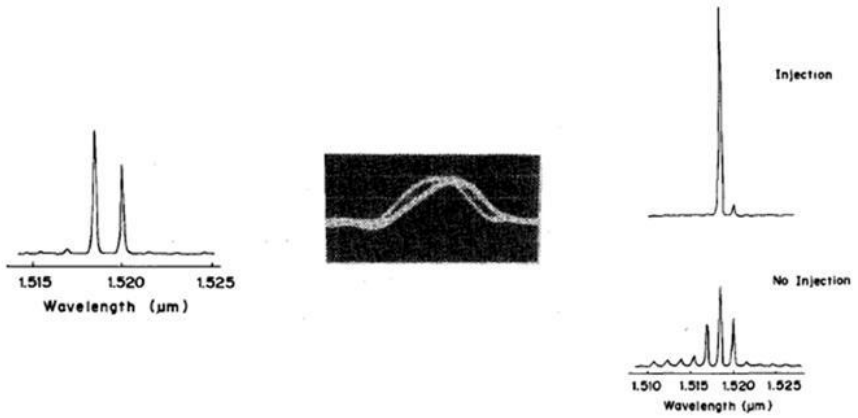

Figure 2.19: Simple graphic explaining mode-partition noise and how optical injection reduces mode partition noise by suppressing Fabry–Pérot modes [44].

2.11. Marginally Locked Optical Injection

In an attempt to parameterize optical injection-locking dynamics such as mode suppression effects, experimental data has been collected corresponding to the experimentally observed onset of stable-locking [33]. Figure 2.20 graphically shows how a marginal increase in injection strength at zero detuning conditions can significantly amplify the injected mode. In this experiment, a marginal increase in external power ratio of 1.4 dB resulted in an approximate increase of 1.4 dB in amplitude of the injected mode, taking the necessary optical power from the non-injected Fabry–Pérot longitudinal modes [33]. In this thesis, a communication architecture is proposed which will utilize this amplification with the SSB technique discussed above to create an all-optical microwave envelope detector.

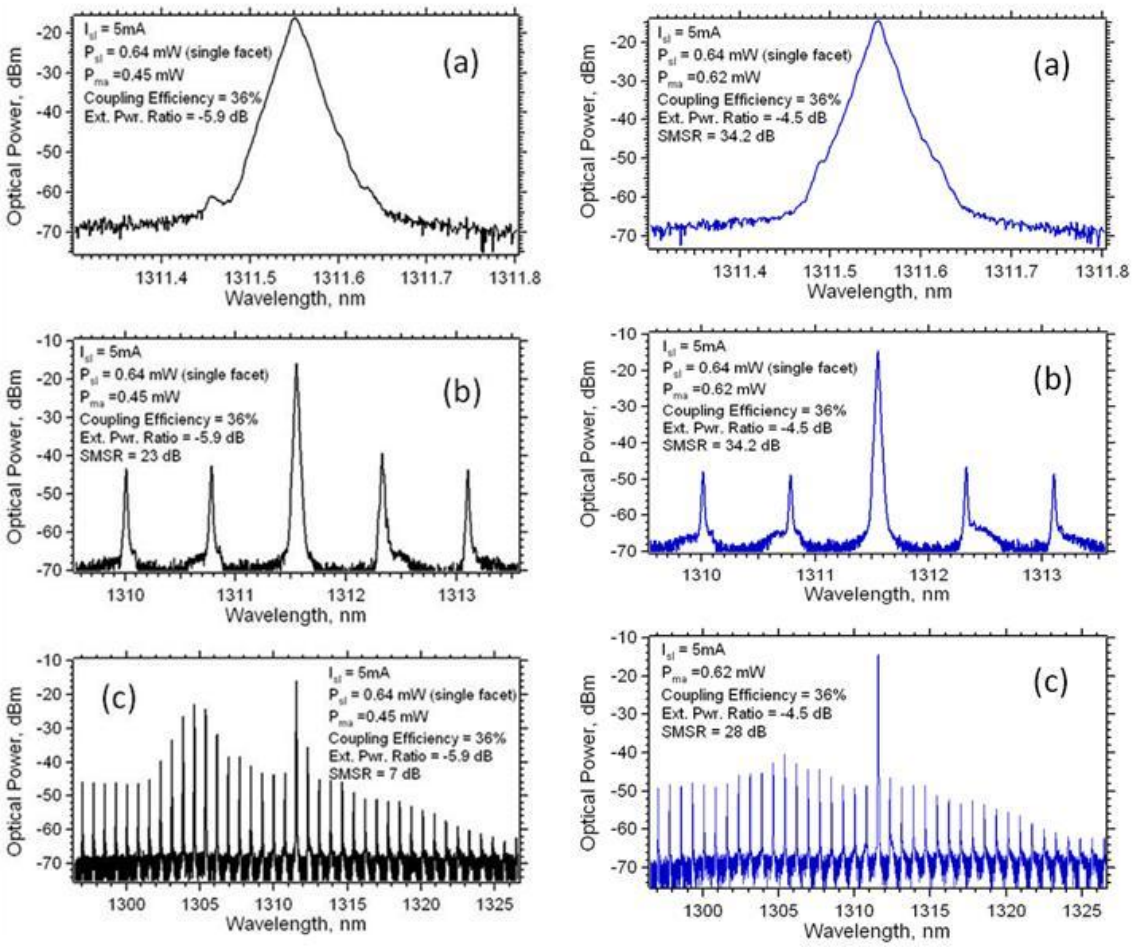

Figure 2.20: Optical spectra showing the onset of stably-locked optical injection at zero detuning frequency, left, external power ratio -5.9 dB, right, external power ratio -4.5 dB. Notice the significant suppression of Fabry–Pérot side modes, amplification of injected mode and suppression of relaxation oscillation frequency [33].

2.12. Suppression of the Relaxation Oscillation Frequency

Of additional interest in the data shown in Figure 2.20 is, what appears to be, the suppression of a relaxation oscillation frequency at 1311.46 nm under an external injection ratio of -5.9dB compared to a -4.5 dB injection ratio where this feature is absent [33]. The relaxation oscillation frequency contributes to the non-flat nature of the pass-

band of directly modulated semiconductor lasers as simulated with the Chebychev filter in Figure 6.16 (appendix A).

2.13. Suppression of Wavelength Chirp

The concept of wavelength chirp further reduces long-haul, high-speed optical transmission through optical fibers in directly modulated lasers. As previously noted, chirp is caused by variations in the output wavelength of the lasers due to carrier induced changes in the refractive index, n, during direct modulation of the bias current. This effect causes the optical spectrum or linewidth to widen under modulation. In 1985 N. A. Olson reported "Chirp-Free Transmission over 82.5 km of single-mode fiber at 2 Gbit/s with injection-locked DFB Semiconductor lasers." This resulted in and the highest bit-rate-distance product at that time of 1.65E11 km b/s and was achieved only by stably locking a DFB semiconductor laser and directly modulating it [18].

Under stably-locked optical injection, the center frequency is held constant over a frequency range, Δf governed by the equation [18]:

$$\Delta f = \frac{1}{2\pi\tau_p}\left(\frac{P_{in}}{P_1}\right)^{\frac{1}{2}} \tag{18}$$

Where P_{in} is the injected optical power and P_1 is the free-running slave laser power as measured inside the laser cavity. The photon lifetime, τ_p is governed by equation [18]:

$$\tau_P = \left[\tfrac{c}{n}\left(\alpha + \tfrac{1}{L}\ln\left(\tfrac{1}{R}\right)\right)\right]^{-1} \tag{19}$$

Where c is the speed of light, n is the index of refraction, α is the internal losses, L is the length of the laser cavity, and R is the facet reflectivity [18].

Further research into wavelength chirp found that a communication signal could be 'pre-chirped' to account for the dispersion of the channel. This idea effectively pulsed the slower moving wavelength components first and the faster wavelengths last so by the end of the channel the group of photons arrived at the same time. This required foreknowledge of the channel length, carrier wavelength, and dispersion coefficient, which proved impractical for reconfigurable optical communications networks.

Chirp is not eliminated completely as suggested in 1985 [18] but instead is a function of detuning frequency and injection strength. Chirp reduction is measured by the metric chirp-to-power ratio (CPR) with units of GHz/mW. Low CPR values are better than high values. CPR is reduced as a function of increasing injection strength and increasing negative (so decreased) detuning frequency. For an injection power ratio of 4 dB and -100 GHz detuning frequency, the CPR is approximately one one-thousanth (-30 dB) the CPR of the same laser under free running conditions [22].

2.14. P1 Dynamic State of Optical Injection

Semiconductor laser are intently nonlinear devices because of the complex relationship between their optical gain on both the carrier electron and photon densities. Figure 2.21 shows a region of unstable optical injection labeled n.s. above the positive detuning edge of the stably-locked region of optical injection strength and detuning frequencies [22]. Within this region, a rich variety of nonlinear dynamics occur including

periodic oscillation, regular pulsation, quasi-periodic pulsation, and chaotic pulsation. These dynamics vary at microwave frequencies which are widely tunable with low phase noise. Anticipated applications for these photonic microwave sources include broadband wireless access networks, satellite communication systems and photonics based phased-array antennas and radars [46]. The largest portion of this dynamical state is composed of the P1 (P1) state.

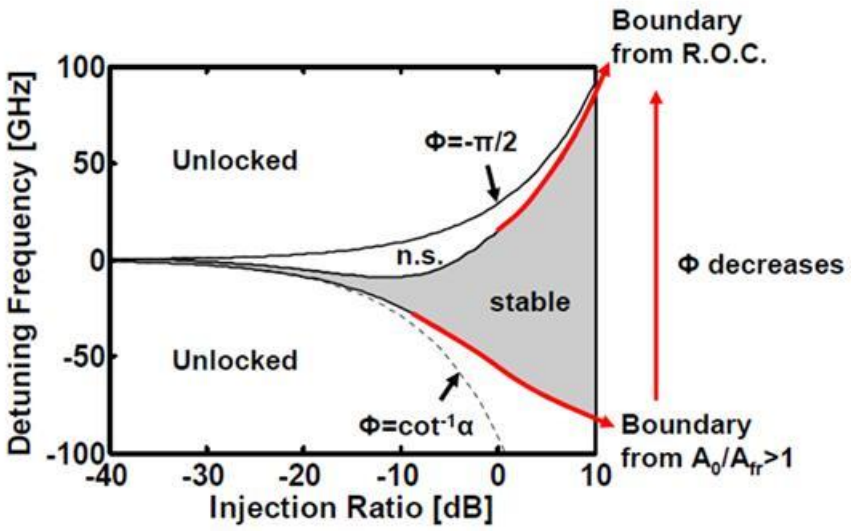

Figure 2.21: Optical injection operation map showing tolerably detuning frequency increases with injection strength. P1 state is located inside the region labeled n.s. [22]

The P1 dynamical state of semiconductor lasers occurs when the dampening ratio of the resonance frequency or relaxation oscillation is zero. This condition can be reached with various combinations of injection strength and frequency detuning. The effect is intensity modulated optical emission from the semiconductor laser that has a frequency dependency on the same operating parameters as stably-locked optical injection [22]. A

range of intensity modulation depths of the P1 microwave frequency on the photonic carrier has been observed, including very large swings of near 100% amplitude modulation depth.

2.15. Enhancing the Relaxation Oscillation Frequency

The P1 dynamic can be largely explained as removing the relaxation oscillation dampening ratio by providing a positive term in the feedback between carrier electrons and electric-field intensity in the active region of the laser diode. The relaxation oscillation frequency increases along with injection strength as shown by the accentuated modulation response associated with increases in the injection strength under stably-locked optical injection in Figure 2.15 [22]. These two effects have been mapped in Figure 2.22, which shows that along the positive detuning edge of the injection-locked region, the carrier density is 1, and resonance frequency increases with respect to the injection strength [22]. This positive detuning edge is referred to as the Hopf bifurcation line [33].

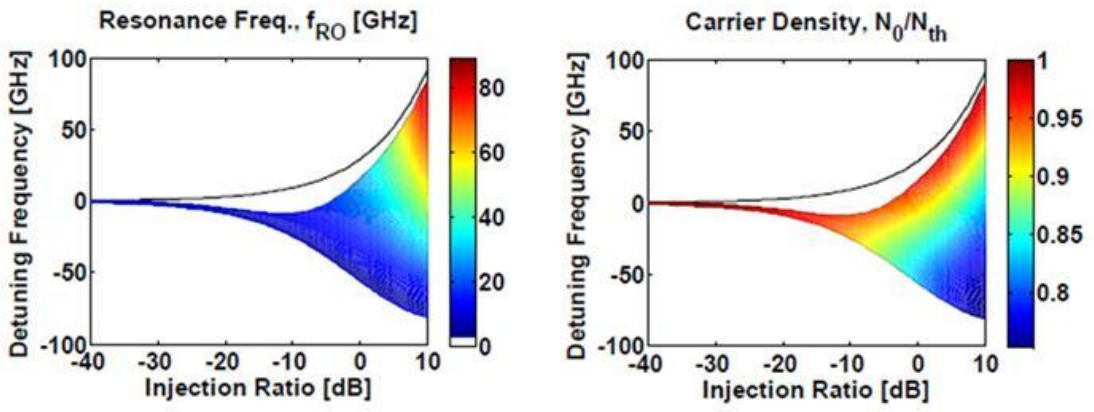

Figure 2.22: Operational map of the stably locked region of optical injection showing resonance frequency increases with optical injection strength (left) and carrier density must be less than one for stable locking (right) [22].

The dampening coefficient of the resonance frequency is useful for describing the peak of the modulation response while the inside of the injection-locked region can be described by $\gamma = \gamma_0 - g\left(N_0 - N_{th}\right)$. In this equation, γ is the injection-locked dampening ratio, γ_0 is the slave laser's free-running dampening term. Gain, g, is a function of current while N_0 and N_{th} are related to the number of carrier electrons available in the active region an those at the threshold carrier density level respectively. Under a range of optical injection and positive frequency detuning conditions, $\gamma_0 = g\left(N_0 - N_{th}\right)$ creates the unstable optical output, which, under the right conditions for P1 oscillation, purely oscillates at a microwave frequency approximately equal to both the frequency detuning and the relaxation oscillation frequency. The P1 oscillation frequency dependence on optical injection strength and detuning frequency allows the optical generation of frequency modulated communication symbols, where the baseband amplitude modulated

communication signal drives the injection strength and/or detuning frequency of coupled semiconductor lasers.

2.16. Modulating the P1 Dynamical State

Operating within this regime can be complex so an operation stability map can be generated as a guide for potential operating points within the dynamical state. Figure 2.23 shows one such operational stability map for a semiconductor laser under a set bias current. This operational state diagram has been plotted with respect to the injection coupling rate which is proportional to the external injection strength [33].

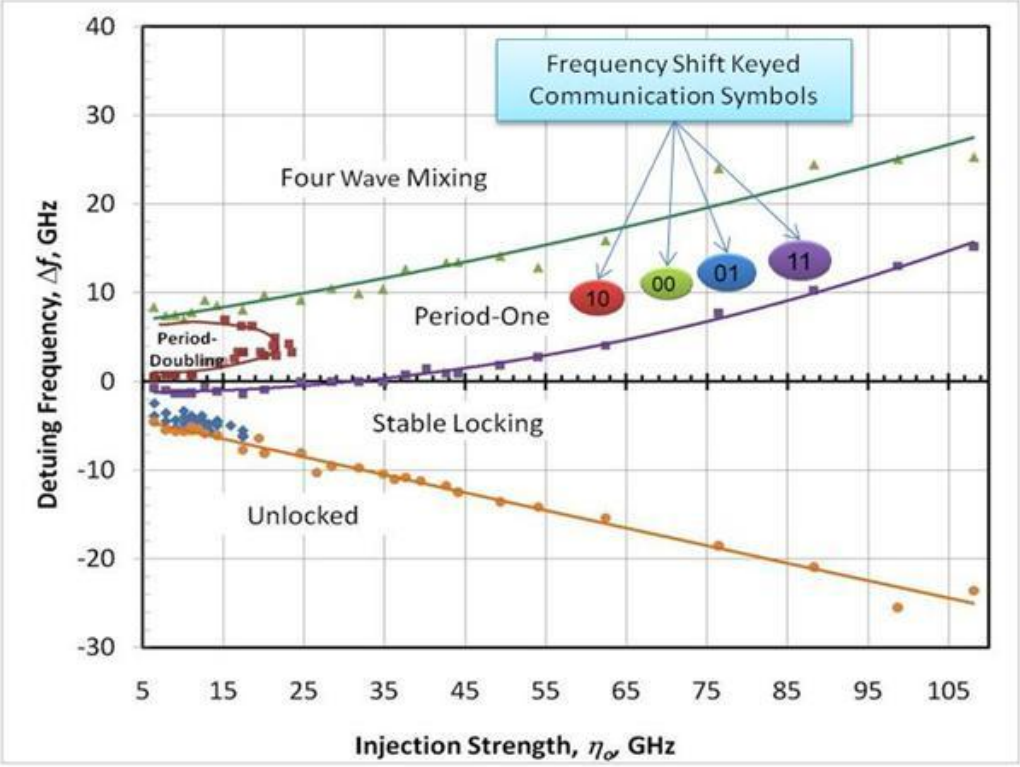

Figure 2.23: Operation stability map of an optically injected semiconductor laser [33].

The P1 dynamic of optical injection allows a second method of single-sideband modulation in much the same way as stably-locked optical injection can provide single sideband modulation. In the stably-locked case, the support of single-sideband or double-sideband modulation is driven by the detuning frequency. In the P1 state, SSB can be achieved at the same detuning frequency, but with different injection strengths. Figure 2.24 shows an example SSB and DSB P1 states created with the same detuning frequency but different injection strength ratios.

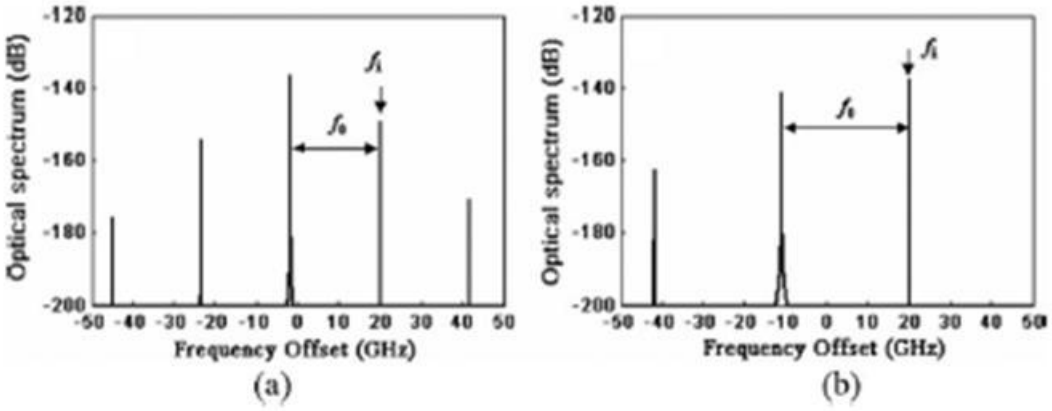

Figure 2.24: Optical spectra of two representative P1 states reached with the same detuning frequency of 20 GHz, but different injection strengths: (a) DSB P1 of 21.68 GHz (b) SSB P1 state of 30.92 GHz with injection ratio ≈4 times (a) [46].

2.17. Spectral Characteristics of the P1 Dynamic

The P1 dynamic has frequency components analogous to the four-wave-mixing effect. When two optical signals with very close carrier wavelengths are guided through the same medium their electric-field magnitudes combine, sometimes canceling, sometimes amplifying. This interaction, known as four-wave mixing, produces amplitude

modulation of the carrier, with the modulation frequency equal to the difference between the two carrier frequencies. The important distinction between four-wave mixing and P1 dynamic is that the P1 dynamic does not produce as much random phase noise. The random phase noise from four-wave mixing limits how close wavelength division multiplexed carriers can be on the same fiber. Furthermore, the resulting carrier optical linewidth is narrower for P1 dynamic than steady state and wider for four wave mixing. Also, the resulting bandwidth or Q-factor of the microwave 'beat frequency' is significantly higher for P1 than it is for four wave mixing.

The P1 dynamic is eclipsed by the opto-electronic oscillator (OEO) when it comes to tonal purity. The OEO uses a laser cavity as an energy storage device and a length of fiber for a delay loop that feeds into a photo-detector that drives an RF amplifier, narrow band filter, and back into the laser diodes bias current. A dual-loop OEO operating at 10 GHz has achieved a high quality factor with low phase noise of -140 dBc/Hz at 10 kHz. Frequency tuning has been achieved for OEOs by mechanically stretching the fiber optic feedback loop, a difficult process to implement in practice. It also has been achieved by taking advantage of the fiber dispersion coefficient and temperature tuning the laser diode to produce different wavelength, and thus time delayed feedback. This also is very difficult, and is not practical for embedded systems [46]. A comparison of photonic microwave generation techniques is given in Table 2.

The fundamental frequency of the P1 state, on the other hand, increases nearly linearly with the increase of injection strength for a set detuning frequency. Alternatively, it increases with the detuning frequency for a given injection strength. These FM signals

are more tolerant to detrimental effects caused by fiber nonlinearities than AM signals are. These microwave frequencies can be widely tunable, starting near the free-running relaxation oscillation frequency and extending to many times that of the semiconductor laser diode.

2.18. Photonic Microwave Applications

The application of photonic microwave generation and propagation in Radio-Over-Fiber technology holds great promise for ‘4G mobile communication systems’ as it allows the broadcast of radio signals without the complex electronics required for local oscillators at every base station. A network architect could choose to generate the frequency modulated signal at the base station and distribute that signal to any number of distributed antennas, geographically separated to prevent interference. The use of optical injection to create microwave frequencies on a photonic carrier significantly decreases the complexity of the microwave transmitter, which requires only a photo detector and antenna. Figure 2.25 illustrates one potential distributed access wireless network implementing radio-over-fiber technology for the distribution of microwave signals.

Table 2: A comparison of different photonic microwave techniques [46]

Techniques	Electronics	Tunability	Maximum Frequency	Microwave Linewidth	Single Sideband	Modulation Type	Stability	Optical Loss
Direct modulation	Moderate	Fair	30 GHz	Determined by source	Special design required	AM	Good	None
Optical heterodyne	Simple	Good	~ THz	Broad	Yes	/	Poor	None
OPLL	Complicated	Fair	330 GHz	Narrow (~mHz)	Yes	/	Good	None
Dual-mode laser	Complicated	Good	42 GHz	Moderate (~MHz)	Yes	/	Poor	None
External modulation	Moderate	Fair	40 GHz	Determined by source	Special design required	AM/PM	Good	Large
Mode locking	Moderate	Poor	30 GHz	Narrow (~Hz-mHz)	No	/	Good	Large
OEO	Complicated	Poor	75 GHz	Narrow (~mHz)	No	AM/PM	Good	Large
Period-one dynamics	Simple	Good	100 GHz	Moderate (~MHz-mHz)	Yes	FM	Poor	None

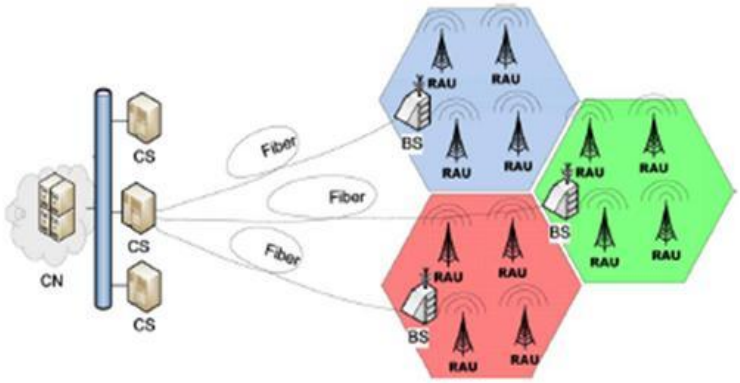

Figure 2.25: A potential architecture for a wireless distributed access system. CN: core network; CS: central station; BS: base station; RAU: remote antenna unit [46].

2.19. Conclusion

The optical injection of directly modulated semiconductor lasers has been shown to significantly enhance the modulation response and reduce the linewidth over free-running directly-modulated lasers. These improvements suggest that simpler modulation architecture for long-haul base-band telecommunications is possible.

Stably-locked optical injection has been employed to increase signal power and reduce noise power. It has been employed as a means of SSB modulation and has demonstrated suppression of mode quantization noise. Stably-locked optical injection has been shown to reduce the nonlinearities associated with direct modulation, including reduced overshoot due to the relaxation oscillation frequency while maintaining fast rise time and symmetric temporal response.

Furthermore, the parameterization of the complex dynamics of optical injection opens the possibility for photonics to reduce the size, weight, and complexity of microwave applications in radar and communications applications. The next chapter demonstrates the use of these parameters, namely detuning frequency and injection strength, for direct access to high frequency microwave modulation on an optical carrier using baseband electronics. It also demonstrates significant microwave stability under large-signal modulation.

3. Methodology

This chapter focuses on the procedures taken in the laboratory and contains specific information to allow a follow-on researcher to repeat and build on the results of these experiments. These experiments demonstrate the ability to use baseband electronics to directly access the orthogonal microwave frequency communication domain without the traditional high-frequency support electronics necessary to reach these high-frequencies.

This chapter is broken into three parts. Section 3.1 describes of the laboratory equipment and setup that applies to both stably-locked and P1 states of optical injection. Section 3.2 explains the investigation process to measure the increase in bit-rate-distance product of a stably-locked Fabry–Pérot laser over its free-running state. Section 3.3 summarizes the measurements taken to verify the ability to place communication symbols on the P1 dynamical state of the injected Fabry–Pérot laser.

3.1. Optical Injection Equipment and Setup

Ideally, the only difference between optical injection-locking (OIL) and the P1 (P1) dynamical states is the injection strength and the detuning frequency. Largely, this is the case for these experiments, and the difference between the experimental setups will be noted as necessary. Figure 3.1 depicts the physical setup used in our optical injection work and allows discussion of each component.

3.1.1. Optical Injection Laboratory Setup

The single-mode master laser is coupled to a polarization-maintaining (PM) SMF with a FC/PC connector. Its output is fed into a polarization maintaining tunable fiber amplifier using a FC/PC-to-FC/APC PM patch cable whose, output is connected through a polarization rotator, which has a free-space optical path that can be conveniently blocked with an opaque object. The output from the polarization rotator is connected to port 1 of a PM Optical Circulator with FC/APC terminators.

Port 2 of the PM optical circulator injects (reflection style) the Fabry–Pérot slave laser using a PM FC/APC-to-FC/PC patch cable. Both the maser laser and slave laser's bias current and temperature are separately controlled with their own laser diode controllers.

Port 3 of the optical circulator is fed into a low-noise optical amplifier which is then transmitted through fiber spools of length 1, 1.7, 10, 20 and 30 km which could be connected in series for as much as 62.7 km of Corning SMF-28e+ fiber. When necessary, a third fiber amplifier is used to compensate for attenuation through the fiber. The output of the channel is then divided by a 90/10 fiber splitter with the 10% output going to an optical spectrum analyzer and the 90% port going to a linear fiber attenuator followed by a high-speed photo detector.

The microwave output of the photo detector is fed into the input pin of the SyntheSys Research BERTScope model 7500A through Coaxial cables with standard SMA connectors. The BERTScope then compares the voltage measured on its input port to a threshold voltage and time delay to create the received bit-stream. The received bit

stream is then compared with the output bit stream. In this way, the BERTScope is able to measure and report the bit error ratio of the communication system. The output of the photo detector can also be fed into an electrical spectrum analyzer or an oscilloscope if desired.

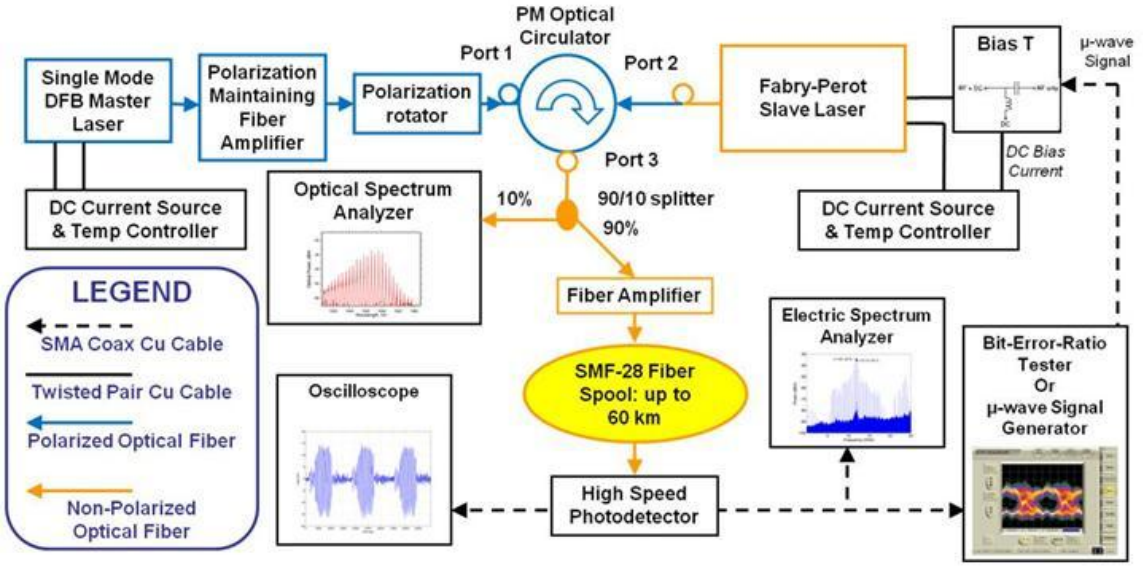

Figure 3.1: Generic experimental setup of optical injection experiments. The BERT Scope proved to be most useful for stably locked optical injection while the electric spectrum analyzer proved most useful for detection in P1 dynamic.

3.1.2. Master Laser

The continuous wave master laser was one component that did change between OIL and P1 dynamic experiments. For the OIL setup, an acceptable but significant difference between the center wavelength of the DFB (master) and Fabry–Pérot (slave) laser was compensated for by injecting a supported longitudinal side-mode of the FP laser. The DFB master laser was manufactured by JDS Uniphase in a butterfly package

which prevented direct modulation of its bias current. Its temperature and bias current was controlled by a Stanford Research Systems Laser Diode Controller Model LDC501.

The master laser for the P1 dynamical state experiments was a Velocity tunable laser diode, (New Focus model 6328); this highly-tunable device was packaged such that direct modulation of its bias current was not possible. The maser laser's wavelength could be finely tuned/changed using a piezoelectric controller. This master was able to provide wider tunability, 1507-1584 nm, and improved wavelength control when compared to the temperature tuned JSDU DFB laser diode; this feature allowed greater flexibility on which FP mode to inject the ability to precisely control the detuning frequency.

3.1.3. Slave Laser

The slave lasers used in this research were all standard fiber pigtailed quantum-well Fabry–Pérot laser diodes in TO-56 packages from Thorlabs; their threshold currents varied from device to device. The Thorlabs LM9LP, the laser mount used for the Fabry-Pérot slaves allowed direct modulation of the bias current through a built-in bias-tee with an SMA connector. One PM Fabry–Pérot slave laser and two non-PM Fabry–Pérot slave lasers were available for testing. All three were connected to a fiber-optic patch cable, PM or non-PM as appropriate, with FC/PC connectors.

The DC bias current and the temperature controller for the slave laser(s) were controlled using Stanford Research Systems Laser Diode Controller(s) Model LDC501. This model has a built-in PID controller as well as an 'auto detect' function that can be

run to calculate the PID coefficients for critically damped temperature control. This feature was utilized most when P1 experiments were attempted for better detuning frequency control. The symptom of poorly chosen PID coefficients for the LDC501 was an unstable temperature which oscillated, in one case un-damped.

3.1.4. Fiber Amplifiers and Attenuators

Low-noise fiber amplifiers and attenuators allow laser bias currents and detuning characteristics to remain constant while allowing compensation for linear fiber attenuation. The optical output from the master laser was fed into a PriTel Inc. polarization maintaining fiber amplifier (model PMFA-30), whose amplification could be adjusted to change the injection strength without modifying the detuning frequency or raising the noise floor. The output of the 90-10 splitter was amplified by the PriTel Inc non-PM fiber amplifier (model number LNHPFA-30) before transmission. Their ability to amplify or attenuate without distorting the wavelength or SNR was a key attribute in measuring the bit-rate-distance product. The fiber attenuator allowed adjustment of the optical power before the high-speed photo detector to control any nonlinear effects optical intensity could have and also to protect the detector from over exposure to light.

3.1.5. Fiber Connectors and Patch Cables

The use of fiber-optic patch cables versus free-space optical paths provided significantly simpler means of optically coupling the devices in the experiment. This came at the cost of increased attenuation, channel distortion, reflective feedback,

polarization and phase distortion. FC/APC connectors were used as often as possible to reduce reflections and polarization maintaining fiber was used to minimize polarization dependent distortion. When possible the cables and connectors were taped to the optical bench to prevent physical motion and avoid thermal fluctuations. Finally, physically changing the experimental setup was avoided as much as possible by taking as much data as feasible from a single setup during the same day.

The optical circulator is PM with FC/APC connectors and Port 3 was connected to a 90-10 splitter which is also FC/APC connected but non-PM. PM fiber connectors and patch cables should allow more stable and controlled experimental behavior including less sensitivity to stress, temperature or other physical environmental factors. With this in mind every component short of the transmission line should be PM. Qualitatively, however, the PM connectors behaved more erratically. To compensate, the external injection strength was measured by disconnecting a non-PM FC/APC connection. That proved to behave more predictably than FC/PC connectors or PM cables.

3.1.6. Optical Spectrum Analyzer

The Ando AQ6317B Optical Spectrum Analyzer was used in this research to directly measure optical spectra. Its normal position in the experiment was to measure the optical spectra from the 10% port of the 90-10 splitter which was connected using a non-PM FC/APC patch cable. Measuring the full-strength optical signal marginally improved as its dynamic range is approximately 60 dB. Ando guarantees spectral resolution of 0.015 nm (≈1.87 GHz) or better when it is placed in 0.010 nm resolution setting and

guarantees better than 5% accuracy for resolution settings of 0.050 nm (≈6.24 GHz) or higher. The data traces can be saved to comma-separated text files and subsequently downloaded to a floppy disc.

3.1.7. High-Speed Photo Detector

There were three different models of photo detectors used in these experiments. Two were manufactured by New Focus Inc. (models 1444 and 1414), and the other was manufactured by Thor Labs (model SIR5-SC). ThorLabs guarantees the SIR5-SC has a 3-dB bandwidth of 5 GHz or greater. This device is quite appropriate for PAM data rates of ≈1Gbps and has a relatively high input capacitance (compared to the New Focus' PDs) which improved the repeatability of the signals, creating a cleaner, more predictable communication symbol. However, this low-pass filter feature completely eliminates its usefulness in P1 dynamic research as P1 can be much higher than 5 GHz.

The New Focus Model 1444 photo detector is optimized for high-speed baseband modulation with a very fast rise-time of 19 ps or faster and is critically damped, to avoid ringing. The New Focus Model 1414 photo detector on the other hand is optimized for frequency-domain applications, such as the P1 dynamic research, and has a flat response for both frequency and phase up to 25 GHz.

3.1.8. Bit Error Ratio Tester and Eye Diagram Analyzer

The SyntheSys Research Inc. (model 7500A) BERTScope was the tool used most for the Bit-rate-distance Product measurements taken in the OIL investigations and was

used to generate baseband PAM signals for All-Optical Microwave symbol generation in the P1 research. Figure 3.2 shows several useful metrics created by the BertScope's Eye analyzer. After transmitting polar rectangular signals through a system who's output is connected to the receive port of the BERTScope, the received information is stored in a 2-dimensional matrix as shown in an Excel document on the bottom right of Figure 3.2, forms an eye and analyzes the results.

When a BERT is performed, for a given threshold time and voltage, the result is displayed on the DETECTOR screen. The BERTScope's Detector interface allows user-defined or automatic detection of optimal threshold values for the Bit Error Ratio Test (BERT). The algorithm for automatic detection of threshold values simply uses the average voltage measured as the voltage threshold and the mean distance between rising and falling edge for time delay threshold. That simple test works well for symmetric eyes and simulates common algorithms employed in actual PAM receivers. This is not effective when the rise-time does not equal the fall-time, or when there is any nonlinearity or hysteresis in the system.

The eye analyzer provides several different tools to qualitatively assess the performance of the communication system from the eye diagram, including the eye diagram itself. An example is shown in the upper right of Figure 3.2 with an example sample threshold value chosen, and marked with an orange dot.

The Q-factor and jitter peak of the eye diagram are metrics that are available from the BERTScope. Example screenshots of these two metrics are shown in the middle two images of Figure 3.2 where the optimal time and voltage thresholds and estimated

optimal bit error ratio (BER) are displayed and circled in red. These values are calculated based on measured BER with respect to voltage and time thresholds.

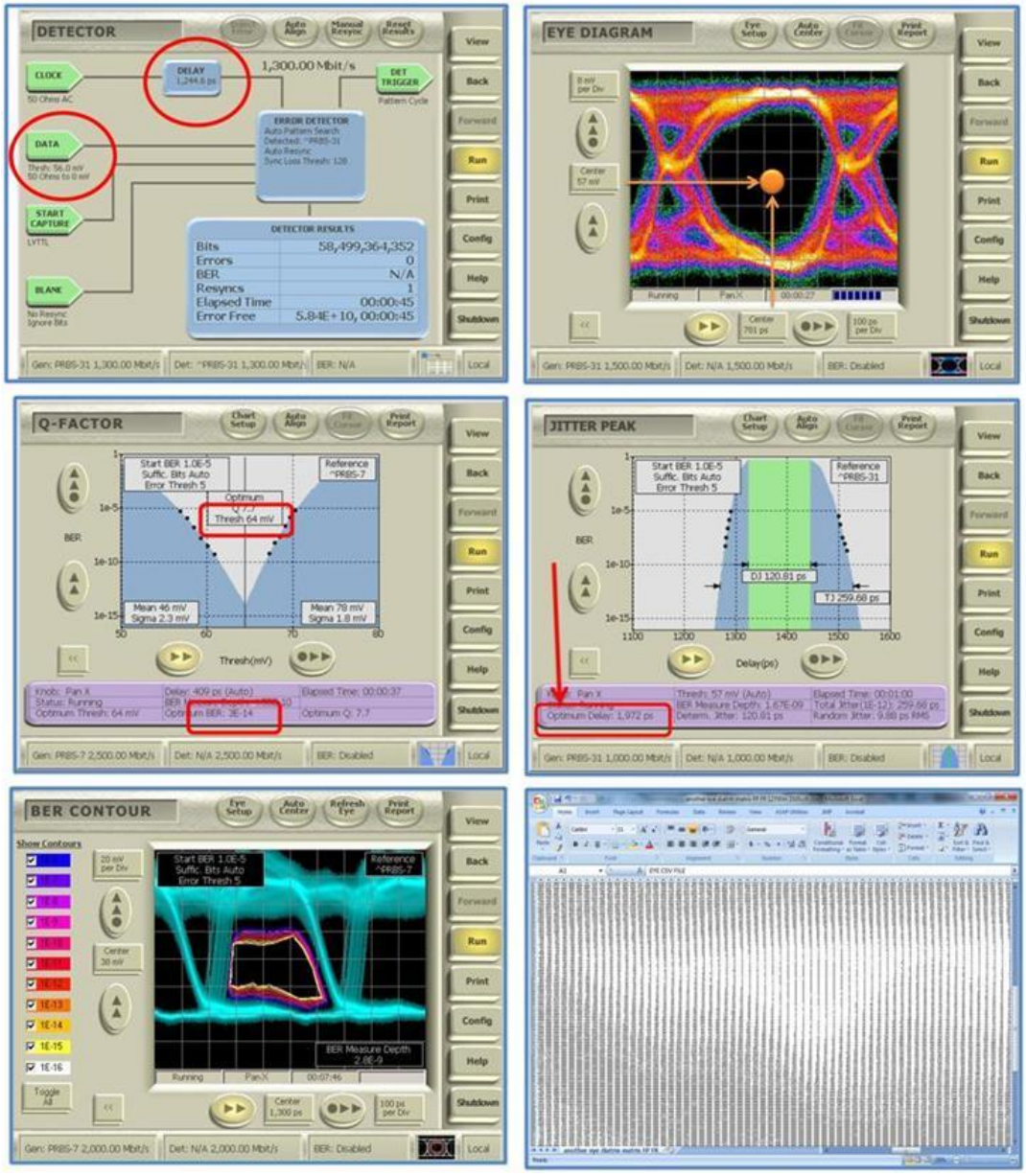

Figure 3.2: Several of the useful features provided by the BERTScope Eye Analyzer are showcased here. The detector interface, the eye diagram, Q-Factor test, BER contour. All of these analysis features are computed using the two-dimensional matrices which can be exported in comma-separated-value form as displayed in Excel in the bottom right.

A final metric used to qualitatively assess the quality of an eye is called the BER Contour. The BER Contour draws equal-BER lines; these lines are not actually measured, but are instead calculated from Q-factor-like measurements and a curve is fit to those measured points in much the same way as the Q-factor test estimate 'optimum BER.' This metric is useful in estimating the steepness of the edge of an eye, the amount of time wasted, in this case approximately 200 to 250 ps, and the amount of signal strength wasted, in this case ≈40mV.

3.2. Measuring Process of increase in Bit-rate-distance Product

The Bit-rate-distance product is conceptually simple to measure: find the operating bit-rate through a given length of fiber at which a marginal increase in either bit-rate or distance would prevent the system from communicating at a tolerable BER, then simply multiply and report the BL product. Repeat for both free-running and optically injection-locked lasers and the test is complete. The difficulty in measuring the Bit-rate-distance product is finding the optimal voltage and time-delay threshold and ensuring **all else equal**.

All else cannot be equal between OIL and free-running operation for the same optimal marginal BER. Either the bit rate, or the distance, or both must change. As discussed in chapter 2, many characteristics about the modulation of a semiconductor laser change under stably-locked optical injection from its free-running state. Furthermore, distance cannot be reduced infinitely. The modulation response of the bias tee (inherent electric parasitic) will eventually prevent the bit-rate-distance product from

being measured. For example, a Fabry–Pérot laser that can barely communicate at 1 Gbps through 10 km of SMF might not be able to be modulated at 10 Gbps through any length fiber and certainly will not respond to a signal at 100 Gbps. The metric of Power Penalty, sketched in Figure 3.3, attempts to compensate for these issues.

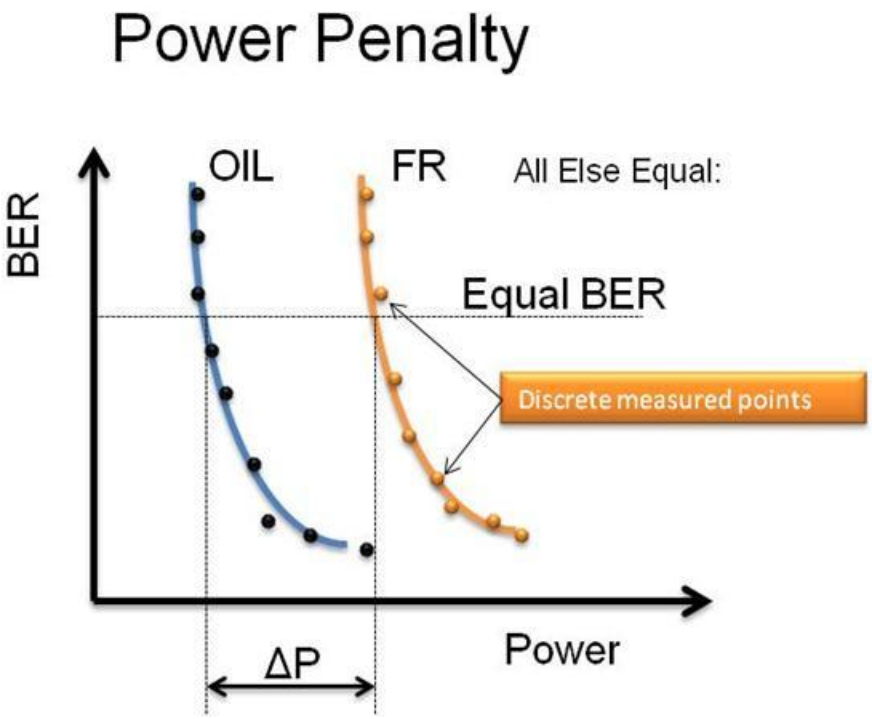

Figure 3.3: Sketch of a notional power penalty (ΔP) measurement. The shift in power required to communicate with the same BER is the power penalty. This could be for any characteristic like distance or bit-rate holding all else equal.

A power penalty can be measured for any changes in the communication system. The characteristics of interest in this experiment include bit rate, distance and optical injection (as pictured). The metric captures the idea that for a given signal inhibition, an increase in signal power can compensate for it. Assuming the communication inhibition keeps the shape of the BER-versus-power curve the same, than the power penalty is

simply the shift along the power axis from one curve to the other. Each discrete measured point must be made for the optimum BER found for the operating conditions. Figure 3.4 shows the process of detecting and recording the optimal threshold values.

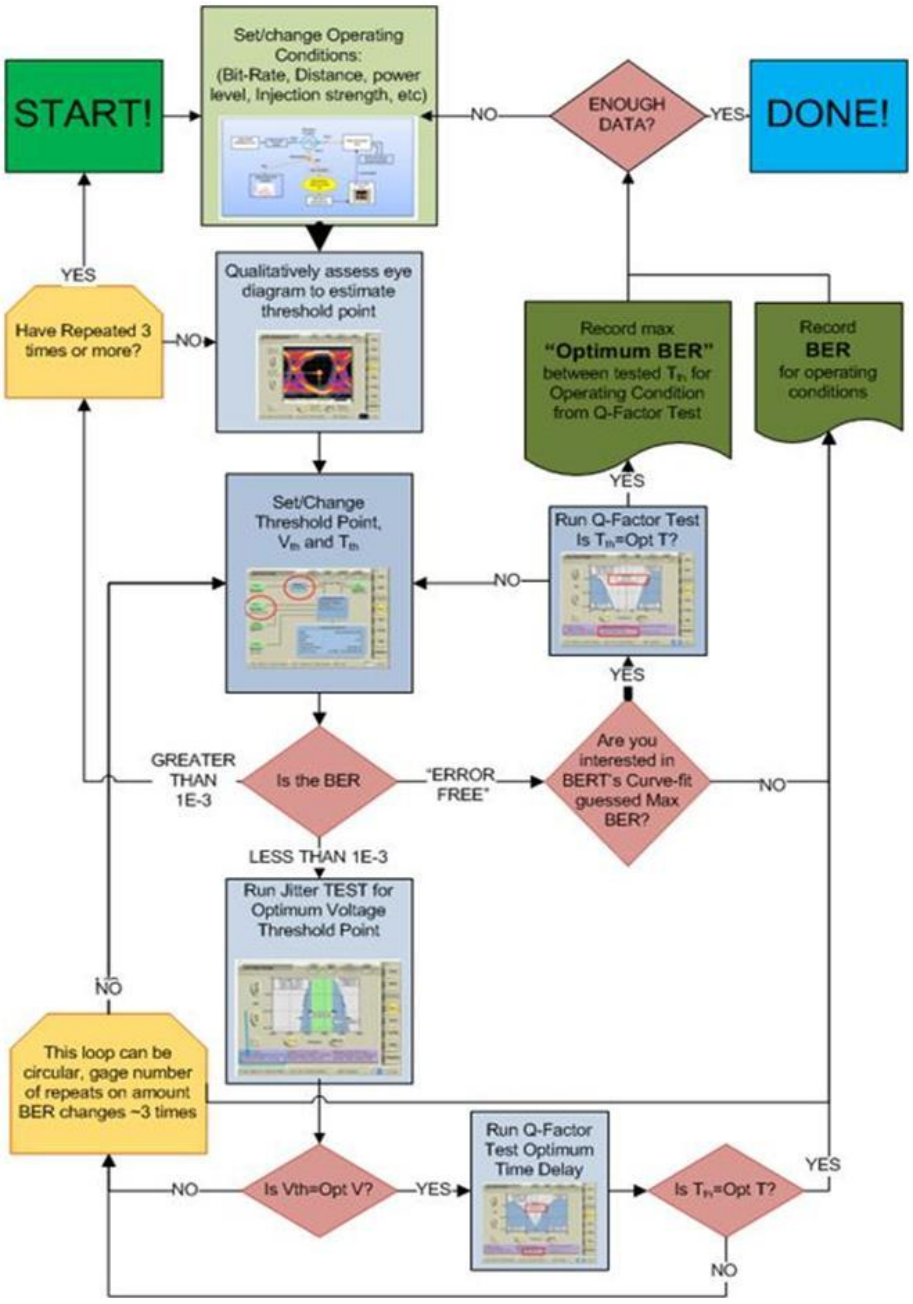

Figure 3.4: Decision process for detecting and recording best possible Voltage and Time delay threshold value and its associated optimal BER.

The first step is to set the communication operating conditions of interest. Those conditions include bit rate, modulation depth, injection strength, detuning frequency (≈0 GHz for stably-locked), optical power into the photo detector or transmission channel, center wavelength, fiber length, bit pattern (user defined or Pseudo-random bit sequences) and so on. After the physical adjustment to the laboratory setup is complete, the BERT is started. This will allow the BERTScope to measure and create an eye diagram which should be viewed for a qualitative assessment of the communication channel.

Several important metrics can be taken directly from the eye diagram including rise-time, fall-time, data unit interval, amplitude, and peak-to-peak jitter. The important characteristic to observe when finding the optimal threshold values is the location of the lowest probability of detecting a signal voltage and time; this location is in the darkest part of the eye. If a dark part of the eye does not exist, then the system cannot communicate and adjustments must be made to the transmitter's configuration. After finding the apparent 'optimal' location, the voltage and time points in the detector are set to these values and BER is measured.

If the BERT returns no errors, it will report "Error Free" and the number of seconds it has been running "Error Free." This does not mean that the communication channel has an infinitesimal BER though, it simply means that the channel has been observed to perform with better than one in however many bits had transmitted. Depending on the nature of the measurement being taken, it may be sufficient to simply

record “Error Free for X bits” where X is the number of bits transmitted. Otherwise, if an estimate of the optimum BER is desired, running a Q-factor test is appropriate.

The Q-factor test measures BER for different voltage values at the specified time delay. The BERTScope can automatically detect this time delay threshold, or, for better accuracy, can calculate it from a jitter test. The longer the Q-factor test runs, the deeper the BER measurement depth gets, and the closer the optimal BER estimate gets to the actual optimal BER value. This estimate can be helpful in finding the shape of the BER vs. power curve when calculating power penalty.

If a BERT for a given time and voltage threshold value generates a BER between 1E-3 and 1E-11 then the BERTScope measures the actual optimal BER within a few minutes. Note that measuring a BER better than 1E-12 in a 500 Mbps link takes over 33 minutes. While a BER better than 1E-11 takes 3 to 4 minutes and measuring a BER over 1E-10 it only takes 20 seconds. Thus, it is reasonable to measure the real BER if it is more than 1E-11. On the other hand, if it is more than 1E-3, the BER measurement will likely have too high a variance to be useful in reporting power penalty or bit-rate-distance product metrics.

For the bit-rate-distance product calculated in this experiment, the desired BER was 1E-9. So when metrics of 5E-10<BER<5E-8 were found, considerable time and effort were used to search for optimal threshold values.

3.3. P1 Dynamic

The overall objective of our P1 research was to determine the feasibility of encoding data onto the P1 state of the optically injected semiconductor laser. With this applicability determination in mind, the stability and noise of the modulated signal were of considerable interest.

The most important portion of this investigation/demonstration was to show that a significantly higher microwave sub-carrier frequency could be produced well beyond what the laser's electronics could support. This was accomplished in much the same way as the stably locked optical injection was accomplished. Relying entirely on the unstable dynamical state of positively detuned, strongly injected semiconductor lasers for the high frequency modulation, and relying on the baseband electronics for the relatively low-frequency data encoding.

Once a P1 state was reached, the bias current of the slave laser was large-signal modulated in much the same way as if it were stably locked. This created Consecutively Sequenced Spread-Spectrum communication symbols on a widely tunable carrier frequency, consistent with IEEE 802.11a wireless standard. Put another way, it was an optically carried, microwave frequency with a square wave envelope.

This optically carried On-Off-Shift-Keyed (OOSK) signal was transported over 50 km of fiber to the New Focus 1444 photo detector. The output of the photodetector was analyzed on an oscilloscope, electrical spectrum analyzer, and/or BERTScope to validate the P1 signal was indeed being modulated. Observing that, the optical signal was then fed into the ThorLabs photodetector with a cutoff frequency of 5 GHz and the low-

pass filter built in. It displayed the baseband interference consistent with Consecutively Sequenced Spread Spectrum communication symbols. This baseband interference is not usually a problem as CSSS signals are usually transmitted wirelessly where no baseband communications happen. To employ CSSS over a fiber link a negative feedback will need to be employed to the baseband signals receiver so it can de-convolve the CSSS signal with its own. This added complexity may prove to limit CSSS or other forms of OOSK microwave subcarrier signals in telecommunications. Other forms of microwave communications exist that do not interfere with baseband communications.

The first stage of a coherent heterodyne detector was created for the output of the photodetector and a 3 kHz sinusoidal envelope carried by the 500 Mbps square-wave pulses was observed as expected on an oscilloscope. Phase locked-loops have been demonstrated with bandwidths on the order of 10s of megahertz, so this signal is ready for the next stage of the coherent demodulator. Further demodulation work should be done including electronic envelope detection, multi-phase heterodyne detection, and all-optical envelope detection; these ideas will be discussed further in chapter 5.

An impediment to using the P1 frequency as a communication subcarrier on an optical signal is the inherent instability of the P1 state. Angular acceleration on the order of 100 MHz/s^2 has been observed on the electrical spectrum analyzer while the P1 state was un- modulated. The P1 state seems to stabilize if the **P1** frequency is equal to an **odd-integer multiple** of **one-half** the **Bit-Rate**. Stated another way, the symbol period should allow for an integer number of ½ P1 wavelengths.

Two competing hypothesis explain this observation. The first is that the high quality of the BERTScope actually allows a small harmonic (the 31st harmonic of 500 Mbps square wave is 7.75 GHz for example) of the square wave PAM baseband signal (see appendix A) to be created and passed through the bias tee onto the slave laser diode, and this small-signal is enough to stabilize the P1 frequency. Further testing and analysis is required to accept or reject this hypothesis.

The other hypothesis is that the large-signal fundamental harmonic of the modulating square wave is causing the P1 frequency to completely stop and restart again. The high-voltage state does not last a long for the P1 state to wander off frequency before being shut back off when a low-voltage modulation occurs. These two competing hypothesis will be difficult to deconvolve as a perfect square wave cannot be created without the 31st harmonic and an exclusive fundamental modulation cannot be generated without changing the injection strength and detuning frequency of the injecting lasers. While a local oscillator and an RF amplifier can create a pure, large-signal sinusoid to directly modulate the bias current, it will be unable to couple without changing the injection strength and detuning frequency. When the sinusoid is high, the injection strength will be lower and the detuning frequency will be lower than when the sinusoid is in a low state.

The stabilization of the P1 frequency in this manner has a margin of error that appears to be proportional to the amount the P1 frequency wanders when it is not being modulated. To perform that experiment the electrical spectrum analyzer was set in ‘100 sweep average’ mode at a relatively fine 100 kHz resolution bandwidth and allowed to

run for several minutes. A small plateau was measured with two spikes on either edge. As long as a modulation rate with an odd-multiple of the fundamental harmonic fell inside those two spikes was used, the P1 frequency was found to stabilize.

4. Analysis and Results

This chapter is broken into two parts, the first discusses the measurements taken under optically injection-locked (OIL) conditions while the second presents observations made under P1 dynamical injection conditions. Since OIL affects both the modulation response (S21) and the linewidth of the directly modulated laser, the OIL discussion focuses largely on characterizing how improvements to each (S21 or linewidth) affect the optical communications link. The results of our work showed that OIL improved the bit-rate-distance product of the Fabry–Pérot laser under investigation by over 25 times.

The majority of the P1 measurements performed investigated the effects produced by varying the modulation parameters (modulation rates, modulation depths, and P1 frequency range) and the ease of shifting/modifying the microwave subcarrier frequency. The P1 setup produced consecutively sequenced spread spectrum (CSSS) communication symbols that were not orthogonal to the baseband communication symbol. This baseband component was filtered out electrically after the photodetector to prepare it for transmission wirelessly and demonstrate its potential as an orthogonal communication channel.

4.1. Stably Locked Optical Injection Improvement

This section's focus is to experimentally demonstrate and theoretically describe improvements to the bit-rate-distance product with respect to chromatic dispersion and wavelength chirp of an injection-locked Fabry–Pérot laser diode over different lengths of SMF. After characterizing the free-running capabilities and distance limitation of the

Fabry–Pérot laser, the bit-rate-distance product is shown to improve by a factor of 25 under stable OIL. The data shows that the bit rate-distance product improvement is due to both the suppression of the unlocked multi-longitudinal modes of the Fabry–Pérot laser and chirp resulting from the large-signal modulation driving the laser.

Observations show a faster rise-time, reduced jitter, suppressed overshoot, and diminished ringing in the eye diagrams collected under OIL, with only a slight degradation in modulation efficiency. These observations confirm performance expectations from the S21 plots published for other systems in the literature. Further, the observed changes to the eye diagrams are in agreement with expected results. These include variations in the ringing and overshoot observed in the eye diagrams collected which coincided with changes in detuning frequency, an anticipated result given the dependence of the shape of the S21 curve on the detuning frequency.

Our work shows the ability to couple two devices, one designed for high-speed modulation and one designed for single-mode operation, in order to yield a transmission system far more capable than either device operating in singular fashion. In this experiment, the high-speed device is a multi-mode slave laser capable of a 4.5 Gbps data rate when connected in an end-to-end configuration (0 km) using a 7-bit pseudo random sequence (PRBS-7) of unipolar rectangular PAM symbols; at this data rate and bit sequence, the bit error rate (BER) has been both measured “error free” and 6.8E-11 over one minute of operation.

While capable of high-speed operation in end-to-end configuration, the multi-longitudinal mode nature of the device and the associated fiber dispersion (≈17.4

ps/nm·km) introduced by SMF at 1550 nm limits the transmission distance capability as described in Chapter 2. Physically, the microwave modulation is on each of the laser's longitudinal modes and each propagates through the fiber at a slightly different velocity; upon arrival at the photodiode, the modulated signal is, in general, out of phase and the modulation washes out limiting the transmission distance. To counter this limitation, the modulation speed must be reduced accordingly or a dispersion mitigation approach must be implemented. The optical power spectra of the free-running Fabry–Pérot laser where the mode peaks have been fit using a Lorentzian function in order to determine the FWHM is given in Figure 4.1.

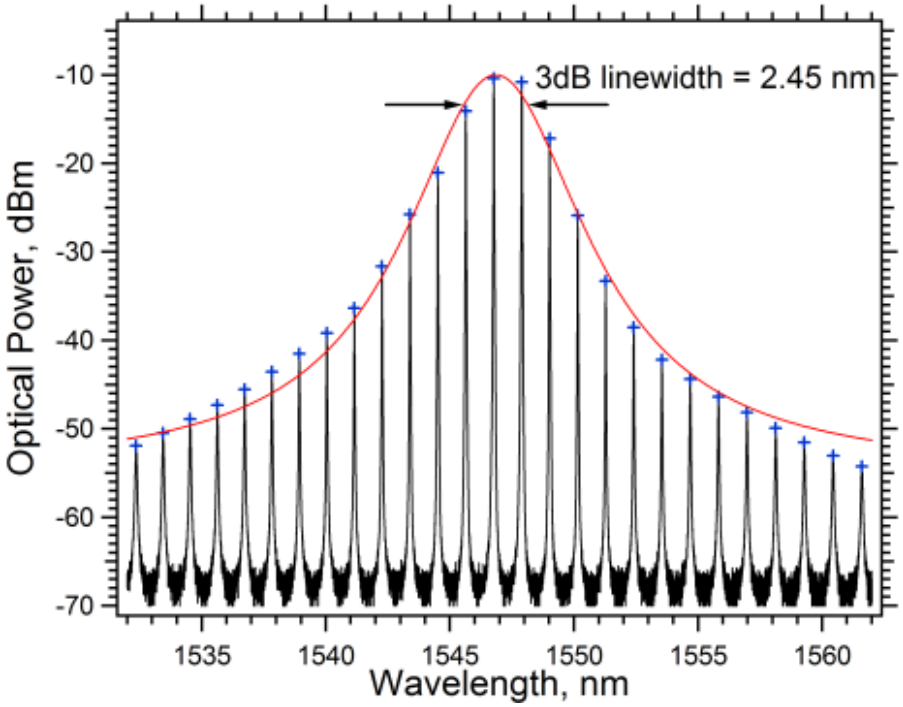

Figure 4.1: Optical power spectra of the free-running Fabry–Pérot laser with the mode peaks fit with a Lorentzian in order to determine the full width half maximum.

The detrimental impact of dispersion and wavelength chirp over 10 km is illustrated in Figure 4.2, where the device is modulated at 1 Gbps. An unacceptable bit error ratio (BER) of 4.6E-4 was measured, indicated by the green (low occurrence) signal traces covering the eye opening. Over 10 km, the total dispersion is calculated to be 0.43 ns (17.4 ps·nm-1·km-1 x 10 km x 2.45 nm) using equation (1), giving a maximum non-return to zero bit rate of 2.3 Gbps at this distance (unipolar rectangular PAM is non-return-to zero, see appendix A). This calculation and the unacceptable BER at 1 Gbps and 10 km points to the bit rate-distance product being limited strongly by **both** chromatic dispersion and wavelength chirp. The bit-rate-distance product of the free-running laser was experimentally determined to be 7.5 Gbps·km for a BER threshold of ≈10E-9.

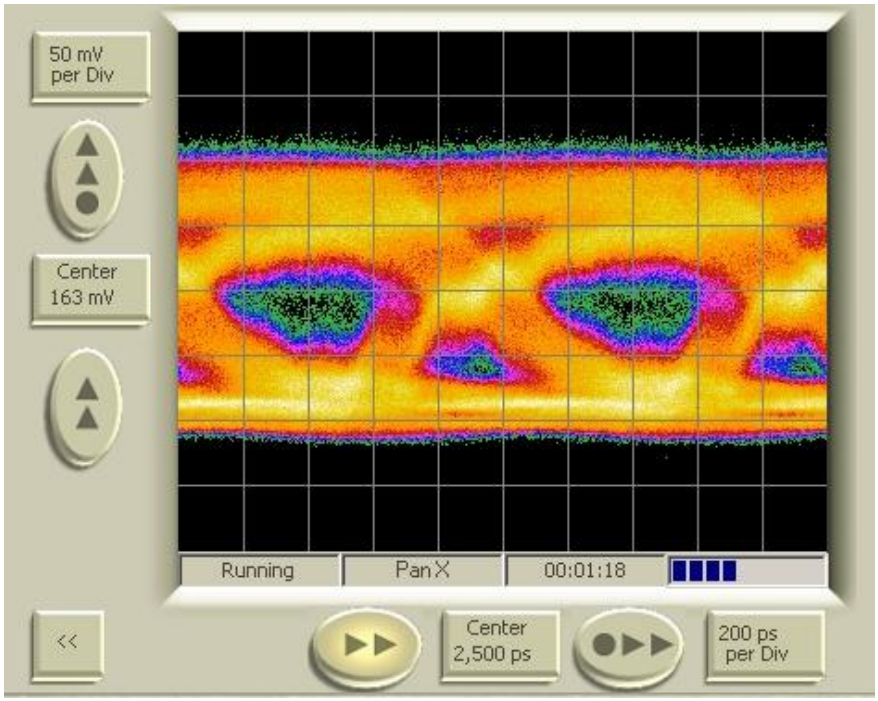

Figure 4.2: 'Closed eye' over 10 km of SMF-28 and 1 Gbps using PRBS-7 unipolar rectangular PAM direct modulation where max BER measured was 4.6E-4.

The maximum achievable bit rate for the injection-locked laser over 60 km was measured to be 3.125 Gbps with a BER better than 1E-12 using a PRPS7 signal. The resultant eye over 60 km at 3.125 Gbps is shown in Figure 4.3 on the left. The maximum bit-rate-distance product is calculated to be 187.5 Gbps-km, an improvement of 25X over the free-running case for the same BER. Figure 4.3 on the right, shows the optical spectra under stable OIL where the SMSR was greater than 45 dB. Continued work showed an insensitivity of the BER over varied wavelength detuning conditions given that stable OIL (SMSR > 35 dB) was maintained. Contrary to expectations, the modulation response of the injection-locked laser showed no improvement over the free-running case, leading to the conclusion that the RC parasitics associated with the diode laser mount and package are the primary limiting factors in the modulation speed of the injected laser investigated in this work.

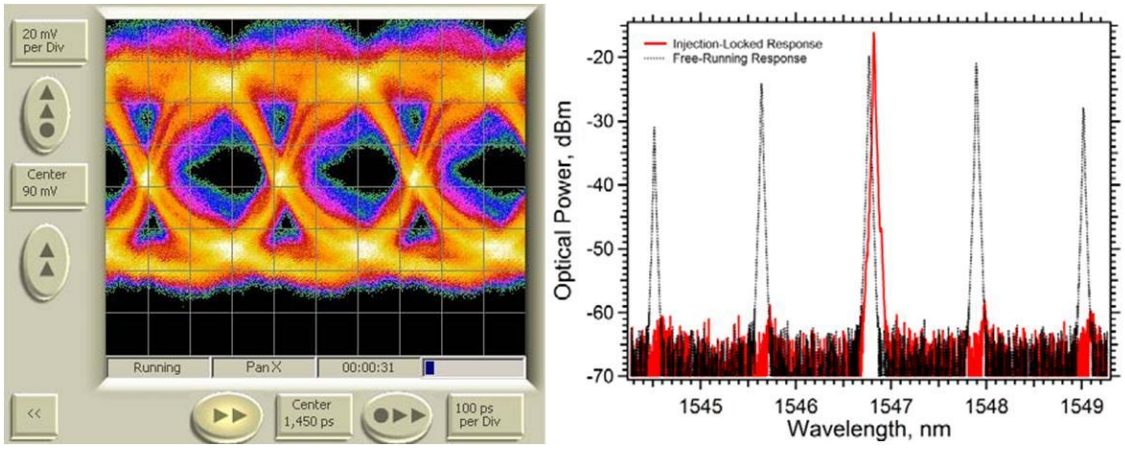

Figure 4.3: Left, Eye diagram observed using a PRBS-7 bit sequence at 3.125 Gbps over 60 km of SMF. The data unit interval is 320 ps, and the rise, fall, and peak-to-peak jitter times are measured by the BERT to be 137 ps, 154 ps, and 137 ps respectively. Right, Optical power spectra over a 5 nm span showing the 45 dB SMSR achieved under stable OIL. The wavelength detuning was 50 pm ($\Delta\lambda = \lambda_{master} - \lambda_{slave}$). The external injection ratio, measured at Port 1, was held constant at 5.05 dB or ($10Log_{10}(P_{master}/P_{slave})$).

Figure 4.4 further illustrates the improvements to the communications link achieve, a side-by-side comparison of measured eye diagrams for free-running and OIL lasers under consistent modulation conditions.

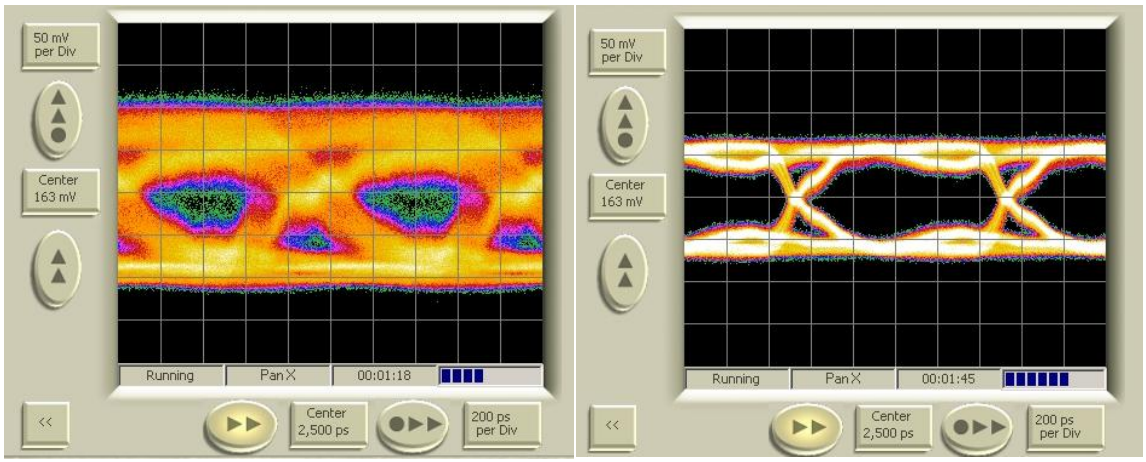

Figure 4.4. (a) Closed eye over 10 km of SMF-28 and 1 Gbps using PRBS-7 where the bit error ratio was 4.6 x 10-4. (b) Open eye under stable OIL over 10 km of SMF-28 and 1 Gbps using PRBS-7; the measured BER was greater than of 10-11.

4.1.1. Characterizing the Free-Running Operational Parameters

The first step to determine the bit-rate-distance product improvement for a Fabry–Pérot laser under stably locked optical injection is to first characterize the laser under free-running conditions. The objective is to find that marginal point at which a very small increase in bit-rate or distance pushes the BER to an undesirably high level and below which, little BER benefit is achieved. Figure 4.5 shows the complexity of finding this marginal point because of the nonlinear dependence of BER on bit-rate and between BER and distance. Notice how a small change in fiber length, only 700 meters, resulted in a significant change to the maximum modulation rate between 1km and 1.7 km, while

between 11.7 and 12.7 km the difference in bit-rate for the same BER is minimal. The minor increase in bit-rate at 0km compared to 1km further illustrates the hypothesis that the system is being modulation-response limited at low-distance, high-data-rate conditions. Notice also that a small change in bit-rate between 1.5 and 2 G bps for 1.7 km of fiber resulted in dramatic increases in BER while between 2 and 2.5 Gbps, the change was relatively minor.

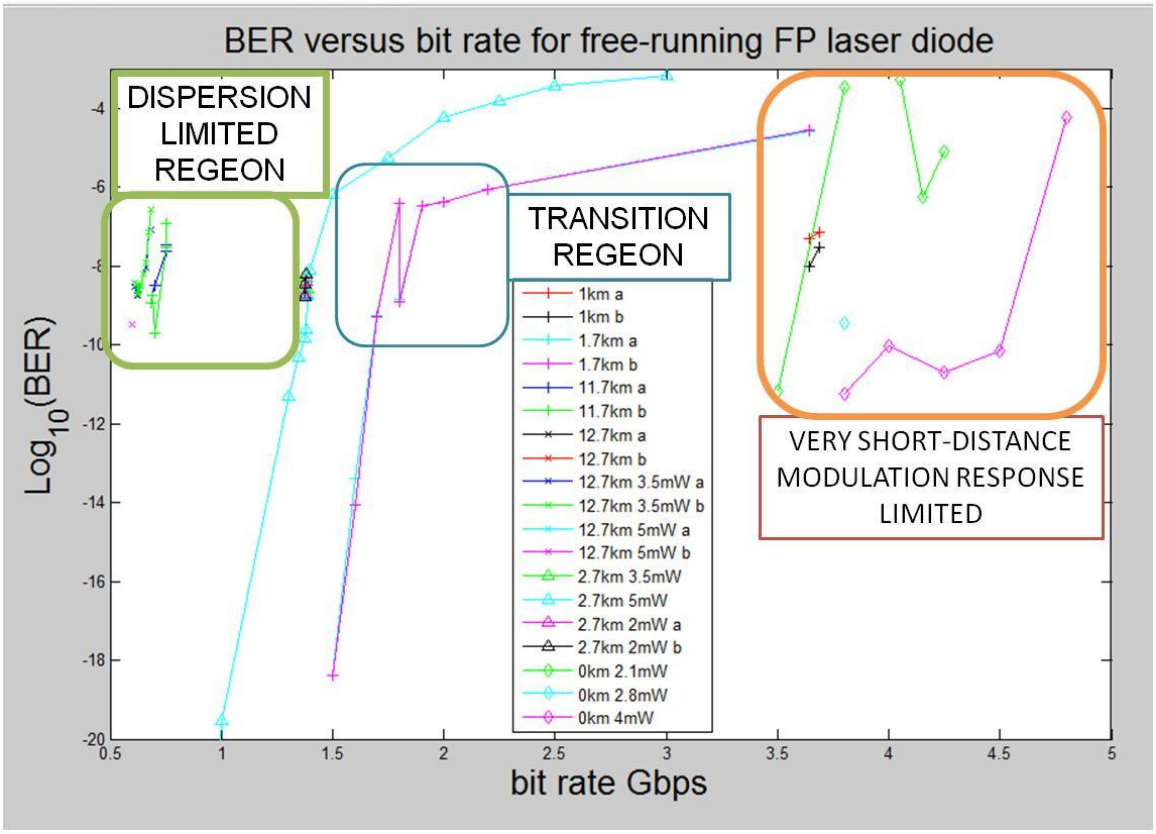

Figure 4.5: BER compared to bit rate for the same Fabry–Pérot laser under free-running conditions.

An interesting phenomenon, likely coincidental, occurs at modulation rates near the trade-off between modulation-rate limiting conditions and dispersion limiting conditions. Here, there appears a region where a slight reduction in bit-rate actually increases the BER instead of decreasing it. This appears to be due to the relaxation oscillation frequency, with a likely minimal BER where an integer number of relaxation oscillation wavelengths can fit inside a single communication symbol. This laser diode appears to have a relaxation oscillation frequency between 7.5 and 8 GHz as shown in Figure 4.6.

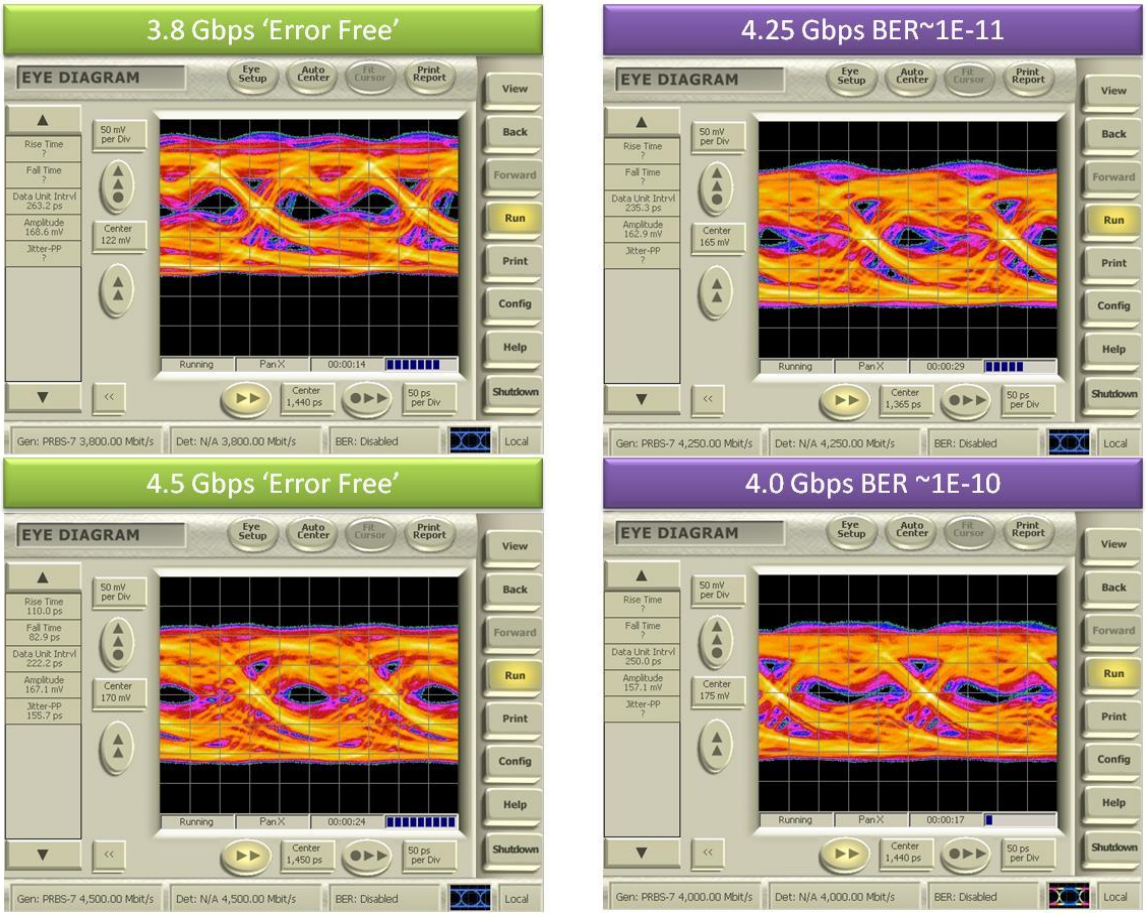

Figure 4.6: BER's sensitivity to relaxation oscillation frequency of approximately 7.6 GHz.

At the data rate of 3.8 Gbps, two full relaxation oscillation periods fit in a single communication symbol, implying a relaxation oscillation frequency of 7.6 GHz, however, time is required for the laser to transition into and out of the relaxation oscillation period, so the free-running relaxation oscillation frequency is slightly above 7.6 GHz. Other data rates represented in Figure 4.6 near 3.8 GHz exhibit eye-closure due in part to the inability to fit an integer number of frequencies in a single bit interval. Figure 4.6 also shows how mode partition noise, expected in the modulation of any multi-mode laser diode appears, as expected, in eye diagrams.

4.1.2. OIL Laser's Back-to-Back Bit-Rate Limits

Evidence supports the hypothesis that the modulation response of the electronic packaging, rather than that of the laser diode, is the primary limiting factor in back-to-back bit rate testing and fiber dispersion is the dominant limiting factor only over significant distances, especially under free-running conditions. Support for this hypothesis comes from the fact that the 3-dB cutoff of a laser diode is often located near its relaxation oscillation frequency, which, from Figure 4.6, is likely around 7.6 GHz for this laser. If the modulation response of the electronic packaging is indeed the limiting factor (parasitic capacitance of the electronic packaging inhibit operation to ≈5 Gbps) then any modulation response improvement that the laser diode experiences through the optical injection of this laser using its current electronic mount and packaging will not be reflected in our BER metrics. However, once the modulation rate is within the

electronics' pass-band, the OIL induced improvement to dispersion and chirp will become obvious. Figure 4.7 shows significant degradation of the free-running laser's ability to communicate over 10 km due to optical dispersion.

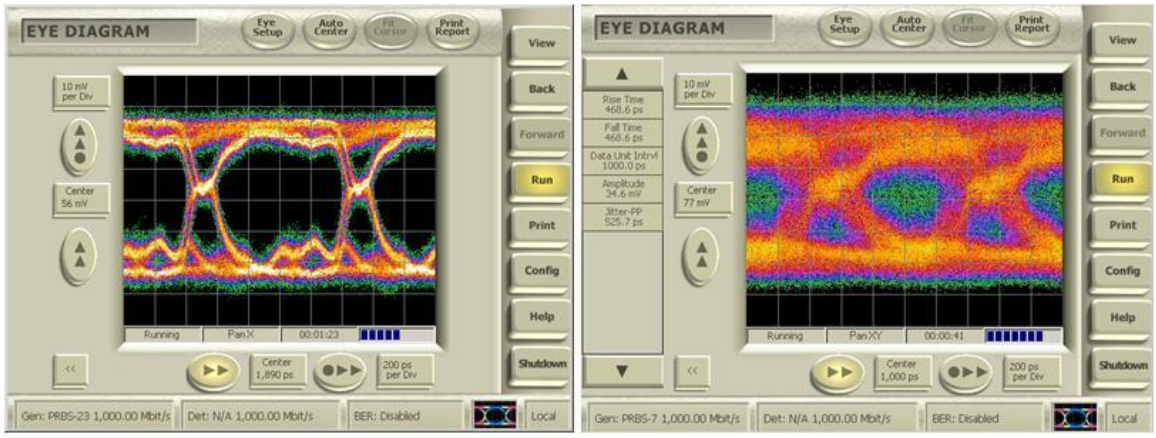

Figure 4.7: Significant EYE degradation due to fiber dispersion on the free-running laser: left 0km, right 10 km.

Figure 4.8 directly compares the performance of a free-running (left) to an optically injection-locked (right) laser diode communicating at the edge of its tolerable BER range through 10 km of fiber. Both experiments show nearly the same BER but for apparently different reasons and with the OIL setup communicating over 4 times as fast.

The eye diagrams in the left column of Figure 4.8 illustrates how a free-running laser diode modulated at 1Gbps encounters significant degradation due to dispersion while the modulation response is still quite good. This is apparent by comparing the amplitude of the high-frequency bit pattern {01010101} to the amplitude of lower-frequency bit patterns {00001111}. Since the amplitudes are nearly equal, good

modulation response at 500MHz. The thick or high variance line drawn for the eye diagram indicates that dispersion limits this communication signal.

A quadrupling of the bit rate for the OIL case is observed in the right column of Figure 4.8 and indicates a modulation-efficiency limitation rather than degradation caused by dispersion. Again comparing the highest frequency to the lowest frequency bit-toggle eye diagrams, the opposite is now seen. At 4.25 Gbps significantly attenuated and asymmetric eye is produced, implying poor modulation response at the highest fundamental frequency of 2.125 GHz. The low variance of the "eye line" indicates robustness against channel dispersive effects unlike its free-running counterpart. The conclusion is that a direct comparison of a bit-rate-distance product between these two tests would result in the unfair comparison of a dispersion-limited communication system to a modulation-response-limited system, and would be inappropriate.

Figure 4.8 supplies further evidence supporting the hypothesis that it is the electronics, not the laser diode, limiting the modulation response. All the OIL tests were performed using the same slave laser electronic packaging and are therefore subject to the same electric parasidics. Under OIL BER results, similar to those obtained for the 0 km, 2.1 mW, free-running, laser of Figure 4.5 (green diamonds) are found. This similarity implies that the effects of chirp and dispersion on the OIL signal are not significant when compared to the modulation limitations of the electronics supporting the OIL laser. Therefore, to make a bit-rate-distance product comparison between OIL and free-running lasers, a length of fiber longer than 10 km is necessary and a bit-rate below 4.25 Gbps is required.

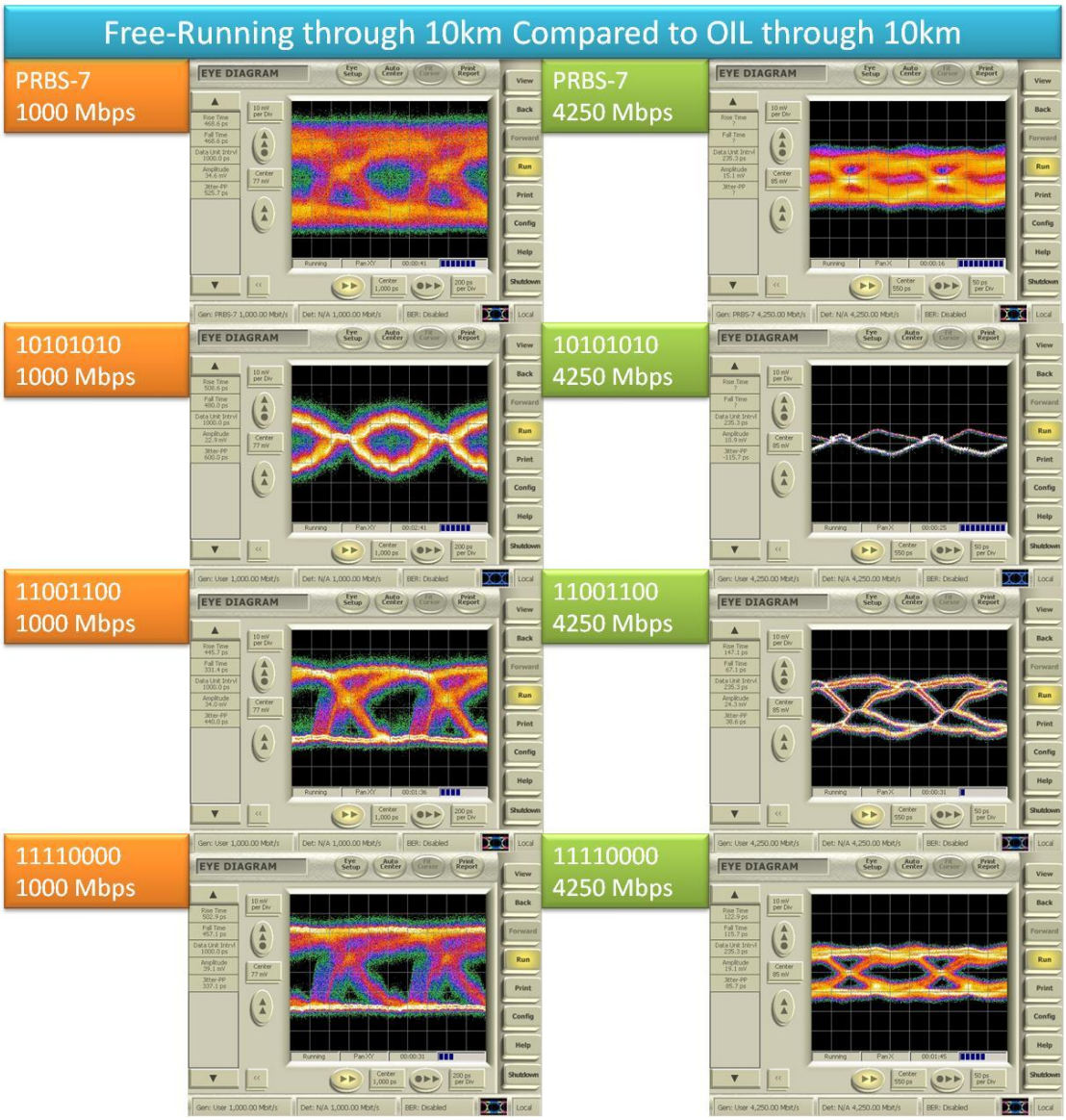

Figure 4.8: A time domain comparison between the maximum bit-rate for 10 km fiber length indicates the free running laser (left) is dispersion limited while the OIL laser (right) appears to be modulation response limited.

Figure 4.9 shows a comparison of a laser diode under free-running and OIL for a high bit-rate condition in the end-to-end configuration. By studying this figure, the effects produced by OIL are highlighted along with the complexity of OIL.

Predictably, the mode-partition noise is absent in the OIL eye. The relaxation oscillation frequency, obvious in the free-running eye is also missing in the OIL eye. This is either due to the dampening effect of heavy optical injection or to the enhanced relaxation oscillation frequency which is a function of detuning frequency and injection strength. In this case, the detuning frequency was maintained close to zero which theoretically yields a 'flat' S21 modulation response. The closely-spaced colors of the OIL eye's line indicate that the steepness of its BER contour is much higher than its free-running counterpart.

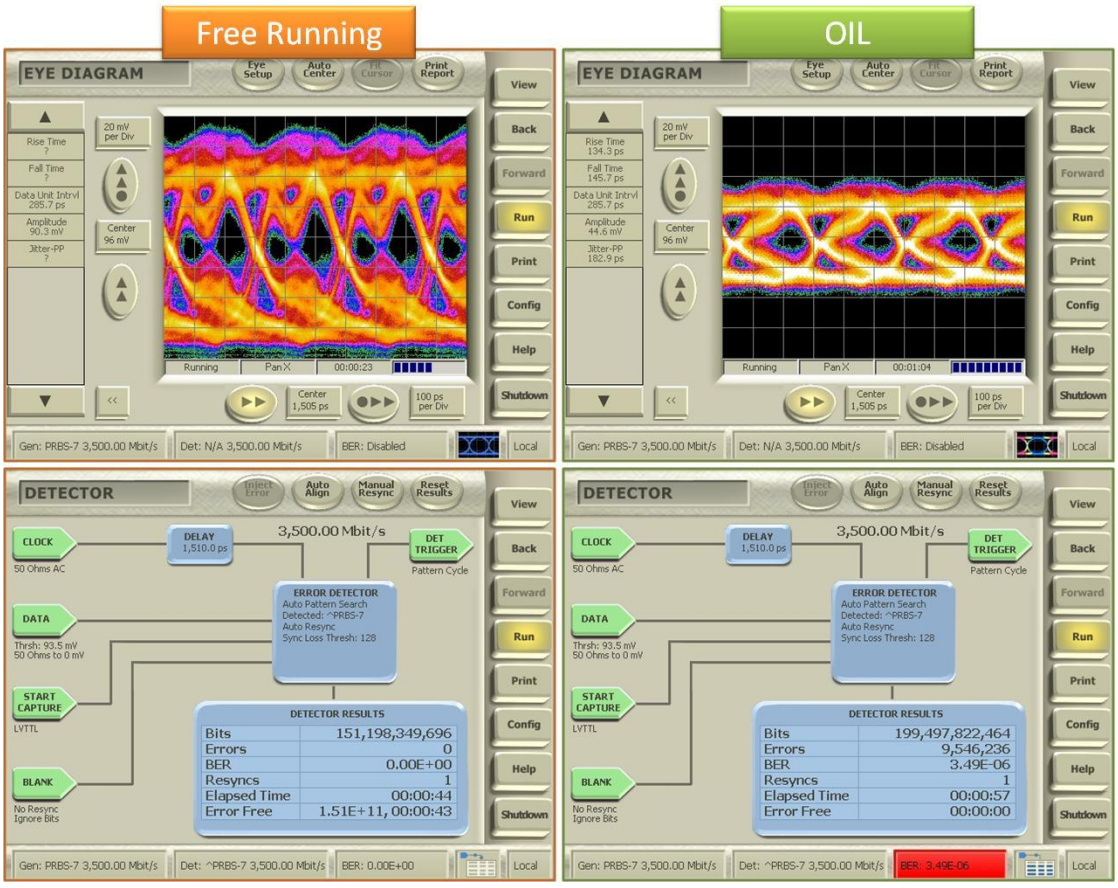

Figure 4.9: Qualitative comparison (top) and BER measurement (bottom) of free-running and OIL laser diodes under 3.5 Gbps modulation.

While both eyes in Figure 4.9 were measured with the same optical power at the photo detector, as indicated by the same threshold voltage, the modulation depth is not the same, as indicated by the relative shortness of the OIL eye compared to the free-running eye. This indicates lower modulation efficiency for the OIL case, a metric which, all-else-equal, counts against the direct modulation capability of the OIL laser. Modulation efficiency is typically overlooked as an insignificant figure of merit in telecommunications.

Digital telecommunications receivers typically measure the average DC shift of an incoming signal and subtract it before performing a sign comparison after its latch-and-hold (see Appendix A). This typical application makes it customary to measure eyes of the same eye height instead of same signal power in telecommunication applications. This is due to the inability in most transmission lines to transmit DC. If that metric is to be used in this case, the OIL signal will benefit significantly and prove to be an even better performer (known from other tests not shown in this figure). However, since the DC optical power was necessary to form the signal in the first place, metrics reported here count the DC-shift against the OIL signal and still show bit-rate-distance product improvement under OIL.

The discussion surrounding issues related to modulation efficiency exemplifies how important it is to parameterize OIL for optical communications applications. A slight change in either the detuning frequency or injection strength can have a dramatic effect on the modulation efficiency which translates to eye-height and BER. Depending on the application, the trade-off between pass-band flatness and signal strength will determine

the optical injection strength and detuning frequency appropriate for a specific application.

4.1.3. Dispersion Limits for OIL Lasers

Back-to-back modulation tests are not able to perform telecommunication capability comparison between two laser diodes because there is an insufficient distance to multiply the bit-rate by to report the bit-rate-distance product or observe dispersive effects. Figure 4.10 shows the bit-rate-distance product for the free-running Fabry–Pérot laser diode used to plot Figure 4.5. The maximum bit-rate-distance product measured with a BER below 1E-9 is the point at which the effects of the relaxation oscillation frequency helped the BER, bit-rate-distance product =8.19 Gbps·km for a BER of 2E-10. Most tests revealed a dispersion limited bit-rate-distance product value between 7.5 Gbps·km and 8.4 Gbps·km for BER between 5E-10 and 1E-8.

To characterize the effects of dispersion on the OIL laser system, the bit rate was held constant while the fiber length was increased. As indicated in Figure 4.9, it can be somewhat ambiguous whether optical injection is advantageous at very-short distances (given the electrical limitations of the laser package). However dispersion effects in the free-running laser can be readily seen at the relatively short metropolitan area distance of 2.7 km where a power penalty between 0.5 and 2 dBm can be measured depending on the BER range of interest (higher power penalty for lower BER due to statistical shape difference between OIL and free-running eye lines). At 2.7 km, however, dispersion characteristics are still insignificant in comparison to modulation-rate parasitic in the OIL

laser. To measure a bit-rate-distance product that is dispersion limited, the fiber length has to be increased.

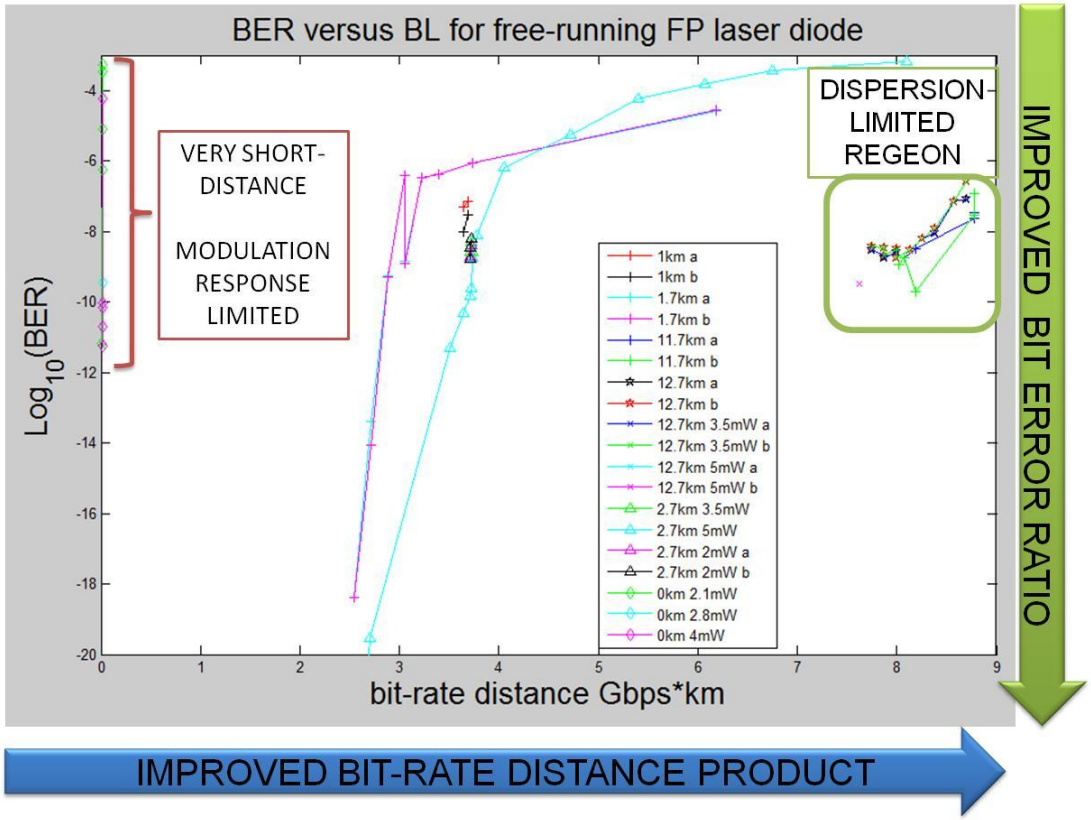

Figure 4.10: BER to bit-rate distance for Free Running Fabry–Pérot laser.

The dispersion-induced power penalty was found to increase more rapidly for increased lengths of SMF for the free-running laser than the OIL laser. This advantage of optical injection locking was best highlighted by the characterization of a link where no amount of optical power could overcome the deleterious dispersive effects when the free-running laser was used as the transmitter while the same laser under injection locking was found to still be dominated by electric modulation parasitics. In order to compare the dispersive effect of the OIL laser to the dispersive effect of the free-running laser, a two-

step measurement was made, one that compared the power penalty of the free-running laser through a shorter length of fiber to an OIL laser through the same shorter length. The second measurement compared the performance achieved when the OIL laser was used to transmit through the longest SMF we had on hand to the OIL through the short-distance.

Figure 4.11 shows these three BER versus power curves. Two curves were through 2.7 km, one OIL and one free-running. The third was OIL through 61.7 km which was not long enough to fully dispersion-limit the OIL laser. As a consequence, the bit-rate was also increased from 1 Gbps to 2.5 Gbps. At one location, around BER=1E-10, the power penalty suffered by the OIL signal through 61.7 km equaled the power penalty suffered by the free-running laser through 2.7 km of fiber. This allows a direct comparison between the two systems at that BER. Here the free-running laser enjoys a bit-rate-distance product of 2.7 Gbps·km while for the same BER and power level for the OIL setup resulted in a bit-rate-distance product of 154.25 Gbps·km for a 57.12 fold improvement. This is dependent on the selected BER and power level. Deployed commercial systems insist on lower BER, which for this system would show an even higher improvement for OIL over free-running lasers.

The divergence between the OIL and free-running lines at low predicted BERs in Figure 4.11 indicates a different line-shape in the free-running laser's eye diagram which reduces the benefits to linear amplification. This divergence implies that the OIL signal needs fewer digital repeaters, where the communication symbol is completely demodulated and re-modulated to overcome simple channel impedance. This is because it

can handle more linear amplifiers before its noise floor interferes too much with its signal.

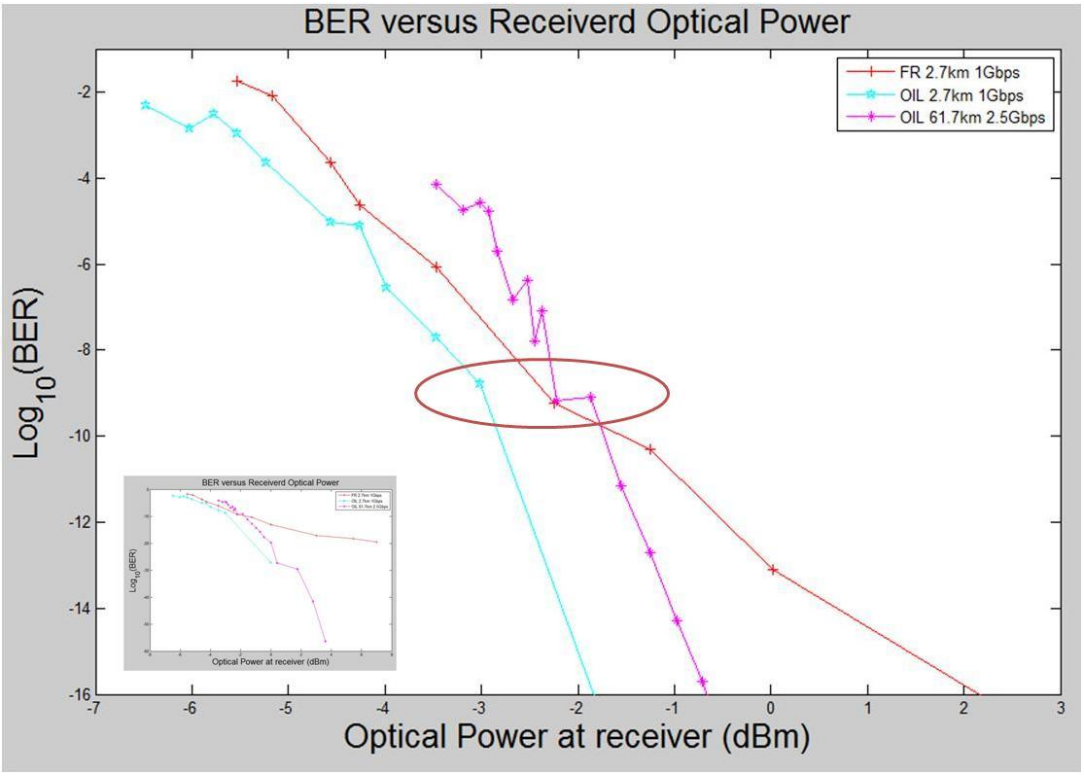

Figure 4.11: BER versus optical signal power plots allow power penalty comparison between operating conditions. Inset shows how plots diverge as predicted optimum BER decreases and the circled area indicates the region where the performance was compared to each other.

Quantitatively, the three points circled in Figure 4.11 are comparable in that they have the same BER following the procedure described in Figure 3.4. Qualitatively, however, they appear quite different from one another. Figure 4.12 provides a side-by-side qualitative view of the communication signal using eye diagrams. The overshoot associated with the relaxation oscillation frequency is present in the free-running case, while the reduced modulation efficiency is observable in the OIL cases. The eye opening

obtained by sending the 2.5 Gbps OIL laser through the full-length of fiber has degraded because of electric parasitics and dispersion related limitations.

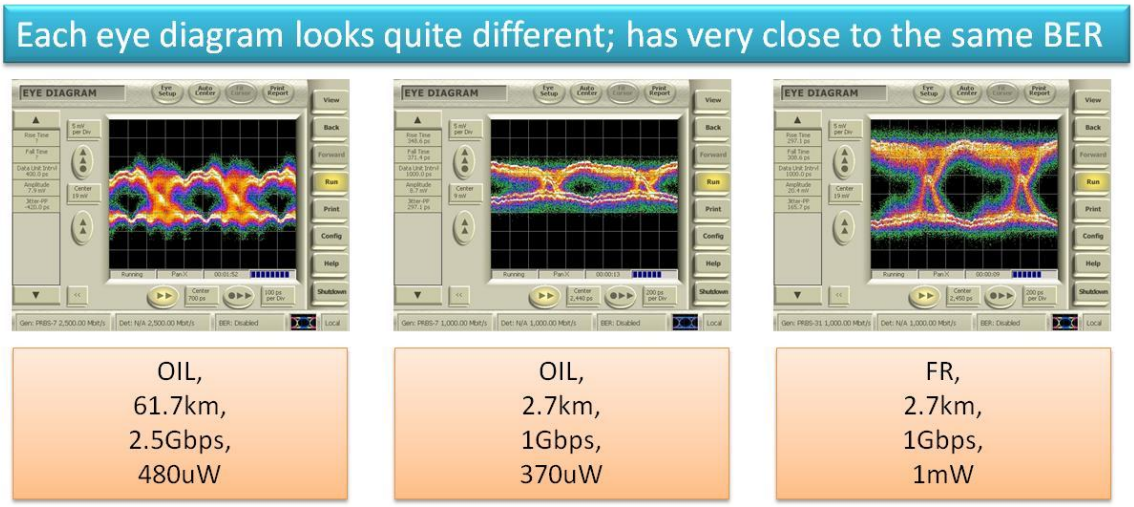

Figure 4.12: These 3 eye diagrams coincide with the three points compared for power penalty between long-distance optically injection-locked (left) short-distance OIL (center) and short distance free-running (right).

4.1.4. OIL Conclusion

In this work we demonstrated an improvement of at least 23 times the bit rate-distance product of a commercial Fabry–Pérot diode laser using OIL. This improvement is attributed to the ability of OIL to improve the SMSR while also reducing wavelength chirp under direct modulation. Using commercial diode lasers, this work proves the ability to couple two devices, one designed for high-speed modulation and one designed for single-mode operation, in order to yield a transmission system far more capable than a similar system using either device alone. Temperature tuning the master laser to each of the Fabry–Pérot modes of the slave laser provides a simple route to WDM. The ability to enhance the modulation bandwidth of multi-mode devices and the bit rate-distance-

product demonstrated over 61.7 km of SMF in this work, shows that OIL of Fabry–Pérot lasers is viable approach towards the realization of a high-speed, long distance directly modulated transmitter.

4.2. Encoding the P1 Dynamic of Optical Injection

The P1 dynamical state (P1), located at the positive detuning edge of the stably locked region, allows the generation of widely tunable microwave frequencies without the use of traditional high-frequency support electronics. This research generates consecutively sequenced spread spectrum (CSSS) communication symbols at widely tunable microwave subcarrier frequencies. These microwave frequencies start as low as the free-running relaxation oscillation frequency just shy of 8 GHz and continue at least to 26 GHz, the cutoff frequency of standard SMA connected coaxial cables.

This high frequency modulation was accomplished using the same support electronics used in our optical injection-locked (OIL) experiments which have cutoff frequencies around 5 GHz. This ultra-wideband on-off-shift-keyed (OOSK) highly tunable signal modulation required no electrical local oscillators except those required for baseband symbol generation. These symbols are consistent with early WiFi (IEEE 802.11A) standards and were transmitted through 50 km of standard optical fiber (SMF-28) on a 1550 nm optical carrier. The results presented in this section demonstrate the P1 dynamic's suitability for the rapidly growing interest in radio-over-fiber communications.

This section starts with general observations and a brief discussion of the free-running or non-modulated P1 signals generated all-optically. Specifically, we focus on data captured from the Optical Spectrum Analyzer (OSA) and Electrical Spectrum

Analyzer (ESA). Time-domain images of communication symbols entering and exiting the P1 state, either from the familiar eye analyzer or from an oscilloscope are presented along with accompanying ESA plots.

This research is unique to the field in that it applies a large-signal baseband modulation to the slave laser's bias current. We also report, for what we believe to be the first time, P1 frequency stability in the context of baseband modulation rate, finding that the P1 frequency stabilizes when it is equal to a harmonic of the fundamental of the modulation rate.

4.2.1. The P1 State

The P1 oscillation state is described as the condition where the slave laser is locked to the injected field and the coupled system oscillates at the injected frequency (f_{inj}) with sidebands at frequencies of $f_{inj} \pm f_r$, where f_r is the enhanced resonance frequency of the optically injected laser. The resultant electric-field of the optically injected slave laser oscillates un-damped towards a steady-state frequency as in a free-running or stably locked semiconductor laser. An example of the P1 state, and its associated electrical power spectrum after the optical signal is passed through a high-speed photodetector, is given in Figure 4.13. These figures, captured with the direct large-signal slave modulation turned off, show the un-damped and enhanced resonance frequency of the injected Fabry–Pérot slave laser, and the microwave frequency whose peak power over average noise power is 30.8 dB.

The optical and corresponding electric spectra shown in Figure 4.13 is an appropriate example of a radio-over-fiber signal that meet the International Telecommunication Union's (ITU) optical wavelength/bandwidth extent allowed for a single wavelength-division multiplexed (WDM) band. The ITU has separated the popular communications wavelengths surrounding 1310 nm and 1550 nm in 50-GHz-wide bands for standardized optical filters, carrier wavelengths, routers, and other communications equipment. As seen on the left in Figure 4.13, harmonics that fall outside of this band (-25 to 25 GHz) are suppressed more than 30 dB and the electric extent is easily contained within the 50 GHz as shown. The ESA reports only the positive half of the electric spectrum, this is because negative frequencies equal positive frequencies in power spectral density, (see Appendix A).

An additional item of interest is the P1 microwave frequency is orthogonal to baseband. This OOSK modulation of the P1 tone creates an average optical intensity change from P1 on state to P1 off state. That average intensity modulation projects energy into baseband, causing some baseband interference.

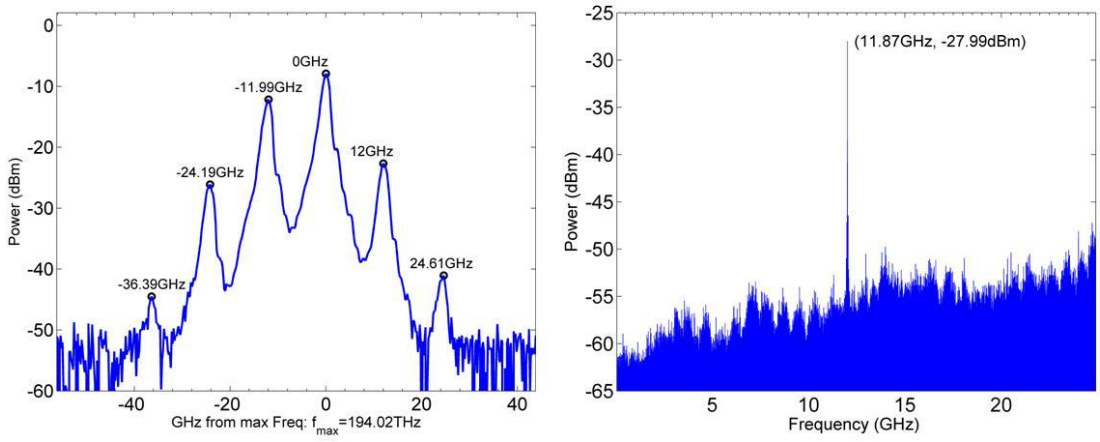

Figure 4.13: Left, optical spectra of the period one state carrying an 11.87 GHz microwave frequency shown on the right.

As discussed in Chapter 2, optical injection provides a method of single-sideband modulation. Figure 4.14 where the optical spectra of the P1 signal appears to be almost exclusively single-sideband modulated. It is important to note that the same average power is present in the P1 spectra as in the free-running spectra and the optical spectrum widens appropriately to accommodate the modulation bandwidth. In order for the spectra to widen, the optical power has to come from somewhere; and in this case it came from a seemingly small but nevertheless significant reduction in peak amplitude as well as the suppression of the remaining non-injected Fabry–Pérot modes, not shown in Figure 4.14.

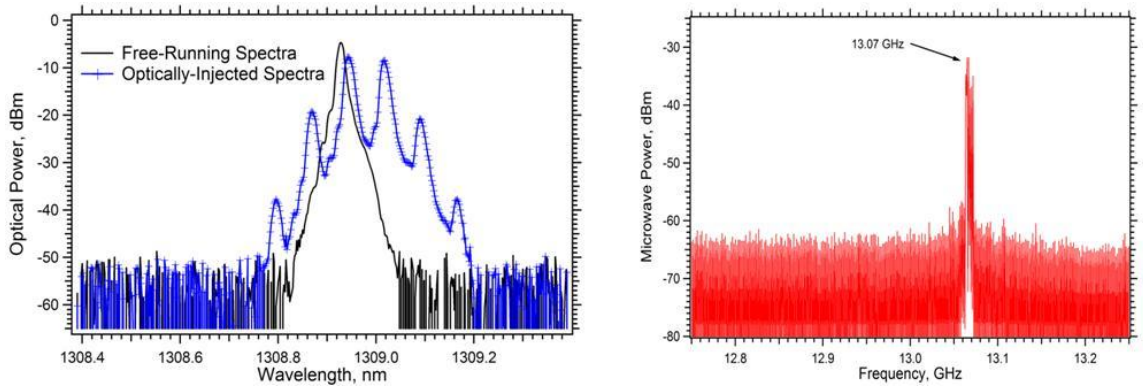

Figure 4.14: Left, OSA trace of P1 optical spectra traced over the free-running optical spectra; Right, ESA plot of the signal output from receiving photodiode.

Here we find that the center frequency of the P1 signal is more than 1.4 GHz higher in Figure 4.14 than in Figure 4.13. This implies an increase in injection strength and/or in detuning frequency occurred with respect to the conditions present in Figure 4.13. Moreover, the spectral width present in the electric spectrum of Figure 4.14 is significantly larger than that found in Figure 4.13. This additional electrical spectral width is shown more clearly in Figure 4.14 because the resolution and video bandwidth on the ESA was improved. In this setting, the ESA took more time to sweep which allowed the P1 frequency time to drift between or even during measurements. This caused the ESA to report lower signal amplitude and higher signal bandwidth than it reported in Figure 4.13.

4.2.2. Stabilizing the P1 Tone

Frequency instability of the P1 signal is one of its biggest drawbacks as it makes many of its microwave applications more difficult to perform, especially when timing

based on its frequency, or applications requiring coherent detection are required. Frequency instability (phase acceleration) as high as 10 MHz/s, though uncommon, has been seen for this laboratory setup. Though movement on the order of 100 kHz has been observed, values in the 1 MHz/s are more common resulting in a very large operational bandwidth for a receiver's phase-locked-loop to match. Figure 4.15 emphasizes the P1 frequency instability issue, showing a near 200 MHz bandwidth that is not smooth.

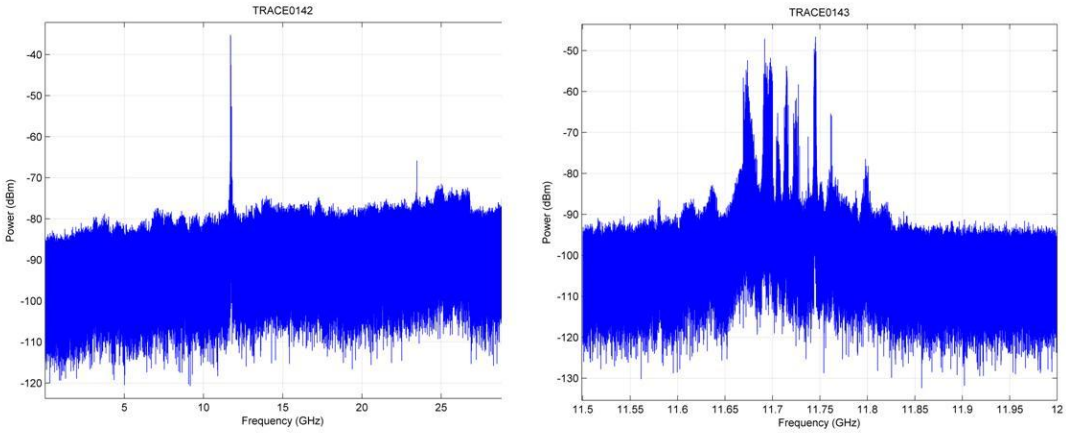

Figure 4.15: Spectrum of ≈11.7 GHz P1 tone from full 25 GHz view (left) and zoomed into the 500 MHz surrounding it (Right).

The effect that modulation has on this P1 tone is quite remarkable in both a qualitative and quantitative sense. Available in the lab are the same baseband modulation electronics which were used in the previous section. This includes the BERTScope which produces unipolar or bipolar rectangular PAM signals and expects to receive and demodulate the same type of signal. As before, this rectangular PAM signal modulates the current of the slave laser diode using a bias tee, and therefore, small-signal analysis

predicts the spectral components of this baseband signal to be simply convolved with the spectral components of the P1 signal. The expected spectrum of the resulting convolution demonstrated in lab is shown in Figure 4.16. Notice the large electrical spectral power located near baseband due to the P1 modulation. This comes from the higher 'average value' or DC shift present during a P1 'on' state.

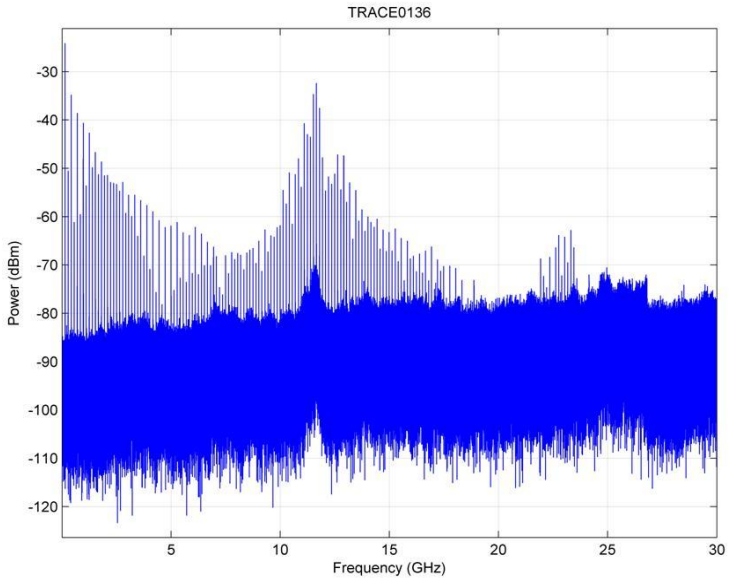

Figure 4.16: P1 modulated with unipolar rectangular PAM at non-random intervals.

The 'wandering' P1 tone, shown on the right of Figure 4.15, was observed to stabilize under modulation. The degree of stabilization was found to be dependent on the modulation rate. The highest degree of stabilization was observed when a significant modulation harmonic fell within the frequency extent of the P1's 'wander'. This is shown explicitly in Figure 4.17 where the range of the P1 is again shown in the top left. In this figure the modulation rates: 1.11Gbps (top right), 1.12Gbps (bottom right), and 1.13Gbps

(bottom left) were chosen for an integer baseband harmonic (the 21st harmonic) to fall inside, inside, and outside the P1 supported range respectively.

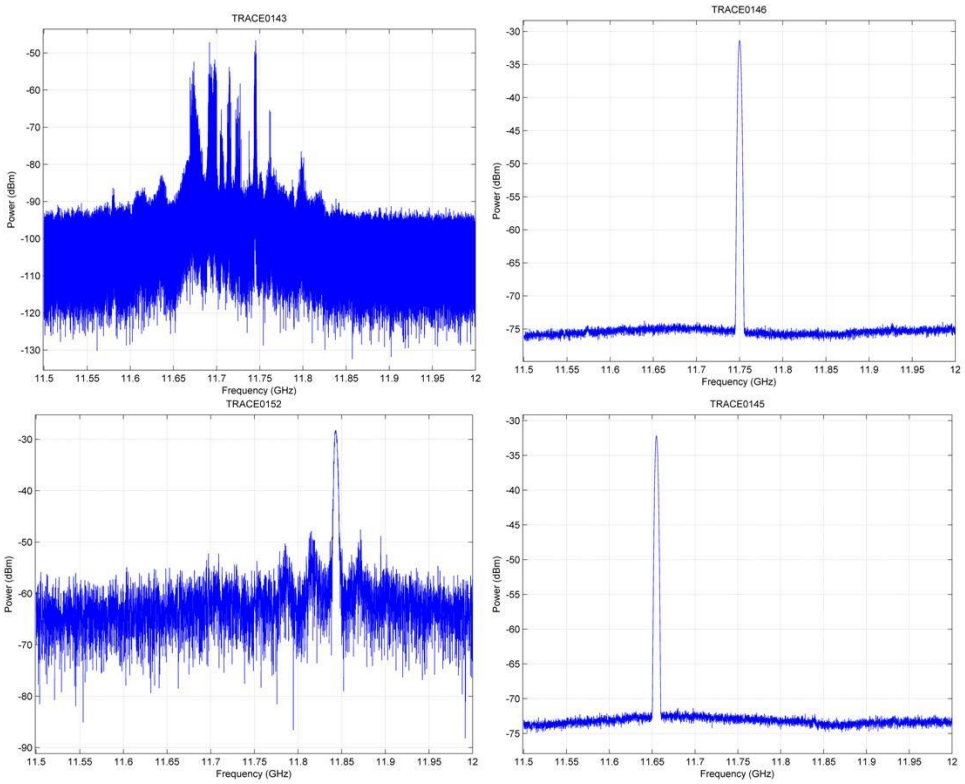

Figure 4.17: Top left: zoomed in view of un-modulated P1 tone; top right: zoomed in view of P1 tone modulated at 1.12 Gbps; bottom right: modulated at 1.11 Gbps; and bottom left: 1.13 Gbps.

The ESA settings were set the same for the three plots of the modulated P1 signal in Figure 4.17. The center frequency was set to 11.75 GHz with a span of 500 MHz, the resolution bandwidth and video bandwidth were both set to 3MHz and the reference level was set to "auto" which produced a -30 dB offset for the plots on the right and -20 dB offset for the plot in the lower left. These settings imply that the raised noise floor in the lower left plot is 10 dB higher than the noise floor in the plots on the right. The

conclusion is that setting the modulation rate to have a higher-order harmonic that lies within the supported P1 region results in 10 dB or better reduction of average noise power.

One hypothesis explaining the significant P1 stability observed under supported modulation conditions is coordination with a high-order baseband harmonic. Enough of the small-signal harmonic produced for the shape of the baseband modulation waveform (in this case, rectangular PAM) is coupling with the slave laser diode, in spite of the low-pass nature of the modulation electronics, to coordinate or synchronize the P1 modulation. The observed harmonic located at 1.1655GHz is the 21^{st} harmonic of the highest fundamental frequency (555MHz) in a 1.11Gbps rectangular PAM modulated alternating bit sequence. The PSD of the 21^{st} harmonics should be approximately -46 dB or one forty-thousandth the power of the fundamental harmonic of a square wave.

A competing hypothesis is that the large-signal sub-harmonic modulation of the slave laser's bias current is correlating the phase of the P1 oscillation at the beginning of the communication symbol. That phase correlation could appear to reduce the frequency instability. Additionally setting the symbol length (in time) appropriately to fit an integer number of P1 oscillations inside the symbol could further reduce inter-symbol interference and generation of phase noise. That reduction in phase noise could explain the reduction in noise floor for wisely chosen communication symbol rates.

An additional qualitative observation (not shown here) was made for a different modulation rate and P1 frequency about the spectral shape of this supported harmonic. While the supported harmonic was scanned at a very fine resolution bandwidth (≈100 Hz

or less) the spectral shape was similar to the spectral shape of a baseband harmonic absent the P1 frequency, measuring straight from the BERTScope to the ESA through a SMA connected coaxial cable. This indicates spectral-shape coupling or following is happening inside the slave laser diode to the spectral-shape of the baseband modulation.

A monotonic large-signal modulation of the slave laser with as few harmonics as possible could potentially reject the hypothesis that high order harmonics are the cause of P1 stability. Care must be taken in such an experiment as nonlinear impedance can produce high-order harmonics from monotonic signals. Furthermore, introducing a modulation scheme which changes the intensity of the slave laser within a single communication symbol could cause intra-symbol P1 instability as shown in Figure 4.18. A small amount of microwave frequency instability can be tolerated in microwave communication systems if the symbol is predictable enough. This direct P1 modulation creates a predictable communication symbol, allowing coherent detection.

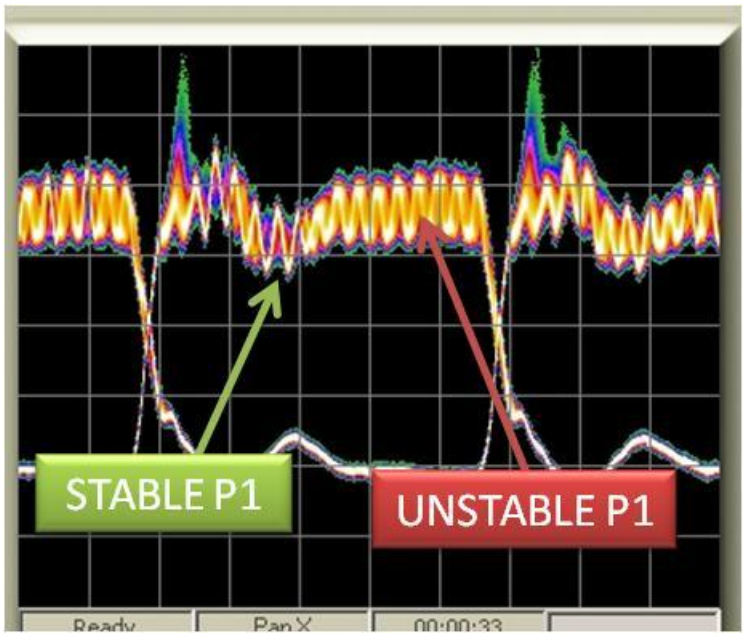

Figure 4.18: Eye diagram of communication signal with region of stable and unstable P1 frequency in the same symbol.

When reducing the spectral components of the baseband modulation signal as suggested, the time-domain representation will lose its flat high and low voltage states as shown in Figure 6.16 appendix A. This will cause the injection strength to change slightly within a given communication symbol due to the modulation power coupling with the slave laser's bias current and thus move the location of the P1 harmonic, or at least the range of the P1 harmonic's wander as observed above. Since this test setup is directly modulating the slave laser's bias current through a bias tee, an increase in bias current due to modulation will reduce both the injection strength ratio and the detuning frequency. Both effects reduce the frequency of the P1 state, as illustrated by the spectral plots in Figure 4.19 where the modulation power has shifted the center harmonic from ≈11.5 GHz to ≈9.75 GHz.

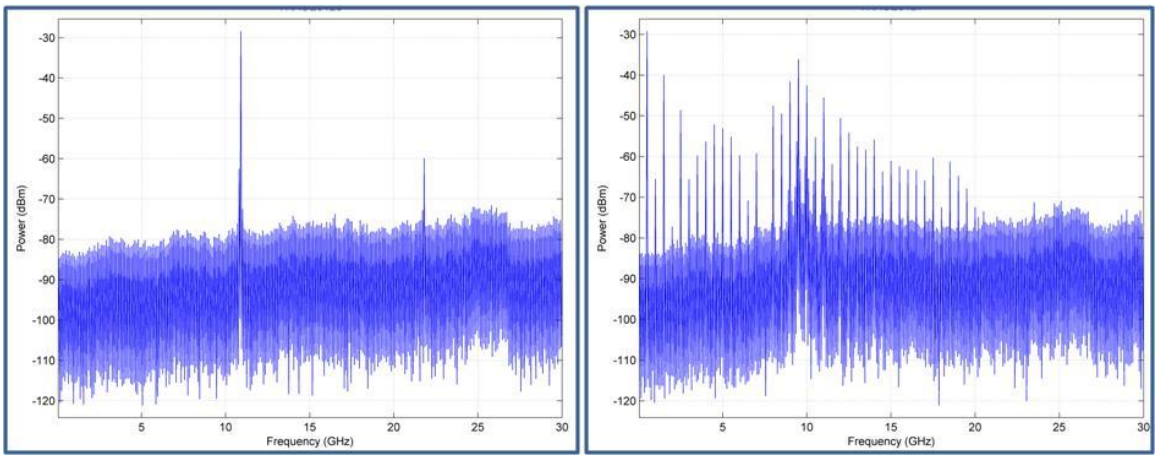

Figure 4.19: A P1 tone (left) under modulation (right) can shift frequency due to the decreased injection strength and detuning frequency.

This is not a trivial characteristic to control. In practice, a stable and controlled P1 frequency is desired as receivers for perfectly stable microwave frequencies are made with less expensive frequency following circuits. For this reason, avoiding modulation-dependent changes in P1 frequency is desirable. In an attempt to characterize this baseband modulation power coupling effect on the P1 frequency, plots of average optical power output from the slave under different modulation depths, rates, and bit-sequence types were created where the average optical output power (Y axis) was measured with respect to the DC bias current (X axis) under a variety of modulation conditions, see Figure 4.20. The results indicate that driving the slave laser well above threshold (approximately 3X), and keeping the modulation depth moderate (near 1V peak-to-peak), reduced the effects of modulation on slave laser intensity. This should minimize the modulation power's effect on the P1 frequency.

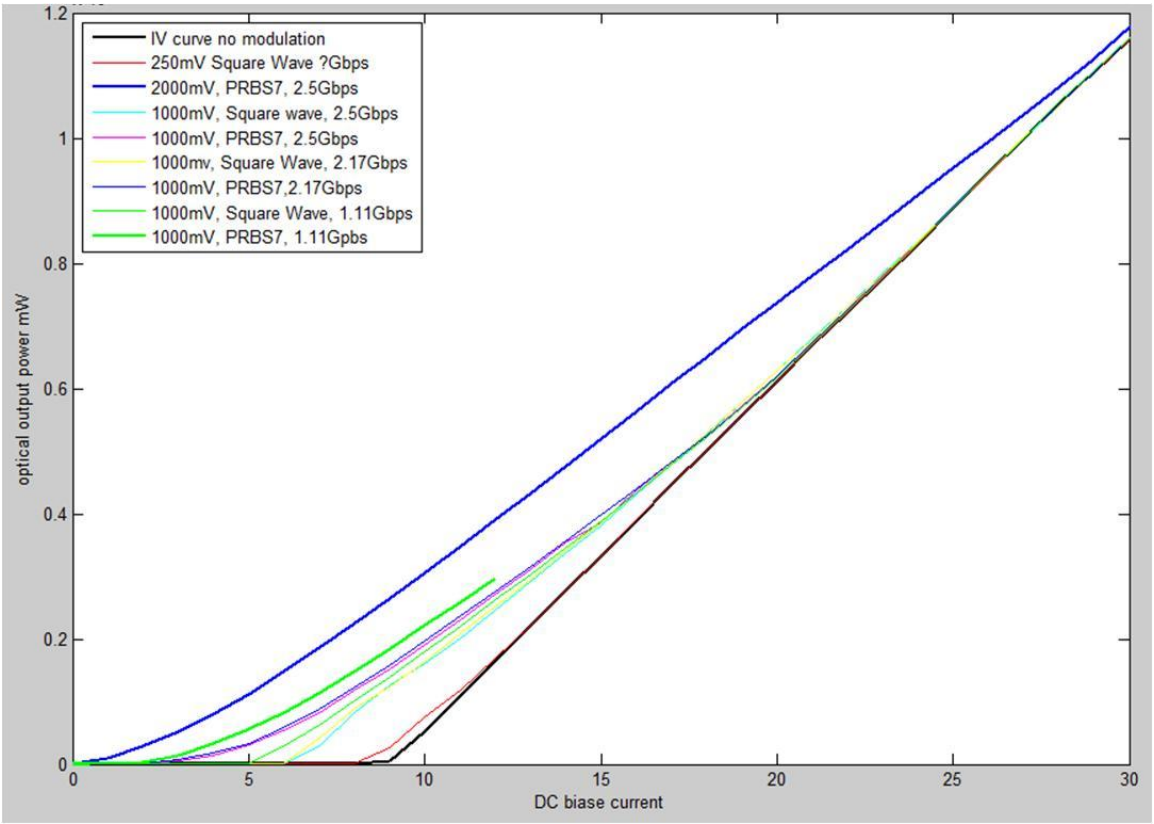

Figure 4.20: Output intensity versus bias current under various modulation conditions.

A communication system's tolerance to carrier frequency shifts is heavily dependent on the type of demodulation used at the receiver unit. Figure 4.21 shows graphically how a communication symbol with a synchronized start time and phase but random frequency appears on an eye analyzer. The top MATLAB simulation allowed frequencies that varied by enough for a $\pi/2$ phase-shift while the bottom included a $3\pi/2$ phase difference in the same communication symbol.

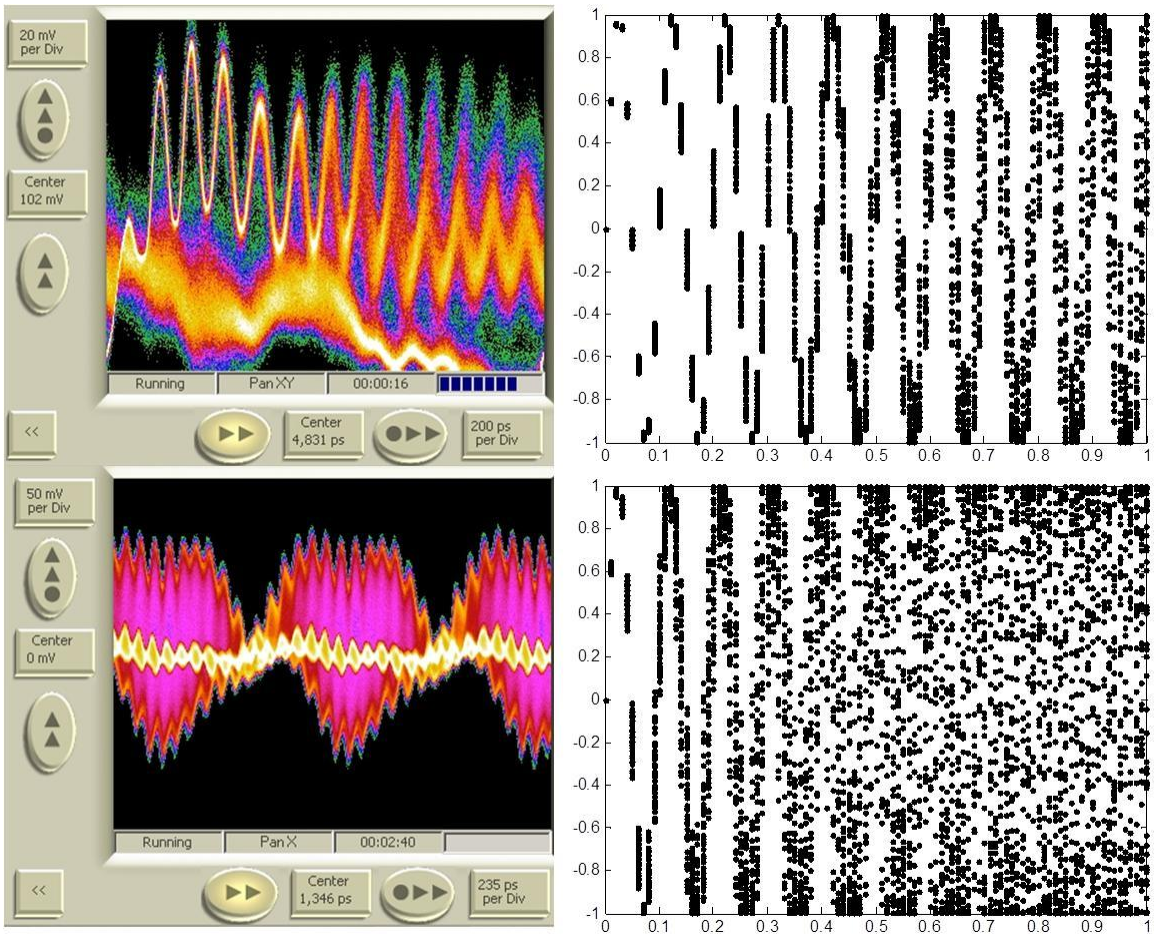

Figure 4.21: Left, BERTScope eye diagrams and right, MATLAB simulations of communication signals with more predictable P1 frequency (top) and less predictable P1 frequencies (bottom). In all cases the initial behavior of the communication symbol is quite predictable.

Recall the competing hypothesis; the P1 stability under modulation is caused by just enough time for an integer number of half-wave lengths of the P1 frequency to fit inside a single communication symbol. This implies that the P1 wavelengths of an unsupported frequency will cancel with delayed versions of itself and leave only harmonics, or, if none can be supported, just a noisy signal, thus increasing the noise floor for non-supported modulation rates. This hypothesis is supported by the time-

domain measurements taken of the P1 symbols. The eye diagrams of the three symbols generated for the spectral plots of Figure 4.17 are shown in Figure 4.22.

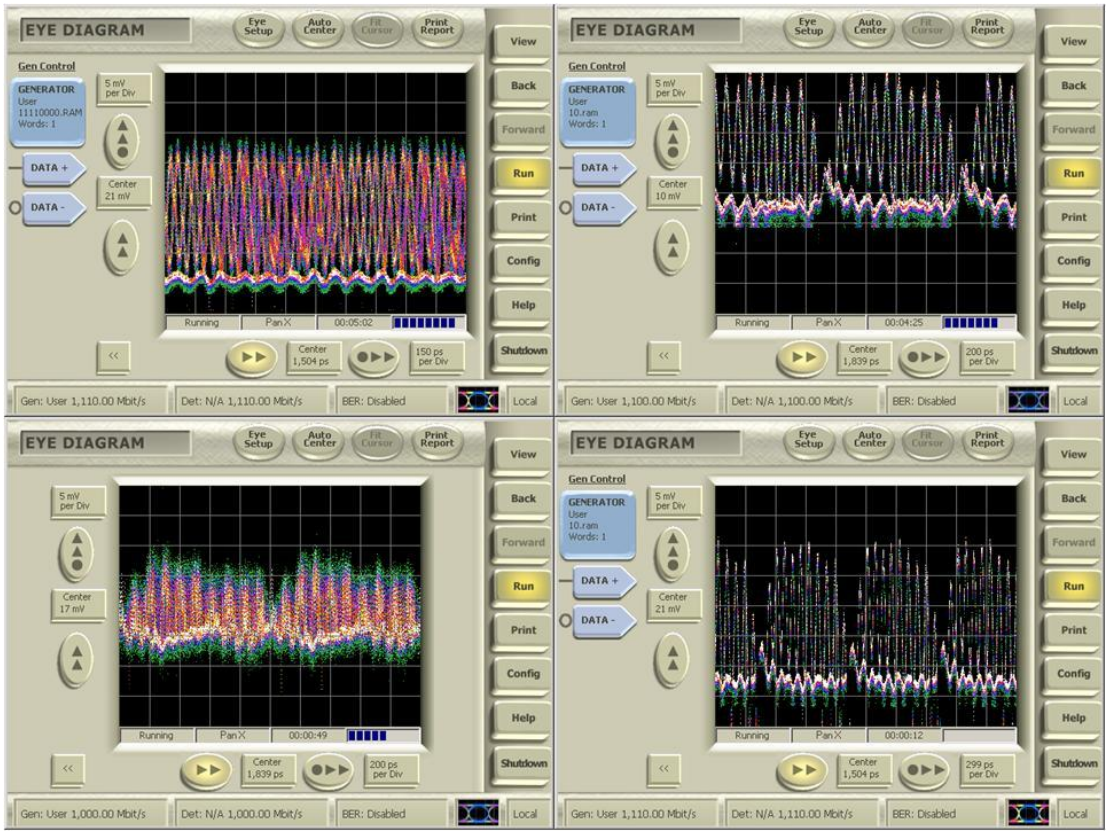

Figure 4.22: top left, overlapping P1 symbols, Top and Bottom right, P1 symbol created with P1 supported harmonic, bottom left, unsupported P1 harmonic. These time-domain representations correspond to the frequency domain signal representations in Figure 4.17.

4.2.3. Demonstration of P1 suitability for Radio-Over-Fiber

The eye diagrams in Figure 4.22 demonstrate the ability to generate predictable, on-off-shift-keyed communication symbols and clearly indicate the importance of choosing symbol-rates compatible with P1 frequency. It also shows that these signals are

all shifted in amplitude. While the P1 symbol is present, the average optical power of these demonstrated symbols is higher than the average optical signal when the P1 symbols are absent. This change in average power means these P1 symbols are not orthogonal with baseband communications on the same channel and wavelength. After this optical signal is converted to an electrical signal at the photo-detector, the baseband component can be filtered out with a high-pass electric filter as demonstrated in Figure 4.23. During transport on the photonic carrier, however, these signals would interfere with any baseband PAM.

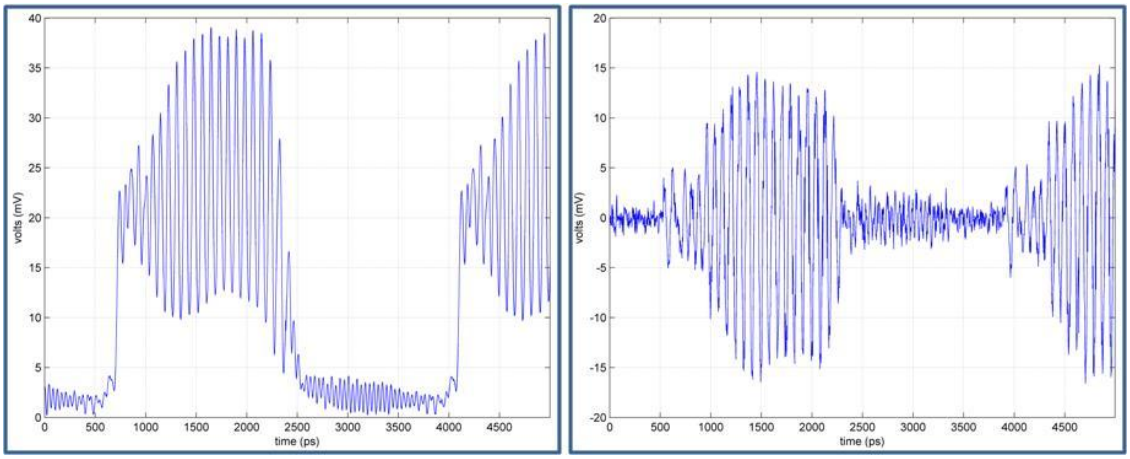

Figure 4.23: Two signals, one with baseband (left) one with base-band modulation removed with an electric high-pass filter (right) on the output of the photo detector.

This P1 frequency can be modulated at different modulation rates as shown in the oscilloscope screenshots in Figure 4.24. The signal on the left is modulated at 1.25 Gbps while the signal on the right is modulated at 591.5 Mbps. The second data-rate was 'discovered' by iteratively adjusting the rate until a maximum modulation depth and ideal shape was found. This implies the P1 frequency is an integer multiple of 295.75 MHz.

These two signals will experience different amounts of dispersion due to the higher data-rate's wider spectral occupancy. However, these signals will experience the same amount of transmission time delay as each other because they are located on the same optical carrier wavelength, which is confirmed by Figure 4.24. To form these images, the negative version of the modulating signal (shown in yellow) was applied directly to the oscilloscope while the positive lead was applied to the bias current of the slave laser diode. Here, the time delay between the two signals was measured to be 41.9550 ns. Corning reports the index of refraction for their fiber is 1.4682 at 1550 nm. This calculation implies that there was 8.567 m of SMF between the BERTScope and oscilloscope. This simple calculation, however, does not elucidate the time delay required for modulation and filtering.

Figure 4.24: Two separate data signals over the same length of fiber experience the same time delay (41.9550 ns) appropriate for 8.566 m SMF at 1550 nm wavelength.

4.2.4. P1 Modulation Summary

This section explored the degree to which the direct-modulation of the P1 dynamical state of semiconductor lasers is suitable for telecommunications applications. This research demonstrated, for the first time, the direct generation of microwave communication symbols without the use of microwave support electronics at data-rates appropriate for long-haul telecommunication applications. It explored the modulation characteristics of widely tunable P1 subcarrier microwave frequencies. It demonstrated the ability to directly generate consecutively sequenced spread-spectrum symbols appropriate for wireless communications. It investigated the parameters, detuning frequency and injection strength, affecting the stability of the P1 frequency under this modulation condition and found that P1's inherent instability could be overcome by setting the P1 frequency equal to a higher-order harmonic of the baseband modulation signal.

4.3. Summary

This chapter is broken into two parts, the first discusses the measurements taken under optically injection-locked (OIL) conditions, while the second presents observations made under P1 dynamical injection conditions. The OIL discussion focuses largely on characterizing how improvements to each (S21 or linewidth) affect the optical communications link. The results of our work showed that OIL improved the bit-rate-distance product of the Fabry–Pérot laser under investigation by over 57 times.

The majority of the P1 measurements performed investigated the effects produced by varying the modulation parameters and the ease of shifting/modifying the microwave

subcarrier frequency. The P1 setup produced consecutively sequenced spread spectrum (CSSS) communication symbols appropriate for transmission wirelessly. This modulation technique demonstrates a unique method of accessing an orthogonal communication channel using only baseband electronics.

5. Conclusions

5.1. Summary

This work presented, for the first time, the application of theoretically derived optical injection parameters for the enhancement of the telecommunication capability of a complete operationally realistic telecommunication system. It exhibited a very wide range of data-rates through representative lengths of SMF. It also demonstrated the encoding of information on the dynamical P1 state of optical injection using baseband electronics by varying the detuning frequency and optical injection strength.

5.2. Key Findings

First, this work verified stably locked optical injections benefit in a relevant communication system. It reported at least 57 times the bit-rate-distance product of a directly-modulated commercial Fabry–Pérot laser using OIL for the same optical signal power. This improvement is attributed to the capabilities of OIL to improve the side-mode suppression ratio (SMSR) and reduce wavelength chirp under direct modulation. This research illustrated the degree to which optical injection can improve the communication capability of a directly modulated laser diode in an end-to-end telecommunication application.

Using commercial diode lasers, this research proved the ability to couple two devices, one designed for high-speed modulation and one designed for single-mode operation, to yield a transmission system far more capable of either device operating in

singular fashion. It also confirmed the enhancement of the modulation bandwidth of multi-mode devices. The bit rate-distance product reported over 61.7 km of SMF in this work, confirmed that OIL of Fabry–Pérot lasers is a viable approach towards a high-speed, long-distance capable transmitter.

Second, this work demonstrated the ability to all-optically generate an on-off-shift-keyed widely-tunable P1 microwave subcarrier using large-signal electrical modulation applied directly to the slave laser under CW optical injection. This novel approach used an amplitude-modulated electrical signal to change the slave laser's operating point to generate the microwave sub-carrier signal on an optical signal. This was unique in that it allowed the widely-tunable microwave frequency to be directly generated and transmitted on an optical carrier using only baseband electronics. The generated microwave signal was carried over 50 km of single-mode fiber to confirm the applicability of the directly-modulated slave in the P1 state for radio-over-fiber.

5.3. Contributions

This study demonstrated the engineering application of the theoretically derived optical injection parameters (frequency detuning and injection strength) to enhance telecommunications using operationally-representative, commercial off-the-shelf equipment. This research performed experiments in two generic areas of optically injected guided-wave optical telecommunications: stably-locked and period-one state. Both areas involved direct-modulation of semiconductor lasers under optical injection.

Both experiments involved the use of support electronics with baseband (low-pass filter) response limited to frequencies below 5GHz.

All key components of the system were composed of readily available commercial off-the-shelf equipment. This research effectively raises the "technology readiness level" of optical injection for telecommunication from 4 to 5. This work demonstrated technology maturity by using theoretical parameters to describe the interaction between individually studied components. This to created a complete end-to-end telecommunication system representative of operational environment.

This stably-locked optical injection research presented reputable bit-rate-distance products for optical communications using relatively inexpensive commercial off-the-shelf components. It confirmed the ability to couple two devices, one designed for high speed modulation and one designed for single mode operation, in order to yield a transmission system far more capable of either device operating in singular fashion. The investigation of an injection-locked Fabry-Perot laser showed a 57 fold improvement to the bit rate-distance product compared to the free-running case when received optical power is considered. This result highlights the reduction of linewidth and wavelength chirp in a directly-modulated injection-locked laser.

Large-signal direct-modulation of a diode laser optically-injected into P1 operation was shown to produce consecutively sequenced spread-spectrum microwave communication signal consistent with IEEE 802.11a (WiFi) standard. The signal was highly tunable and transmitted over 50 km, suitable for radio-over-fiber applications. The P1 signal was shown to stabilize under specific modulation rates, in some cases

improving the signal to noise ratio more than 10dB for marginal changes in modulation rates.

Temperature tuning of the master laser to each of the Fabry-Perot modes of the slave laser provides a simple approach for WDM applications. The ability to enhance the modulation bandwidth of multi-mode devices, and the bit rate-distance product demonstrated over 60 km of SMF in this work, shows that OIL of Fabry-Perot lasers is a viable approach towards a high-speed, long distance capable transmitter.

5.4. Future Work

The field of optical injection is rich with research opportunities. As with any time and resource constrained research, there are still significant untested hypotheses waiting to be rejected or accepted. This section discusses only a few of those hypotheses and research areas.

5.4.1. General Purpose Network Analyzer

A general purpose network analyzer (PNA) is the tool best suited for measuring the modulation response between any two ports of a passive or active network (including microwave reflections from the same port). A PNA measures impedance, VSWR, loss, gain, isolation, and group delay. This work referenced several “S21” plots, generated by PNAs, in other research, but never reported any of its own. This research would benefit from testing both the electronic packaging of the slave laser and the laser diode itself. In particular, it would add value to the section 4.1.2 discussing the slave laser’s back-to-

back modulation limits. While this research was able to conclude the electronics limit the modulation response, it did not measure the 3-dB cutoff modulation response.

5.4.2. Monotonic Direct Modulation

This research focused on using an end-to-end logical bit-error-ratio tester that used TTL type logic for both its output and input ports. This was appropriate for demonstrating a complete telecommunication system. In general, testing should take TTL logic (as would appear from the output port of a transmitter), transform it for transportation through the channel, and convert it back to TTL for the telecommunication receiver. However, the spread-spectrum nature of rectangular PAM leaves some ambiguity between a systems' time-domain response compared to its frequency domain response. One example of this ambiguity was noted in Chapter 4 while discussing the stability of the P1 frequency:

- Did the very-small amplitude high-frequency signal (21^{st} harmonic) located at the same P1 frequency from the BERT that stabilized the P1?

- Did the large-signal fundamental harmonic that correlated the phase of the P1 signal at the beginning of the communication symbol?

Amplifying the monotonic signal from a local oscillator through a microwave amplifier fed into the bias-tee of the semiconductor laser would satisfy the removal of the

high-frequency (31^{st} harmonic) component from the modulating electronic signal. However, the non-linear nature of the bias-tee might create that harmonic again. Therefore, measuring the spectral content of the optical signal through a high-speed photodetector would be prudent.

This page intentionally left blank.

6. Appendix A

6.1. Baseband Modulation and Demodulation

When a transmitting Boolean logic digital device communicates information to a receiving Boolean logic digital device, it does not need to know exactly how the receiving device internally represents **B**inary dig**IT**s or bits, processes these bits, or even the rate at which it handles bits. What is necessary is that the two devices agree on the logical content. The cartoon in Figure 6.1 depicts how communication systems move information from a transmitter to a receiver through a channel and Figure 6.2 illustrates how bits in error effect communications and how the effect is measured at the physical transport networking layer.

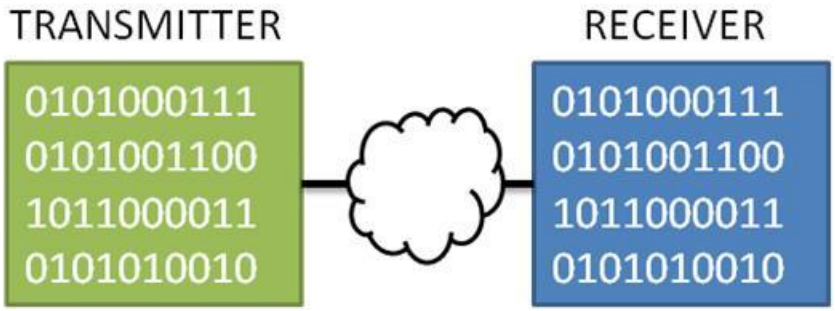

Figure 6.1: Cartoon of binary digital data communication

A metric of how well the receiver and transmitter agree on the logical content of communicated data is the quotient of the number of bits in error divided by the total number of bits transmitted and is called the Bit Error Ratio (BER). In practice a BER greater than .0125 is not very useful, so in practice, reporting BER quotients in the form

of XE-Y, is cleaner [23]. For example, a common BER such as 6.8E-8 means 68 bits in error per billion total bits transmitted.

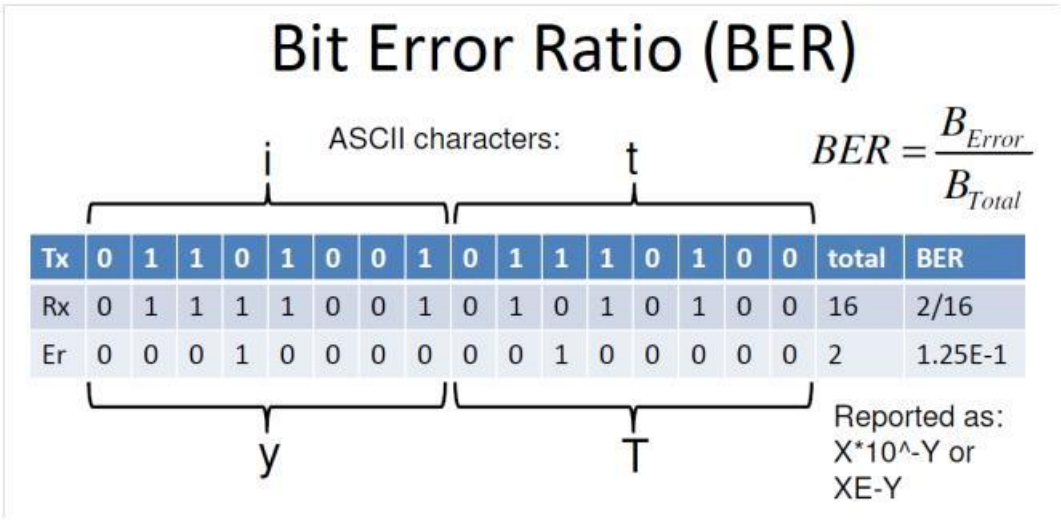

Figure 6.2: Illustrates the bit error ratio by showing an intended bit string, ASCII "it" with two bits in error which transformed "it" to "yT" leaving a BER quotient of 1.25E-1.

The simplest way to represent a bit is with a logic voltage level. If two logic chips use the same external logic level or line voltage then simply connecting the data output pin of the transmitter to the data input pin of the receiver and synchronizing with a common clock yields a simple digital communication system. Assigning logical bits to voltage levels in this way describes a baseband digital communication technique known as binary pulse-amplitude modulation (PAM) [23].

In telecommunications, the term baseband refers to an electrical signal whose spectral content is measured from 0 Hz and does not utilize a sinusoidal carrier signal. This can be quite confusing. The fundamental harmonic or the minimum bandwidth

required for a 10 gigabit per second (Gbps) baseband square wave communication link is 5 gigahertz (GHz) while the carrier frequency of an FM radio station is approximately 100 MHz. The FM radio signal is not considered baseband, even though its peak spectral power is well below the 10 Gbps baseband signal.

Baseband modulation techniques encode information directly on the amplitude, width, position or shape of a pulse and do not rely on a sinusoidal carrier signal. A good communications system takes the baseband communication symbol from the transmitter's data output pin and creates the same communication symbol for the receiver's data input pin as quickly as possible, even if the receiver is thousands of kilometers away. Common baseband pulse modulation schemes include pulse-width modulation (PWM) used to control servo motors, pulse-position modulation (PPM) used in optical communications and, the most commonly used form of digital communication modulation, pulse-amplitude modulation (PAM) shown in Figure 6.3 [23].

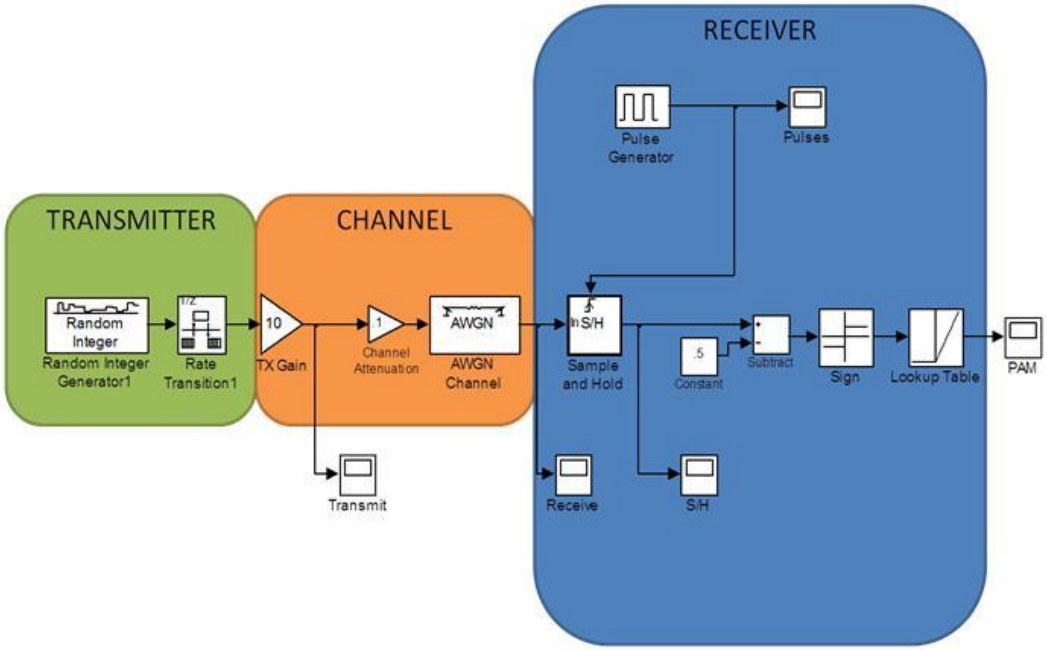

Figure 6.3: SIMULINK model of a simple Pulse Amplitude Modulated digital Communication System.

In its most basic form, digital communication systems can be thought of as physical extensions of logical processes that occur inside a logical chipset. The voltage plots from running the Simulink model shown in Figure 6.4 help illustrate the digital communication process. First a transmitter, represented here by a random number generator, converts its logic bit rate (bits per second or bps) into a PAM signal, represented by the rate transition block in Simulink. The system then amplifies that PAM signal in preparation for transmission through the channel where it is attenuated and experiences additive white Gaussian noise. The signal output from the channel is fed into the analog input pin of a sample-and-hold circuit shown in Figure 6.5 whose sample

frequency and symbol phase is controlled by the frequency and phase of a local clock or pulse generator.

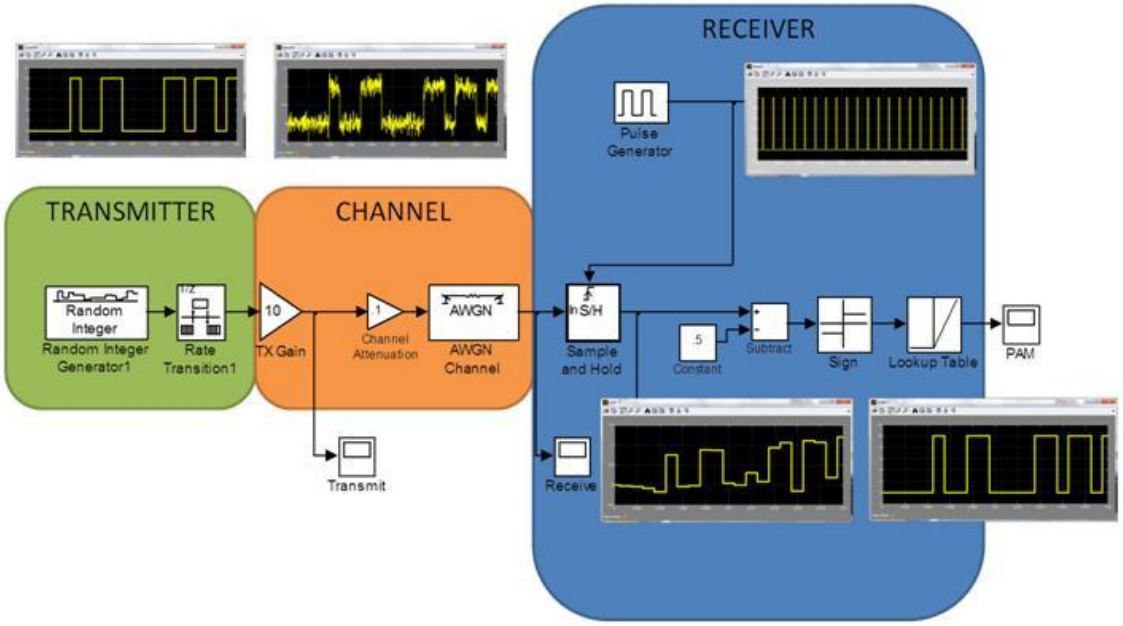

Figure 6.4: The time domain plots of signals as they are processed by the simple PAM digital communication system helps illustrate how a simple PAM system works.

The analog output signal from the sample and hold is then compared to an optimal offset voltage and is transformed to the receiver's logic voltage for processing, and represents the receiver's bit rate. This step, simulated by the lookup table block, is known as "maximum likelihood decision…" most likely a 1 or 0 bit, "…based on a-priori decision criteria," here represented by the frequency and phase of the pulse generator as well as the offset voltage value stored in the receiver [12]. A useful tool for finding the a-priori decision criteria is a voltage versus delay time histogram of the communication signal called an eye diagram, which will be discussed later. Thinking of the receiver in

this way is a bit too rigorous for binary amplitude-shift keyed signals but is quite useful for more complex baseband symbols like PPM, PWM, and multi-level PAM, where more than 1 bit can be represented with a single communication symbol.

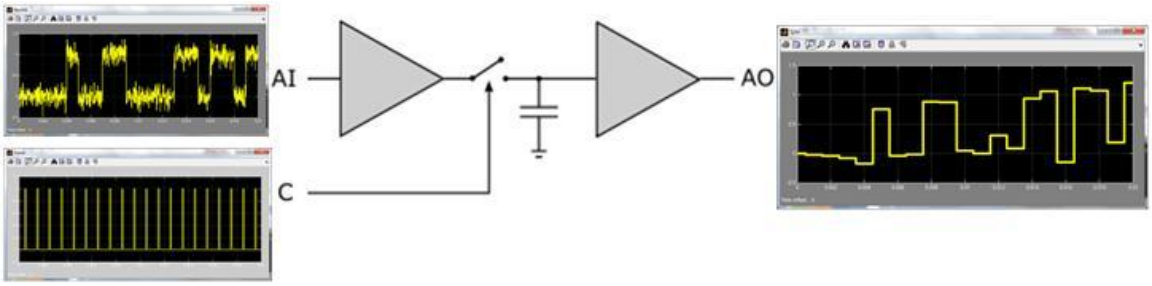

Figure 6.5: A simplified sample and hold circuit diagram, AI is analog input, C is local clock or control input and AO is analog output.

An example of a pulse-amplitude modulated digital communication standard is the 5 Volt I^2C communication standard which defines the communication protocol between digital logic chips, usually on the same printed circuit board as positive 5 volts being treated as logic value 1 and 0 volts treated as logic value 0 with a voltage tolerance of .7 volts, very similar to the simple digital communications system simulation shown in Figure 6.3. This rectangular PAM standard works well for short communication distances and slow data rates in spectrally unlimited transportation channels.

Baseband communication signals like I^2C quickly become impractical when longer distances or higher data rates are required. Because of this, the baseband signal is up-converted from its baseband state onto a carrier signal for transmission through the channel, then down converted back to baseband before the baseband receiver. For

example, up-converted signals may be in the form of a 2.4 GHz microwave carrier frequency modulated using a directly sequenced spread spectrum (DSSS) approach, better known as WiFi 802.11a, for wireless transportation; alternatively, the baseband signal could be placed onto an 193 THz laser carrier using an on-off-shift-keyed modulation scheme as shown in Figure 6.6, better known as direct-modulation coherent optical communication.

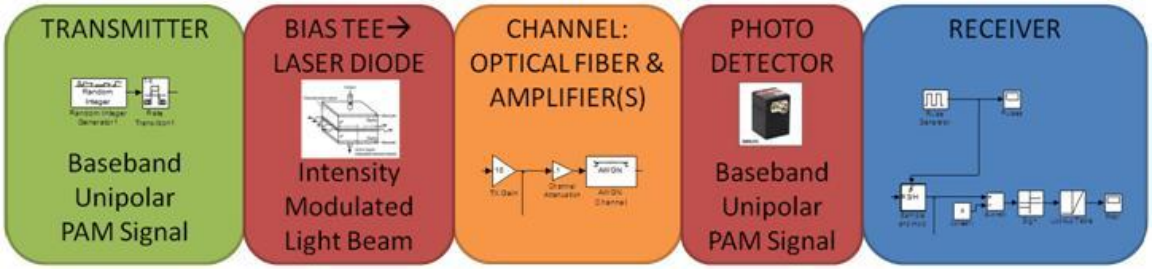

Figure 6.6: Directly Modulated Coherent Optical Communications simply drives a laser diode's bias current with an offset version of a baseband PAM signal.

Directly modulating the bias current of a semiconductor lasers as shown in Figure 6.6 is a simple and compact approach to pass data onto an optical fiber. Intrinsic limitations under direct-modulation such as wavelength chirp and inherent relaxation oscillation frequency constraints impede high-speed and long-distance communications capabilities of laser diodes [3]. Moreover, the electronic packaging of the laser diode also limits the modulation response of the optical communication system (note: the same electrical parasitics noted here limit the RF modulation capabilities of electrical communications, often to a much higher degree) [21].

Since a laser only works when the gain in an optical cavity can overcome the cavity photon loss, there is a threshold current, I_{th} applied to the laser diode, before which, it acts as a simple Light Emitting Diode (LED) whose light output is due to spontaneous emission [24]. Figure 6.7 shows how much more current is required for true on-off-shift keyed (OOSK) modulation than simply amplitude shift keying (ASK) a laser diode operating above the threshold current.

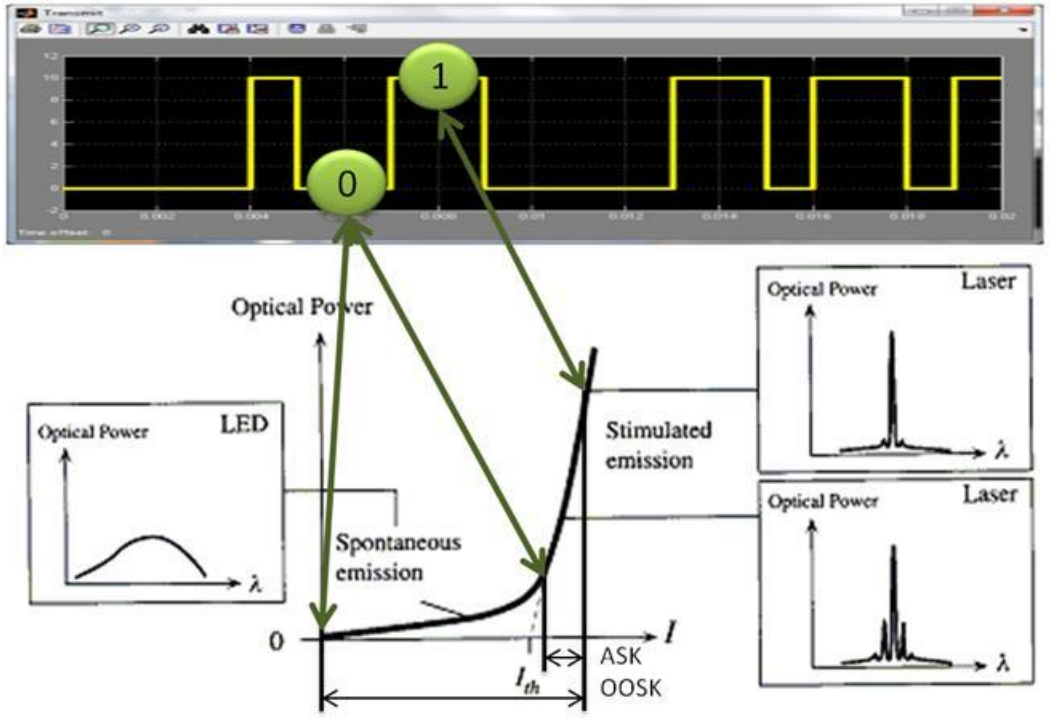

Figure 6.7: Driving the laser diode directly with the PAM communication signal to On-Off-Shift Key (OOSK) the laser diode requires significantly more modulating current then small-signal Amplitude Shift Keying (ASK) of the laser diode through a bias tee [24].

Though ASK optical signals do decrease the voltage differential between logical high and low voltage values, many optical communications systems find it easier to compensate for the optical signal's average intensity (DC) shift than the additive white Gaussian noise (AWGN) introduced for the amplification of the communication signal used to drive the laser diode under OOSK conditions. Because of this advantage, many manufacturers produce laser diode packages which have an SMA cable connectors for the small signal radio frequency (RF) desired to modulate the direct current (DC) bias through a bias tee. A simple circuit diagram of a bias tee is shown in Figure 6.8.

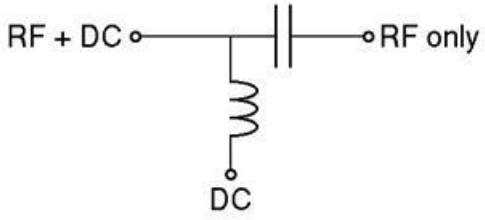

Figure 6.8: Simple circuit diagram of bias tee. The RF+DC port drives the laser diode, the DC port supplies enough current to keep the laser diode current above threshold even under modulation from the RF port.

Ideally, the RF port will pass all alternating current (AC) power at frequencies greater than DC with identical conversion loss at every frequency. Ideally the DC port will pass only Direct Current (DC) power and block all AC power. In practice, however, there is a limit, both high frequency and low frequency, to what can be practically built, and still maintain a flat modulation response. Realistic bias tees couple a finite frequency bandwidth from the RF port and the DC port acts as a low pass filter with a cutoff frequency greater than zero.

The impedance of the capacitor, X_c, and inductor X_L, is described as:

$$X_c = \frac{1}{j2\pi fC} \qquad X_L = j2\pi fL$$

Solving for a high enough impedance to block the RF signal from passing to the DC port reveals that an effective inductor needs to be approximately 1 mH. Commercial inductors with 1 mH inductance have self-resonant frequencies around 1 MHz; several orders of magnitude short of the Accel-RF bias tee shown in Figure 6.9 which is created with more complex circuitry than shown by the simple diagram in Figure 6.8.

Even top performing bias tees, like the one whose spectral response is shown in Figure 6.9, exibits non-ideal behavior. At modulation rates above 4 GHz, the Accel-RF device will attenuate the input signal by approximately 2 to 3 dB compared to the spectral components less than 1 GHz. This non-flat spectral response leads to unintended communication symbol shaping and potential wavelength chirp issues in the output optical signal.

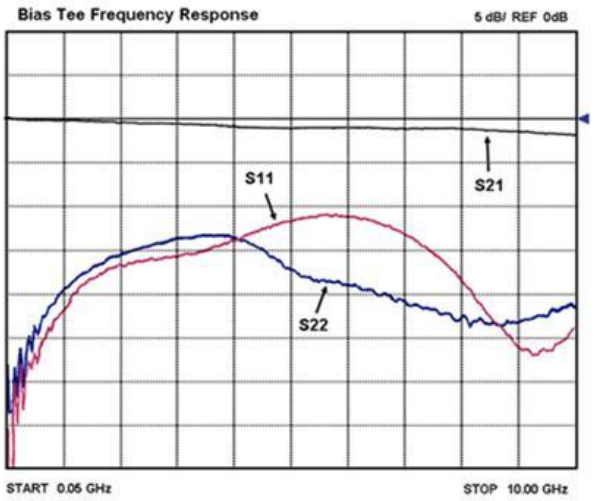

Figure 6.9: Spectral Response of Accel-RF's broadband bias tee, describes how much power applied to the RF port gets translated to the output port with respect to frequency.

6.2. Baseband Power Spectral Density

With some understanding that physical systems have spectral limits to modulation, it is now important to understand how time-domain baseband signals like rectangular pulse amplitude modulation (PAM) is represented in the frequency domain. One familiar baseband signal is a single rectangular polar PAM pulse centered at t=0 with a width $\pm T_b / 2$, the time-domain representation is given in equation (20). The arbitrary data map here points a binary 1 to +A volts and binary 0 to –A volts [23].

$$\begin{aligned} P_{PAM}(t) &= \pm A \quad -\tfrac{T_b}{2} \le t \le \tfrac{T_b}{2} \\ P_{PAM}(t) &= 0 \qquad otherwise \end{aligned} \tag{20}$$

Figure 6.10: Output of a simulated binary rectangular polar PAM signal with A=5V and T_b=1 ms.

The magnitude of the frequency domain representation of a single rectangular pulse is given by the Equation [25]:

$$P_{PAM}(f) = AT_b sinc\left(2\pi\left(\frac{T_b}{2}\right) f\right)$$

The energy of n polar PAM pulses is n times the square of P_{PAM} over the load resistance R_L, usually 1 for ease of analysis [25]:

$$E_{PAM}(f) = \frac{nA^2 T_b^{\,2}}{R_L} sinc^2\left(2\pi\left(\frac{T_b}{2}\right) f\right)$$

Since the sinc(f) function extends from f=-∞ to ∞, these equations are known as 'two sided' spectral density functions. The two-sided power spectral density (PSD) of the PAM signal is E_{PAM} divided by n and T_b shown in equation [25]:

$$PSD_{PAM}(f) = \frac{A^2 T_b}{R_L} sinc^2\left(2\pi\left(\frac{T_b}{2}\right) f\right)$$

The power spectral density of a 1 kbps polar rectangular random PAM signal without AWGN is shown in Figure 6.11, with spectral resolution of approximately 0.19 Hz. The frequency range only extends to positive 25 kHz because the simulation only sampled the signal at 50 thousand samples per second (50 k/2=25 kHz). Ideally, analog systems spectral components extend to infinity. Also, since the simulation has finite length, the PSD is not smooth, while an ideal signal's PSD is smooth. Even so, the envelope clearly demonstrates its $sinc^2$ nature appropriate for this signal's PSD. So, even though the polar rectangular random PAM signal is a baseband signal, spectral components extend to surprisingly high frequencies, and any of the frequencies cut off by non-ideal modulation shapes the time-domain communication symbol.

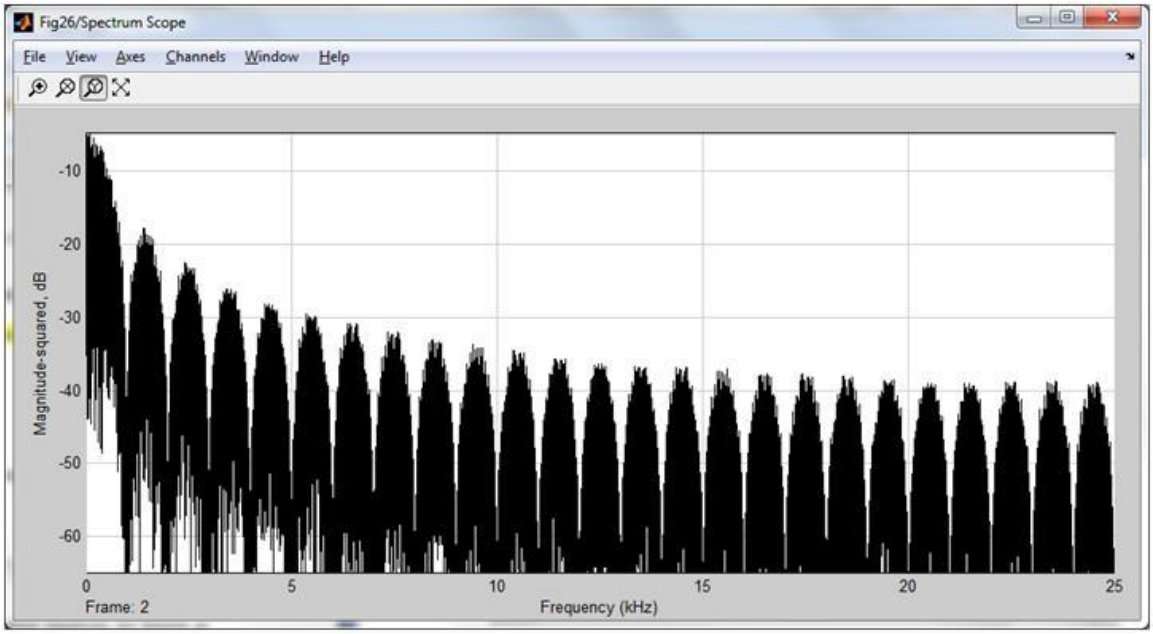

Figure 6.11: The simulated power spectral density of a 1 kbps (null every integer number of 1kHz) sampled at 50 thousand samples per second. Full Nyquist range displayed 25kHz ($f_{samp}/2$).

Numerically integrating the PSD shown in Figure 6.11 provides a way to compare the expected to the actual signal power through band-limited channels. The expected power of the PAM signal is simply the amplitude of the PAM signal squared, divided by the load resistance as shown in the equation below. Table 3 shows the result of the signal power found by summing the power spectral density vector and dividing that sum by the integral of the time domain PAM signal [23].

$$P = \int_{T_b} \frac{\left(P_{PAM}\left(t\right)\right)^2}{R_L} dt = \frac{A^2}{R_L} \tag{21}$$

Table 3: The percentage of total power of a binary rectangular PAM within a given bandwidth.

Bandwidth (Hz)	Percentage of Total Signal Power
$1/T_b$	90%
$2/T_b$	95%
$4/T_b$	97.5%
$8/T_b$	98.75%

Clearly there is decreasing marginal benefit to including higher order harmonics. While the first four harmonics of a rectangular PAM signal contain 97.5% of the total signal power, the next four only contain 1.25%. Though an optical communication system can easily accommodate the 8 kHz of bandwidth necessary to support 98.75% of a 1 kbps rectangular PAM signal, a more appropriate 2 Gbps rectangular PAM signal is simulated in Figure 6.12.

The simulation shows how the fundamental harmonic, in this case a 1 GHz sinusoidal frequency with amplitude $\pi/2$, eventually becomes a 'perfect' square wave, by adding, one-by-one, each odd-harmonic. Each of these many harmonics are represented by a delta function in the power spectral density plot of the eventually completed square wave in Figure 6.14.

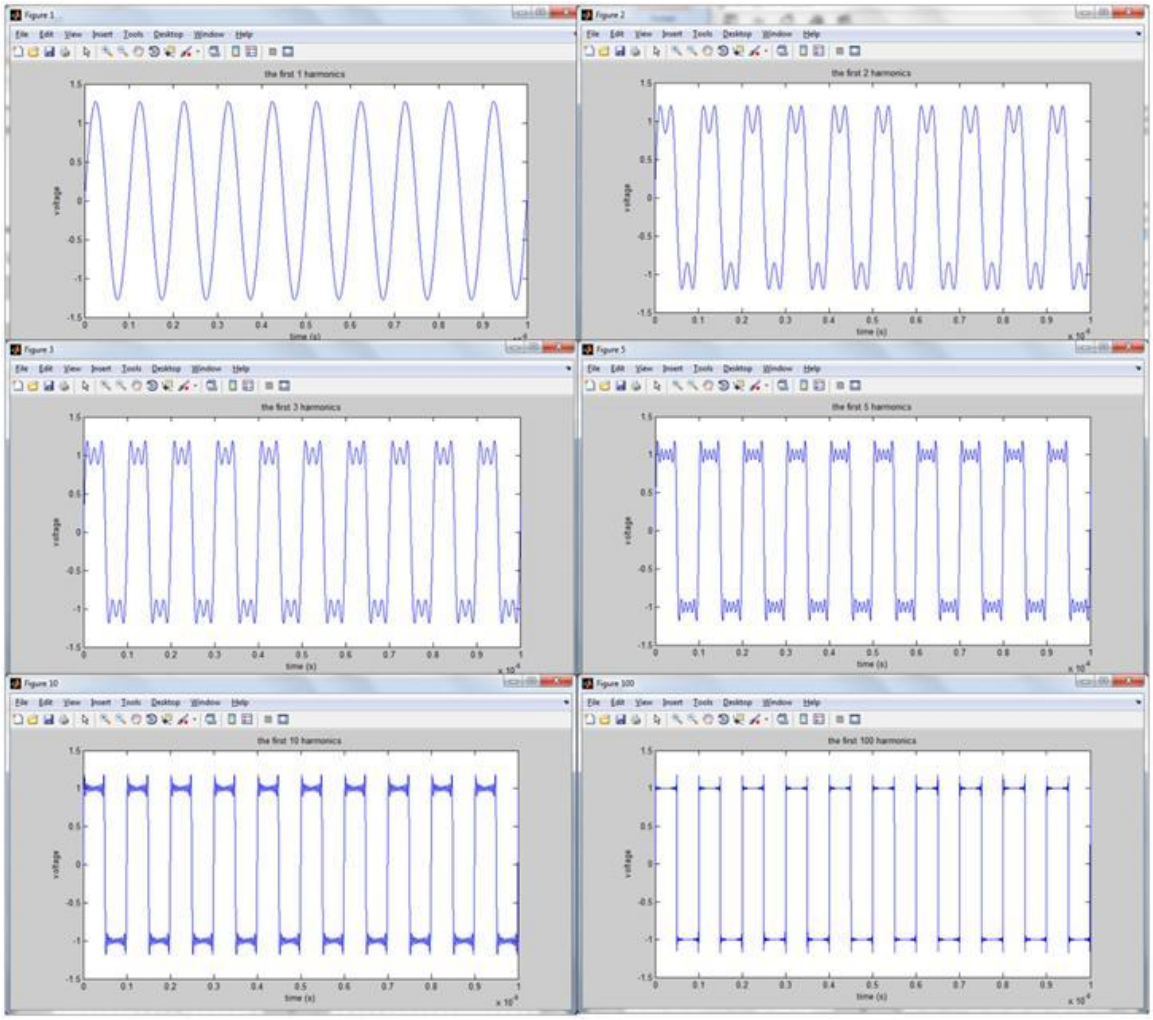

Figure 6.12: Constructing a 2Gbps Square Wave using Fourier series coefficients. Shown here are plots of the waveform created from the first 1, 2, 3, 5, 10, and 100 harmonics.

Representing a rectangular PAM signal as a square wave is appropriate assuming the communication system can modulate frequencies up to that harmonic. The highest fundamental harmonic of a rectangular PAM communication signal happens when the modulator encounters alternating bit sequences such as 0 1 0 1 0 1. The Fourier series representation of a square wave is given by equation (2.7) [25].

$$f(t) = \frac{4A}{\pi} \sum_{k=1,odd}^{\infty} \frac{1}{k} \sin\left(k\left(2\pi f_0\right)t\right) \tag{22}$$

The Fourier series representation provides a rough estimate on the location of the signal's power in the frequency domain. As shown in Figure 6.14, by the 10,000th Fourier series harmonic, the square wave looks almost perfect, and the spectral width of the signal is very wide, nearly 180 GHz. The largest spectral component is the fundamental harmonic of 1 GHz. Since this is a discrete simulation, the maximum frequency measurable is the Nyquist frequency equal to the sampling frequency divided by two. In this case the sample frequency is approximately 3.5E13, so, though the computation would take a very long time, there technically is signal power located past 17 THz.

MATLAB implementation

```
n=10000;
sig10000=zeros(1,length(t));
t=0:tsamp:tsig;
for m=1:n
    sig10000=sig10000+(4./pi())*(1./(2*m-1)).*sin((2*m-1).*pi.*t./tsym);
end
figure(10000)
plot(t,sig10000)
```

Figure 6.13: MATLAB implementation of equation (22), the result of which is shown in Figure 6.14.

Representing random rectangular PAM signals as a sum of Fourier Series Coefficients is only useful for finding approximate bandwidth occupation of signal space. In reality, the Fourier Series requires prior knowledge of every voltage level for all time. This is an inappropriate assumption, as the voltage level will only be known once the bit

is transmitted. To see the effect of this prior knowledge in the Fourier Series representation of a signal, see how the signal starts to ring toward the end of the communication symbol in Figure 6.12 in anticipation of the bit transition, which, from that bit's perspective, occurs in the future. This effect breaks the causality rule of linear systems, and therefore is not present in real systems [26].

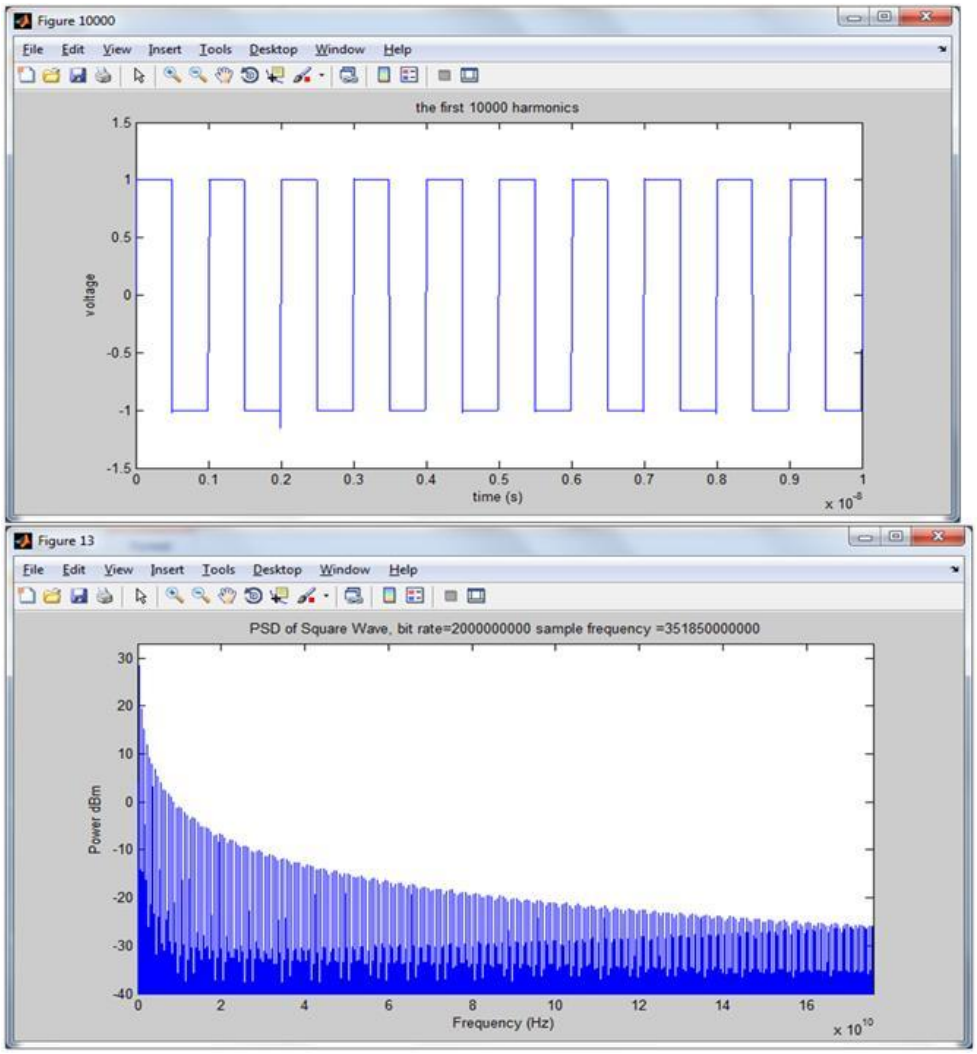

Figure 6.14: Top, time domain representation of a 2Gbps square wave assembled by summing the first 10000 coefficients of the Fourier series of a square wave. Bottom: the power spectral density of the same signal, without AWGN.

A more appropriate representation of a band-limited physical system is a simulation which employs a causal, low-pass filter in the transmission channel, additive white Gaussian noise (AWGN) and a Bit Error Ratio Tester (BERT) which will compare the received bit stream with the transmitted bit stream to measure the performance of the communication system. Figure 6.15 shows the schematic of one such simulation based on Dennis Silage figure 2.9 in Digital Communication Systems Using MATLAB and Simulink [23].

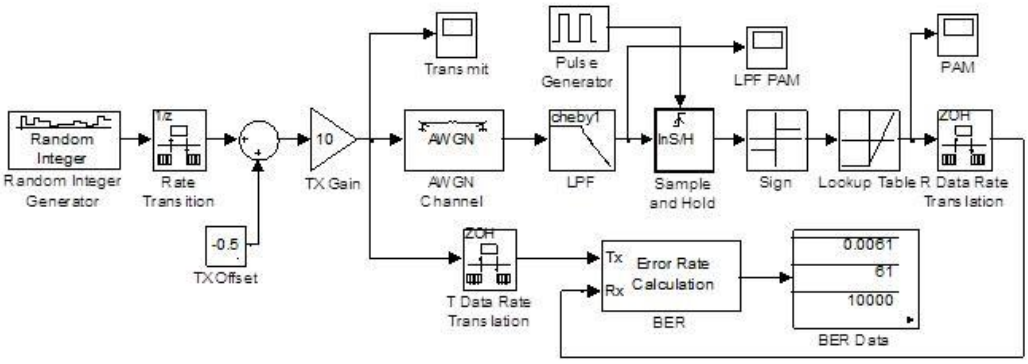

Figure 6.15: Simulink model of band limited binary rectangular PAM communications system.

Running the Simulink model in Figure 6.15 with a bit rate of 1 kbps, no AWGN, and a 9th order Chebyshev type I low-pass filter with a cutoff frequency of 1.2 kHz and a 10% pass-band ripple outputs signals shown in Figure 6.16 [23]. The interesting affects the channel parasitic has on the signal shape include the elimination of all but the fundamental frequency in the higher frequency 0 1 0 1 transitions. Also, the overshoot on the leading edge of the communication symbol is consistent with the anticipated signal

shape predicted by Figure 6.12. The energy required for the increase in amplitude comes from the higher frequency components not transmitted, and accounts for the time delay of one-half the bit interval. Conspicuously absent is the ripple on the trailing edge of the communication symbol. This is because the Chebyshev low-pass filter is causal.

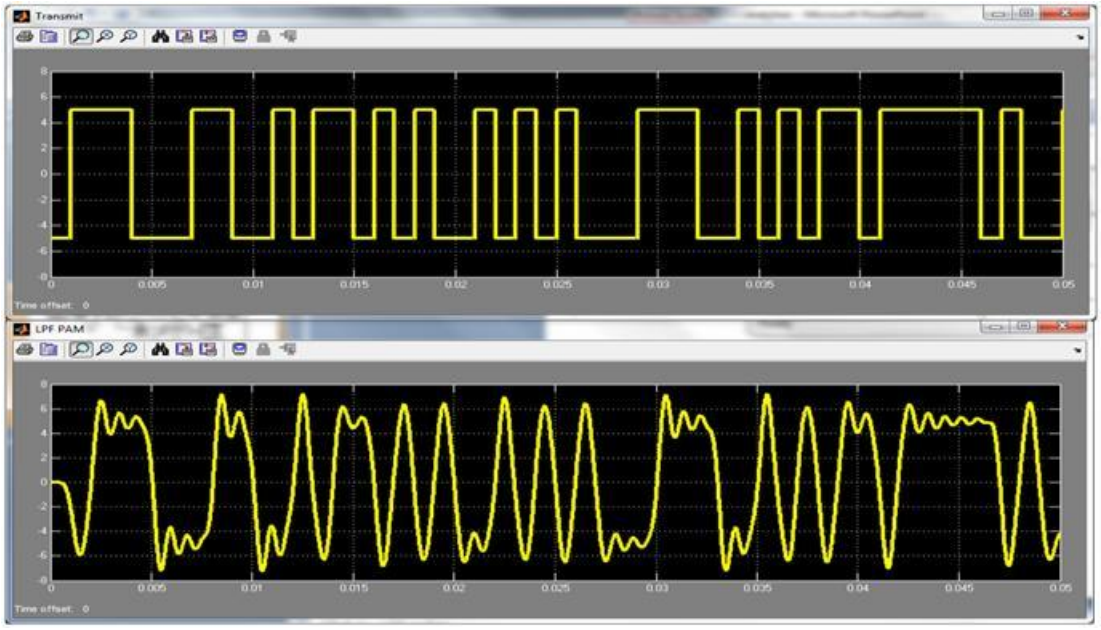

Figure 6.16: Random rectangular PAM signal (top) passed through a Chebyshev type I filter (bottom) without AWGN.

The trailing edge ripple obvious in Figure 6.12 for Fourier series coefficients of 2 or greater helps the communication symbol's overshoot be more predictable. But this requires prior knowledge that the bit is about to transition. Notice how the high voltage in Figure 6.16 is a little higher after strings of 0s than it is after a single 0 or a string of 1s. That's because the construction of a square wave using Fourier series coefficients requires the prior knowledge of the frequency of the square wave [26]. Real systems that use this technique delay the communication signal to account for future bit transitions

before transmission, and anticipate the overshoot. Each pulse shaping filter has its own specific time delay. Generally, increasing the time delay allows the communication symbol to be closer to ideal shape and allows more efficient use of the channel spectral bandwidth. Figure 6.17 shows an example of a shaped pulse signal called raised cosine PAM [23].

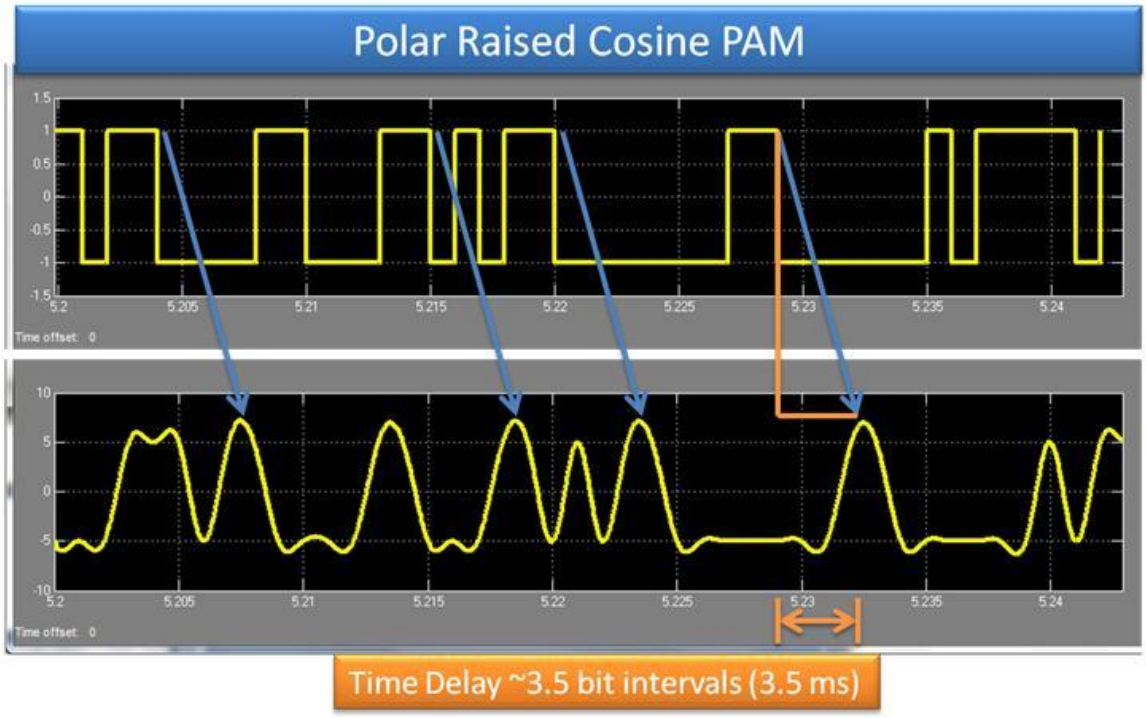

Figure 6.17: Polar Raised Cosine PAM has a more effective use of spectrum, including the trailing edge ripple predicted with the Fourier series coefficients, but requires longer time delay to maintain causality.

In comparison with the unfiltered polar rectangular PAM, which only introduces a time delay equal to half a bit interval to ensure highest probability of detection, raised cosine PAM requires the half-bit interval, plus the time delay associated with the pulse shaping filter, in this case 3 bit intervals. This increase in time delay does allow for more

efficient use of the spectral width of the channel as shown in Figure 6.18 [23] which, in turn, reduces inter symbol interference and allows more effective filtration of AWGN.

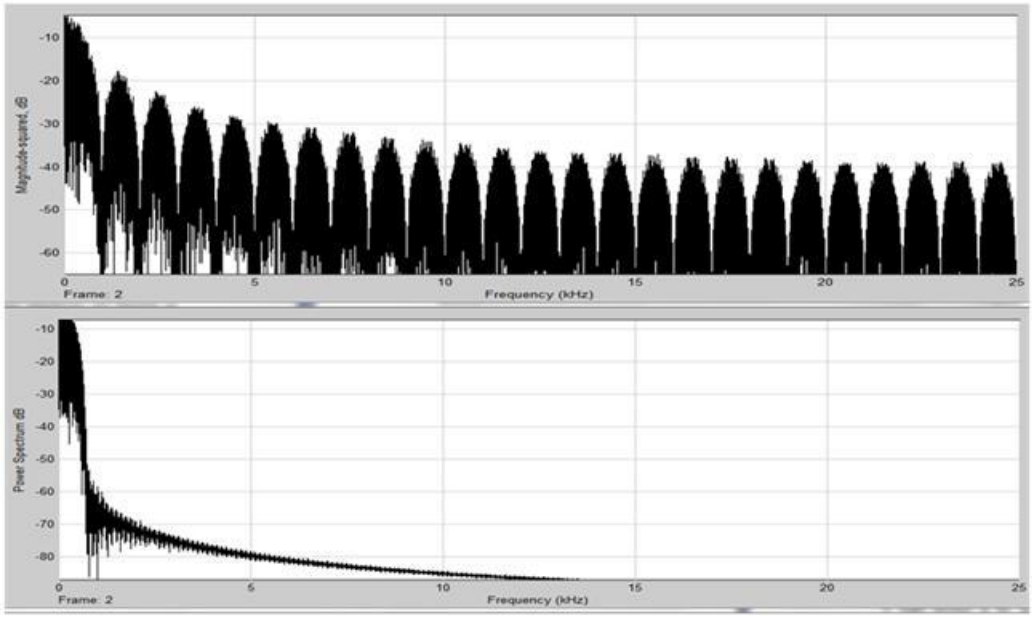

Figure 6.18: Compared to the PSD of random rectangular PAM (top), random raised cosine PAM (bottom) at the same data rate is significantly more efficient.

6.3. Eye Diagrams

The optimal time delay for the sample and hold circuit as well as the optimum offset voltage that provides the lowest bit error ratio is not trivial to observe or calculate in a real system. A few of the major issues affecting communications are additive white Gaussian noise (AWGN), channel attenuation, distortion, and bandwidth, bit-rate instability (jitter), transmission delay, and inter-symbol interference (ISI). An eye-diagram provides an image to qualitatively assess these characteristics and more.

Performing a quantitative bit error ratio test for every possible delay time and voltage would take a prohibitively long period of time. Therefore, to properly measure a bit error ratio of 1E-12 in a 500 Mb/s link would take over 2,000 seconds to perform for a single voltage and time delay point. To get a map of 100 time delay points at 10 different voltage thresholds would then take about 23 days to measure. As a result, the BERT Scope provides a feature called an eye diagram. An eye is a two-dimensional histogram of voltage vs time delay where the probability of occurrence is represented by a different color or intensity dot. Another way of looking at it, an eye diagram places the voltages associated with many random bit sequences on top of each other as shown in Figure 6.19. This eye diagram provides a way of "quickly and intuitively assessing the quality of a digital signal [27]."

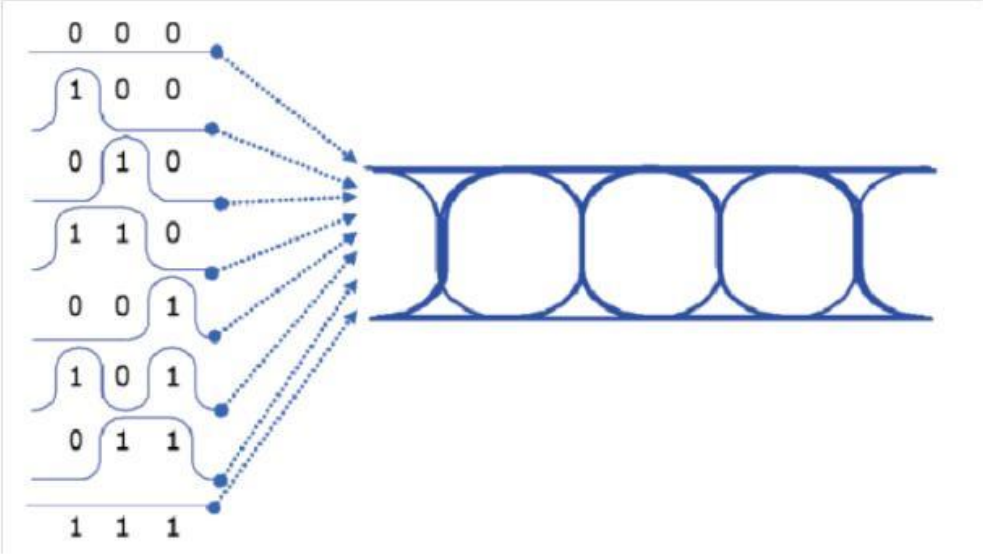

Figure 6.19: Eye diagrams are formed by overlaying bit sequences [27]

For slow data rates, such as the 1 kbps simulations above, an eye diagram is the output of an oscilloscope that has simply held thousands of traces on the screen at once, this is called “persist” on our oscilloscope. What is necessary for that analogy to be true is that the signal displayed on the screen be sampled at least at the Nyquist sampling rate. Figure 6.20 shows a simulated eye diagram formed by overlapping rectangular PAM vectors. The same signal as shown as ‘transmit’ signal in Figure 6.16 [23].

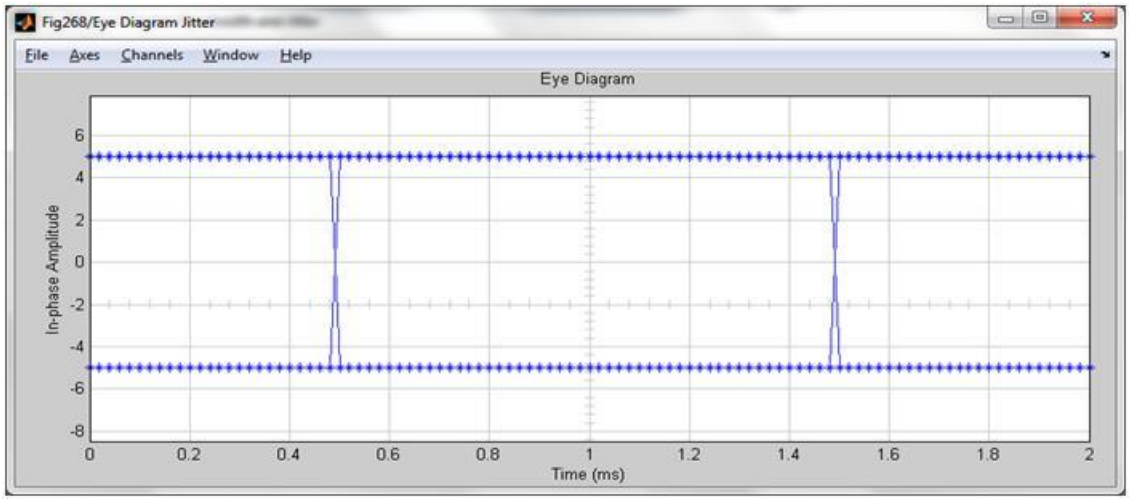

Figure 6.20: A simulated 'perfect eye diagram' created by overlapping hundreds of binary rectangular PAM symbols.

An eye diagram created with the signal after the transmission through the channel looks qualitatively much different. Where the eye diagram in Figure 6.20 appears to have a rise time only because of the sampling frequency of the input signal, the eye diagram in Figure 6.21 has a rise time because the low-pass 9-pole Chebyshev filter representing the spectral limitations of the transmitter and channel has shaped the signal. A Chebyshev low pass filter with its pass-band ripple and steep cutoff slope more closely represents the

spectral response of an optical transmitter than the 9-pole Butterworth filter more common in baseband electronics[23].

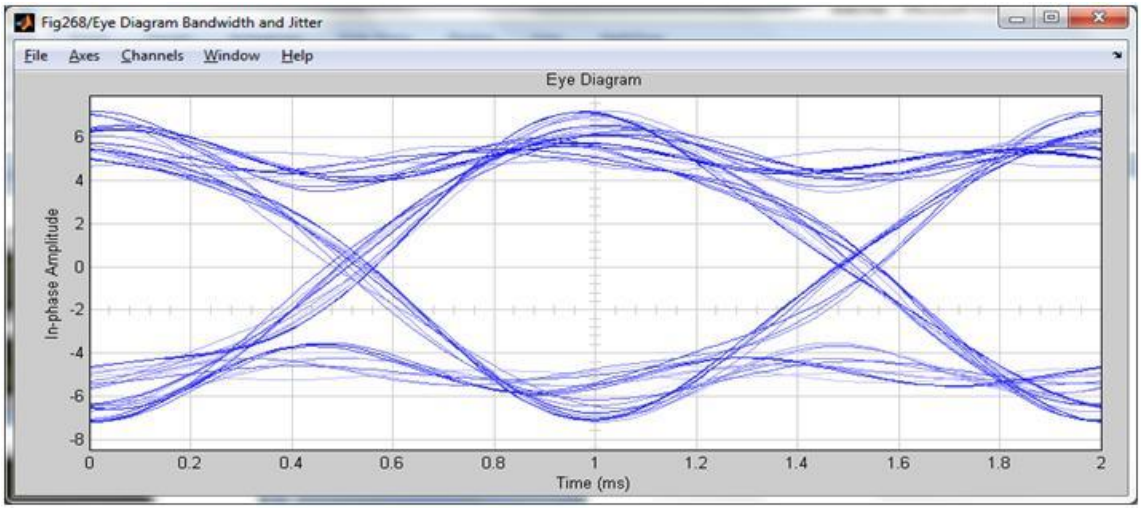

Figure 6.21: Eye diagram formed with the signal output from the 9-pole Chebyshev signal filter in Figure 6.15 by simply overlapping the channel output vector segments.

In a fast physical communication system, a real-world digital sampler will not be able to sample as many points per communication symbol; this slower sampling rate will result in a realistic eye diagram looking much like what is shown in Figure 6.22 [23], without the relational lines shown in Figure 6.21 [23] or, in an eye diagram of a weak optical system shown on the left side of Figure 6.24 [28].

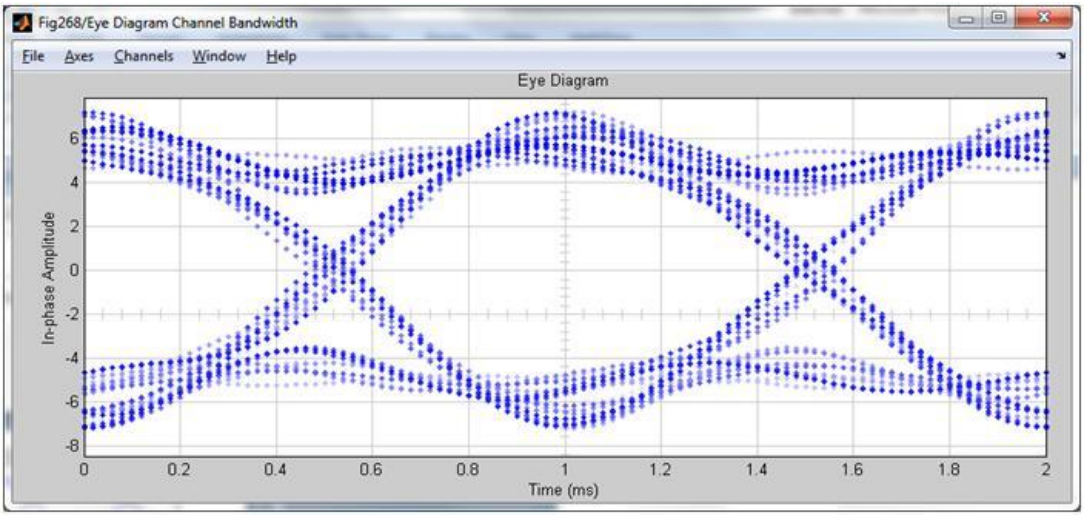

Figure 6.22: Eye diagram formed without drawing a line to connect the sampled points, showing more accurately what an eye diagram of a signal sampled below bit-rate.

In optical communication systems, communication speeds on the order of 5 billion bits per second are common. However, the most advanced analog to digital samplers operate in the tens of millions of samples per second. Even though the sampler measures signals 3 orders of magnitude too slow, it can still form a useful eye diagram using the technique shown in Figure 6.23. The sample rate of an eye diagram analyzer differs from a standard digital sampling oscilloscope which determines its sample rate based on an external clock. An eye diagram analyzer, instead, bases its sample rate on the frequency content of the incoming signal itself, determining on the fly an optimal sample frequency to down-convert optimally into the intermediate frequency [28].

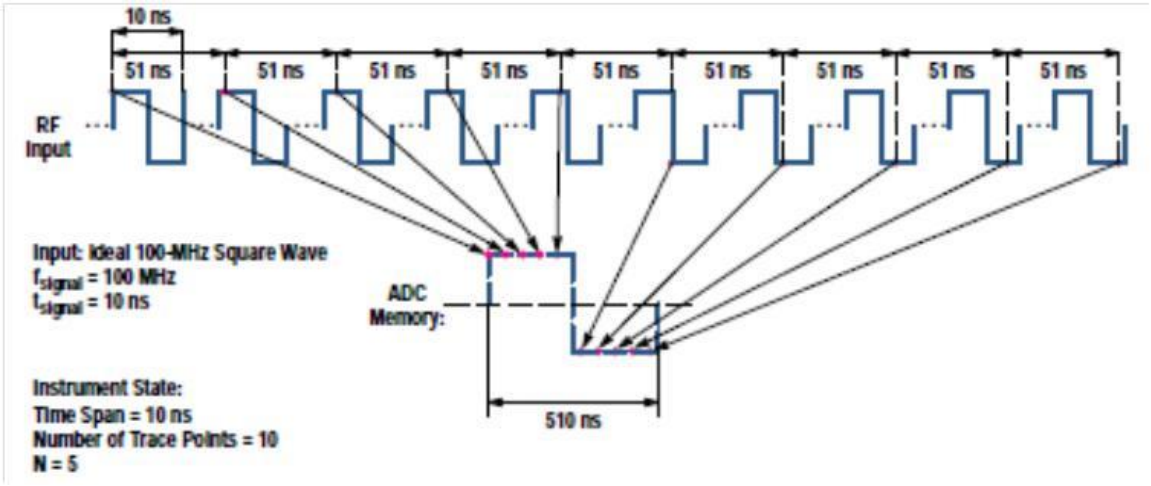

Figure 6.23: Shows how an eye diagram can be formed even as the communication signal of interest is grossly under sampled [28].

Figure 6.23 describes a process called 'harmonic repetitive sampling.' In this process the sampling time, T_s is a function of the fundamental signal period, in this case 10 ns, the time span, the number of trace points, and the maximum sample frequency of the analog to digital converter (ADC). The upper bound on the sample frequency is, of course, the highest sample frequency possible by the analog to digital converter in the eye analyzer. For illustration purposes, the eye analyzer described in Figure 6.23, the HP 71501A, has a maximum sample frequency of 20 million samples per second, making its minimum sample time 50 ns. Equation (23) describes the process of calculating the sample time, T_s [28].

$$T_S = \frac{1}{f_s} = (N \times T_{signal}) + \Delta T$$
$$\Delta T = \frac{Time\,Span}{Number\,of\,Trace\,Points} = \frac{10\,ns}{10} = 1ns \qquad (23)$$

Mandating, that $0 < \Delta T$, it is sufficient to simply solve the equality $Ts = (N \times T_{Signal})$ for an integer value of N to ensure the sample time is longer than the minimum sample time allowed by the ADC. In our example: $50\ ns = (N \times 10\ ns)$ so N=5. For the example in Figure 6.23, the desired number of measured points per symbol is 10, and the symbol time is 10 ns, so $\Delta T = 1\ ns$. This makes the sampling time for the eye analyzer 51 ns, and, to form a single trace of an ideal square wave, the eye analyzer will need to have a sampling time of 510 ns [28].

If the signal of interest really was an ideal square wave, then a standard digital sampling oscilloscope would be a more appropriate tool to measure it. The oscilloscope would simply repeat the above process for about a second, correlate the measured points to a trigger and time average the measured signal to display a clear trace of the square wave. This is not possible; however, in the presence of pseudo random bit sequences (PRBS) as the time average would converge eventually on a DC voltage level, displaying only a flat line for the signal trace. Instead, eye diagrams simply place a small, dim, dot at the measured time delay and voltage. Placing many of these dots on the screen eventually creates a type of two-dimensional histogram as described above. An eye diagram created in this way is shown in Figure 6.24 [28].

From that eye diagram, however, it is difficult to determine whether eye closure is caused by noise, inter-symbol interference, mismatch noise, or jitter. To provide this relational information between different points, the eye analyzer repeats the same PRBS many times so the whole PRBS pattern can be measured at the desired sample rate and a relation between each point on the eye diagram can be created. The right graph in Figure

6.24 is a line diagram of the same communications signal measured in the left graph. The line diagram clearly shows the overshoot that the optical communications system is experiencing at the 0 to 1 transition [28].

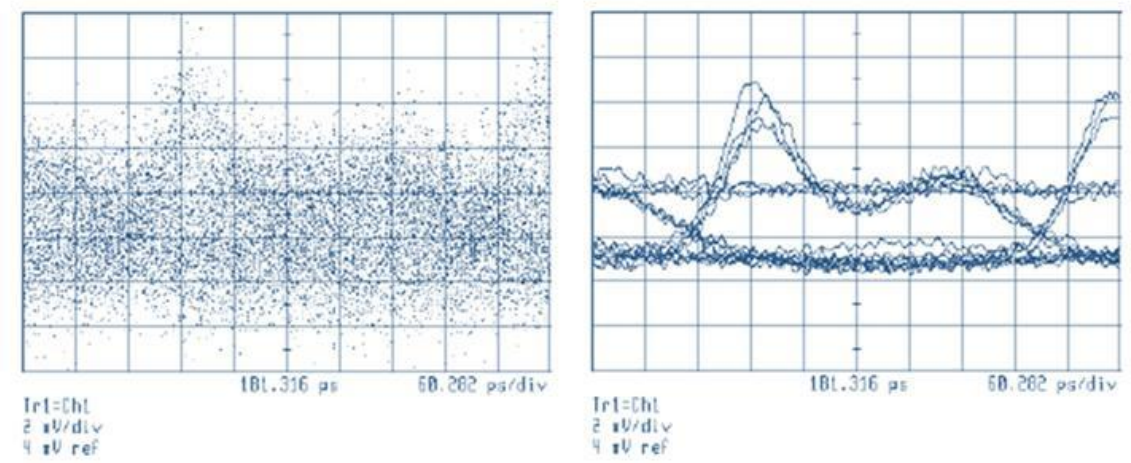

Figure 6.24: Left, eye diagram created by under-sampling a PRBS communication signal losing all relational information between each measured point. Right, eye line diagram, repeats the same PRBS sequence enough to fully sample the entire sequence, keeping relational information between each point [28].

References

[1] Simpson, T. B., "Mapping the nonlinear dynamics of a distributed feedback semiconductor laser subject to external optical injection," *Optics Communications*, 215, 135-151 (2003).

[2] Gavrielides, A., Kovanis, V., and Erneux, T., "Analytical stability boundaries for a semiconductor laser subject to optical injection," *Optics Communications*, 136, 253-256 (1997).

[3] Hwang, S. K., and Liu, J. M., "Dynamical characteristics of an optically-injected semiconductor laser," *Optics Communications*, 183, 195-205 (2000).

[4] Eriksson, S., "Dependence of the experimental stability diagram of an optically-injected laser on the laser current," *Optics Communications*, 210, 343-353 (2002).

[5] Pochet, M., Naderi, N. A., Terry, N., Kovanis, V., and Lester, L. F., "Dynamic behavior of an injection-locked quantum-dash Fabry-Perot laser at zero-detuning," *Optics Express*, 17(23), 20623-20630 (2009).

[6] Chrostowski, L., Faraji, B., Hofmann, W., Amann, M. C., Wieczorek, S., and Chow, W. W., "40 GHz Bandwidth and 64 GHz Resonance Frequency in Injection-Locked 1.55 μm VCSELs," *IEEE Journal of Selected Topics in Quantum Electronics*, 13(5), 1200-1208 (2007).

[7] Lau, E. K., Zhao, X., Sung, H. K., Parekh, D., Chang-Hasnain, C., and Wu, M. C., "Strong optical injection-locked semiconductor lasers demonstrating > 100-GHz resonance frequencies and 80-GHz intrinsic bandwidths," *Optics Express*, 16(9), 6609-6618 (2008).

[8] Hwang, S. K., Liu, J. M., and White, J. K., "Characteristics of Period-One Oscillations in Semiconductor Lasers Subject to Optical Injection," *IEEE Journal of Selected Topics in Quantum Electronics*, 10(5), 974-981 (2004).

[9] Pochet, M., Naderi, N. A., Kovanis, V., and Lester, L. F., "Optically-injected Quantum-dash Lasers at 1550 nm Employed as Highly Tunable Photonic Oscillators," Conference for Lasers and Electro-Optics, San Jose, Ca (2010).

[10] Pochet, M., Naderi, N. A., Li, Y., Kovanis, V., and Lester, L. F., "Tunable Photonic Oscillators Using Optically-injected Quantum-Dash Diode Lasers," *IEEE Photonics Technology Letters*, 22(11), 763-765 (2010).

[11] L. Byoungho. Review of the present status of optical fiber sensors. *Optical Fiber Technology 9(2)*, pp. 57-79. 2003.

[12] B. Sklar . *Digital Communications : Fundamentals and Applications* 2001.

[13] S. Bernard. Digital Communications: Fundamentals and applications. Upper Saddle River, New Jersey 2003.

[14] F. Mogensen, H. Olesen, G. Jacobsen, *J. of Quantum Electron.*, vol. QE-21, pp. 784-793 (1985).

[15] J. M. Liu, H. F. Chen, X. J. Meng, T. B. Simpson, *IEEE Photonics Technology Letters*, vol. 9(10), pp. 1325-1327 (1997).

[16] E. K. Lau, J. W. Liang, M. C. Wu, *J. Sel. Top. Quantum Electron.*, vol 15, pp. 618-633, 2009.

[17] D. J. Malyon, A. P. McDonna, *Elect. Lett.*, Vol. 18(11), pp. 445-447, May 1982.

[18] Olsson, N.; Temkin, H.; Logan, R.; Johnson, L.; Dolan, G.; van der Ziel, J.; Campbell, J.; , "Chirp-free transmission over 82.5 km of single mode fibers at 2 Gbit/s with injection locked DFB semiconductor lasers," *Lightwave Technology, Journal of* , vol.3, no.1, pp. 63- 67, Feb 1985

[19] Z. Xu, Y. J. Wen, W.D. Zhong, C. J. Chae, X. F. Cheng, Y. Wang, C. Lu, J. Shankar, *Optics Express*, Vol. 15(6), pp. 2953- 2962, Mar 2007.

[20] C. C. Lin, Y. C. Chi, H. C. Kuo, P. C. Peng, C. J. Chang-Hasnain, G. R. Lin, *J. of Lightwave Tech*., Vol. 29(6), pp. 830-841, Mar 2011.

[21] N. Naderi, M. Pochet, F. Grillot, N. Terry, V. Kovanis, L. F. Lester, *J. Sel. Top. Quantum Electron.*, vol 15, pp. 563-571, 2009.

[22] Lau, E. K., Wong, L. J., and Wu, M. C., "Enhanced Modulation Characteristics of Optical Injection-Locked Lasers: A Tutorial," *IEEE Journal of Selected Topics in Quantum Electronics*, 15(3), 618-633 (2009).

[23] D. Silage. *Digital Communication Systems using MATLAB® and Simulink®* 2009.

[24] S. O. Kasap, "Optoelectronics and Photonics: Principles and Practices" Prentice Hall, 2001.

[25] F. G. Stremler. *Introduction to Communication Systems* 1990.

[26] C. L. Phillips, J. M. Parr and E. A. Riskin. *Signals, Systems, and Transforms* 2003.

[27] Tektronix, Inc. "Anatomy of an Eye Diagram: Application Note" www.tektronix.com/bertscope, 2010.

[28] C. M. Miller. High-speed digital transmitter characterization using eye diagram analysis. *Hewlett Packard J 45*pp. 29. 1994.

[29] N. A. Naderi, "External control of semiconductor nanostructure lasers," *University of New Mexico,* http://hdl.handle.net/1928/13160 July 2011, 2011.

[30] Lester, L. F., Schaff, W. J., Offsey, S. D., Eastman, L. F., "High-speed Modulation of InGaAs – GaAs Strained-Layer Multiple-Quantum-Well Lasers Fabricated by Chemically Assisted Ion-Beam Etching," *IEEE Photonics Technology Letters*, 3(5), 403-405 (1991).

[31] Matsui, Y., Murai, H., Arahira, S., Kutsuzawa, S., and Ogawa, Y., "30 GHz bandwidth 1.55 μm strain-compensated InGaAlAs-InGaAsP MQW laser," *IEEE Photonics Technology Letters*, 9(1), 25-27 (1997).

[32] K. V. K. K. Prasad. *Principles of Digital Communication Systems and Computer Networks* 2004.

[33] Pochet, Michael, "Characterization of the Dynamics of Optically-Injected Nanostructure Lasers," University of New Mexico, http://hdl.handle.net/1928/11079 July 2010.

[34] T. B. Simpson, J. M. Liu, and A. Gavrielides, *IEEE J. Quantum Electron.*, vol. 32, no. 8, pp. 1456–1469, Aug. 1996.

[35] L. Chrostowski, X. Zhao, and C. J. Chang-Hasnain, "Microwave performance of optically injection-locked VCSELs," *IEEE Trans. Microw.Theory Tech.*, vol. 54, no. 2, pp. 788–796, Feb. 2006.

[36] L. A. Coldren and S. W. Corzine, *Diode Lasers and Photonic Integrated Circuits*. New York: Wiley, 1995.

[37] Liu, J. M., Photonic Devices, Cambridge: Cambridge University Press, 909-912 (2005)

[38] Lau, E. K., Sung, H. K., and Wu, M. C., "Frequency Response Enhancement of Optical-injection Locked Lasers," *IEEE Journal of Quantum Electronics*, 44(1), 90-99 (2008).

[39] P. Spano, S. Piazzolla, andM. Tamburrini, "Frequency and intensity noise in injection-locked semiconductor lasers: Theory and experiments," *IEEE J. Quantum Electron.*, vol. 22, no. 3, pp. 427–435, Mar. 1986.

[40] B. Li, M. I. Memon, G. Yuan, Z. Wang, S. Yu, G. Mezosi, and M. Sorel, "All-optical response of semiconductor ring laser bistable to duo optical injections," in *Proc. Conf. Lasers Electro-Opt.*, San Jose, CA, 2008, pp. 1–2.

[41] L. Chrostowski and W. Shi, "Monolithic injection-locked high-speed semiconductor ring lasers," *J. Lightw. Technol.*, vol. 26, no. 19, pp. 3355–3362, Oct. 2008.

[42] G. H. Smith,D.Novak, and Z. Ahmed, "Technique for optical SSB generation to overcome dispersion penalties in fibre-radio systems," *Electron. Lett.*, vol. 33, pp. 74–75, 1997.

[43] H.-K. Sung, E. K. Lau, and M. C. Wu, "Near-single sideband modulation in strong optical injection locked semiconductor lasers," presented at the Opt. Fiber Commun. Conf., Anaheim, CA, 2006.

[44] K. Iwashita and K. Nakagawa, "Suppression of mode partition noise by laser diode light injection," *IEEE J. Quantum Electron.*, vol. 18, no. 10, pp. 1669–1674, Oct. 1982.

[45] V.V. Vassiliev, V.L. Velichansky, V.S. Ilchenko, M.L. Gorodetsky, L. Hollberg, A.V. Yarovitsky, Narrow-line-width diode laser with a high-Q microsphere resonator, Optics Communications, Volume 158, Issues 1–6, 15 December 1998, Pages 305-312,

[46] Xiao-Qiong Qi; Jia-Ming Liu; , "Photonic Microwave Applications of the Dynamics of Semiconductor Lasers," *Selected Topics in Quantum Electronics, IEEE Journal of* , vol.17, no.5, pp.1198-1211, Sept.-Oct. 2011

REPORT DOCUMENTATION PAGE

Form Approved
OMB No. 074-0188

PLEASE DO NOT RETURN YOUR FORM TO THE ABOVE ADDRESS.

1. REPORT DATE *(DD-MM-YYYY)*	**2. REPORT TYPE**	**3. DATES COVERED** *(From – To)*
22-03-2012	Master's Thesis	Sept 2010 – March 2012

TITLE AND SUBTITLE

Improvements to Optical Communication Capabilities Achieved through the Optical injection of Semiconductor Lasers

5a. CONTRACT NUMBER

5b. GRANT NUMBER

5c. PROGRAM ELEMENT NUMBER

6. AUTHOR(S)

Locke, Timothy P. Captain, USAF

5d. PROJECT NUMBER

5e. TASK NUMBER

5f. WORK UNIT NUMBER

7. PERFORMING ORGANIZATION NAMES(S) AND ADDRESS(S)

Air Force Institute of Technology
Graduate School of Engineering and Management (AFIT/ENGY)
2950 Hobson Way, Building 640
WPAFB OH 45433-8865

8. PERFORMING ORGANIZATION REPORT NUMBER

AFIT-GE-ENG-12-27

9. SPONSORING/MONITORING AGENCY NAME(S) AND ADDRESS(ES)
Air Force Research Laboratory Sensors Directorate (AFRL/RYDP)
Dr. Nicholas G Usechak, Research Engineer
2241 Avionics Circle, Area B Bldg 620
WPAFB OH 45433

10.SPONSOR/MONITOR'SACRONYM(S)
AFRL/RYDP

11. SPONSOR/MONITOR'S REPORT NUMBER(S)

12. DISTRIBUTION/AVAILABILITY STATEMENT

APPROVED FOR PUBLIC RELEASE; DISTRIBUTION UNLIMITED.

13. SUPPLEMENTARY NOTES

14. ABSTRACT

Optically injection locked lasers have shown significant improvement in the modulation capabilities of directly modulated lasers. This research creates a direct-modulated optical communications system to investigate the bit-rate distance improvements achievable using optically injected Fabry-Pérot laser diodes. The injection strength and detuning frequency of the injection signal was varied to determine their impact on the optical communication link's characteristics. This research measured a 25 fold increase in bit-rate distance product using optical injection locking as compared to the injected laser's free-running capability. A 57 fold increase was measured in the bit-rate distance product when signal power is considered in a power-penalty measurement. This increased performance is attributed to the injected signals tolerance to dispersion given its reduced linewidth and chirp.

This work also investigates the suitability of optical injection for radio over fiber applications using the period-one dynamic of optical injection. The all-optically generated, widely tunable microwave subcarrier frequency, well above the 3-dB cutoff frequency of the laser's packaging electronics, was modulated with the same baseband electronics. This optically carried, ultra-wide spread spectrum signal was transported over 50km of standard-single-mode fiber. After detection at a high-speed photo-detector and the baseband modulation component was removed, the resultant signal was found to be suitable for broadcasting with an antenna or added to a frequency division multiplexed channel.

15. SUBJECT TERMS

Semiconductor lasers; Injection-locked lasers; Optical Communications, Bit-rate distance product; Radio-Over-fiber; Spread-Spectrum; Period-One Dynamic; Optically Generated Microwave Frequencies,

6. SECURITY CLASSIFICATION OF:			**17. LIMITATION OF ABSTRACT**	**18. NUMBER OF PAGES**	**19a. NAME OF RESPONSIBLE PERSON**
a. REPORT	**b. ABSTRACT**	**c. THIS PAGE**			Michael C Pochet, Maj. USAF
U	U	U	UU	176	**19b. TELEPHONE NUMBER** (937) 255-6565, ext 4393 (michael.pochet@afit.edu)

Standard Form 298 (Rev. 8-98)
Prescribed by ANSI Std. Z39-18